T H E U N I V E R S I T Y O F M I C H I G A N

COLLEGE OF ENGINEERING
Department of Nuclear Engineering
Radiation-Solid-State Physics Laboratory

Final Report

MICROWAVE INTERACTIONS AT CRYSTAL DEFECT CENTERS

Robert Borcherts
Hossein Azarbayejani
Sophocles Karavelas
Chihiro Kikuchi
Glenn Sherwood

ORA Project 04275

under contract with:

AIR FORCE OFFICE OF SCIENTIFIC RESEARCH
CONTRACT NO. AF 49(638)-987
WASHINGTON, D. C.

administered through:

OFFICE OF RESEARCH ADMINISTRATION ANN ARBOR

January 1963

en gn

UMP053

TABLE OF CONTENTS

TABLE OF CONTENTS (Concluded)

LIST OF TABLES

LIST OF FIGURES

LIST OF FIGURES (Continued)

Part III

LIST OF FIGURES (Concluded)

Part IV

FOREWORD

During the six years that this contract with the Air Force Office of Scientific Research has been in effect, some spectacular developments in quantum electronics have taken place. In 1956, while the first draft of the technical proposal was in preparation, the term "quantum electronics" had not yet been coined. The stated purpose of the proposed program was merely to carry out some basic investigations of chemical and lattice defects in crystalline solids, using electron spin resonance as the tool.

By the end of 1956, however, Bloembergen's suggestion of the solid-state maser became very widely known, and a short time later the feasibility of the suggestion was reported by Scovil, Feher, and Seidel of the Bell Telephone Laboratories. At the Lincoln Laboratory, McWhorter and Meyer discovered maser action in chrome cyanide around the middle of 1957, and on December 20, 1957, the workers at The University of Michigan Willow Run Laboratories observed maser action in pink ruby.

Development of the ruby maser as a device took place very swiftly. During these months after the discovery of maser action in ruby, Townes and Giordemaine, using a tested pink ruby crystal that had been supplied by The University of Michigan workers, announced the successful operation of the radiotelescope maser at the Naval Research Laboratory. A similar device was built later for The University of Michigan radiotelescope. More recently, the ruby maser was used by the workers at the Jet Propulsion Laboratory for the precision determination of the Astronomical Unit (149,589,500 Km). At

the same laboratory, a program evaluating the use of ruby masers for satellite communication is in progress, and it is well known, of course, that a ruby maser is part of the Telstar communication system.

The pink ruby, which previously had been used primarily for phonograph needles, was very soon found to have another important application in a device now popularly called the laser. Soon after theoretical suggestions were offered by Schalow and Townes, T. H. Maiman of the Hughes Research Laboratory and Collins and his co-workers at the Bell Telephone Laboratories reported the predicted phenomenon.

The program carried out under this AFOSR contract is a classical example of the importance of basic research in technological developments. As mentioned earlier, our initial objective was merely to explore the uses of electron spin resonance as a tool to study defects in hard crystalline materials, to which only limited attention had been paid at that time. It was this program that led this principal investigator to examine the merits of such materials as ZnS, MsO, $CaCo_3$, and Al_2O_3 as maser materials, and thus to the observation of maser action pink ruby.

The technological developments in masers and lasers have in turn already raised a number of questions, the answers to which can come only from more intensive basic investigations. One such question is the very old one of energy transfer and transformation mechanisms in solids. We have noticed that the mechanism invoked to explain laser action in solids is different from that needed for luminescence and scintillation phenomena. A program to study these phenomena has been started, with the hope of gaining deeper insight

to energy conversion processes in solids.

In bringing this contract to a close, I wish to thank Mr. Charles F. Yost, now of the Advanced Research Projects Agency, and the various members of the Air Force Office of Scientific Research for the generous support that made our work on the ruby maser at Willow Run possible, and for the continuation of the program to introduce these solid-state concepts and techniques into the research programs of the Department of Nuclear Engineering.

Chihiro Kikuchi
December, 1962

PART I

PROPERTIES OF RUBY AND OTHER SAPPHIRES

by

C. Kikuchi and S. Karavelas

I. INTRODUCTION

For centuries ruby has been highly prized as a gem, but it is only very recently, since the discovery of maser action in ruby, that the industrial importance of this material has come to be appreciated. Before 1957, the Linde Company was the principal supplier of ruby and sapphires. The so-called pink ruby was manufactured by this company to make the so-called sapphire phonograph needles.

The present surge of interest in ruby and related materials stems from the fact that ruby has been shown to be useful as a maser and laser material. Maser, an acronym for Microwave Amplification by Stimulated Emission of Radiation, is a low-noise, high-gain amplifier, for which ruby is the critical material. The ruby maser was used in the Telstar communication system,[1] and at the California Technology Jet Propulsion Laboratory a packaged ruby maser for satellite tracking stations is under evaluation. In scientific application, the ruby maser made possible the precision measurement of the Astronomical Unit, the average distance of the earth from the sun. The precision value of 149,589,500 ± 500 km was obtained by the workers at the Jet Propulsion Laboratory, after making careful analysis of the radar echo from Venus.[2]

Ruby is also used in lasers, a device for the generation of intense coherent optical radiations. The word Laser is an acronym for Light Amplification by Stimulated Emission of Radiation. The industrial and technological uses of this device are still under research and development. It is possible that the device will find applications in communication systems

operating at optical frequencies, and in certain industrial processes such as micro-cutting, micro-etching, and micro-welding. It also seems to be usefull as a medical tool—in coagulating a detached retina onto the eyeball, for example.

A great deal has been said about the usefulness of ruby as a maser and laser material, but few popular expositions attempt to explain why ruby is useful. Consequently, it will be the purpose of this discussion to point out the factors that make ruby behave the way it does.

II. CRYSTAL STRUCTURE

Chemically, ruby is aluminum oxide which contains a small concentration of chromium. Aluminum oxide occurs in two forms; the one that concerns us is known as α-Al_2O_3. In mineralogy, this form is called corundum, and the commercial name of synthetic corundum is sapphire. The commercial sapphire, which is clear, transparent, and colorless, should not be confused with the gem sapphire, which is blue. (In passing, perhaps it should be noted that the technological importance of sapphire is beginning to be realized. For example, according to a recent NASA report, sapphire windows will henceforth be used on satellite solar batteries. Also, sapphire has the very unusual property of high thermal conductivity but low electrical conductivity, in contradiction to the Weidemann-Franz law, which asserts that good electrical conductors are also good thermal conductors. This particular property is used in the laboratory to provide good thermal contact and good electrical insulation.)

There are several varieties of rubies, distinguished by their colors. Gem rubies are deep red, due to the high chromium concentration, whereas the rubies important for masers and lasers are pink, due to the chromium concentration of 0.1% or less.

The crystal structure of sapphire is rather complicated.[3,4] It can be conveniently generated by placing Al_2O_3 molecules at the corners of a cube and stretching the cube along one of the body diagonals. Another Al_2O_3, rotated 180° about the molecular axis with respect to the first molecules, is

placed at the center of this distorted cube. Upon careful examination of this structure, it will be seen that each Al atom is sandwiched between two groups of three oxygens, as shown in Fig. 1. The three oxygens are in a

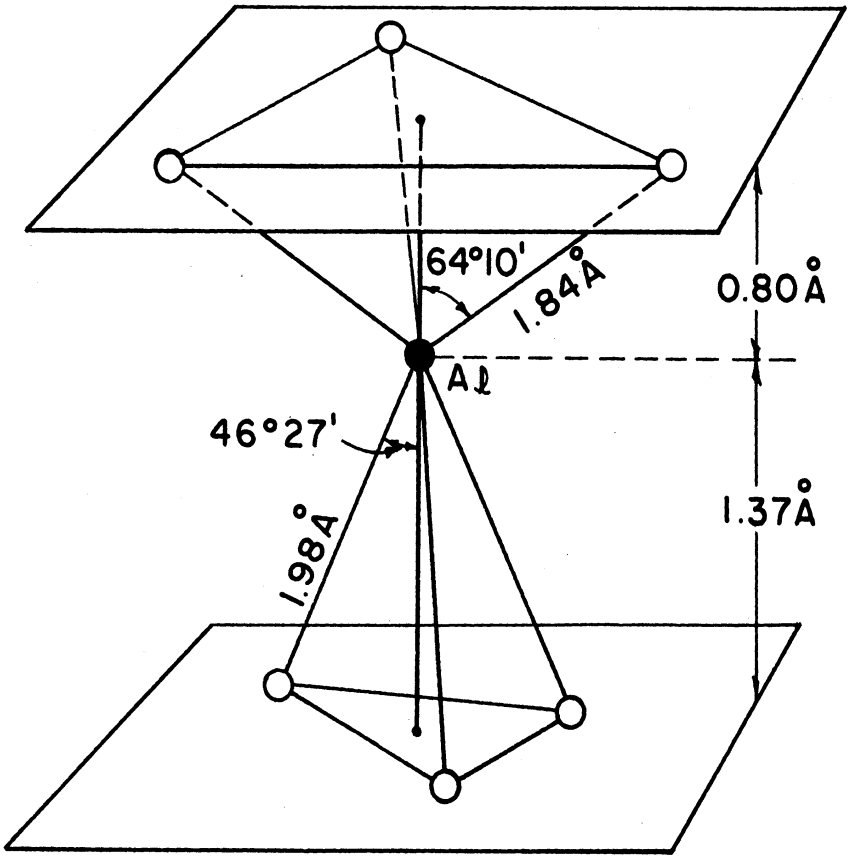

Fig. 1. Coordination of Al atom in α-Al_2O_3.

plane about 1.37Å from the Al site, and the Al-O distance is about 1.98Å, making an angle of 46°27' with the crystal c-axis. The other three oxygens lie in a plane 0.80Å away; the Al-O distance is about 1.84Å and the angle 64°10'. The relative orientations of the two oxygen triangles are not quite 180°. If the oxygens are projected on a horizontal plane, the result shown in Fig. 2 is obtained.

The details of this quantum mechanical calculation is somewhat involved, but the general qualitative features of the energy-level diagram can be predicted readily from group theory. We are concerned with what is called the crystal-field spectra, i.e., the spectrum which arises from electrons making transitions within the 3d shell. For a cubic field, the energy-level diagram would be as shown in Fig. 3:[5]

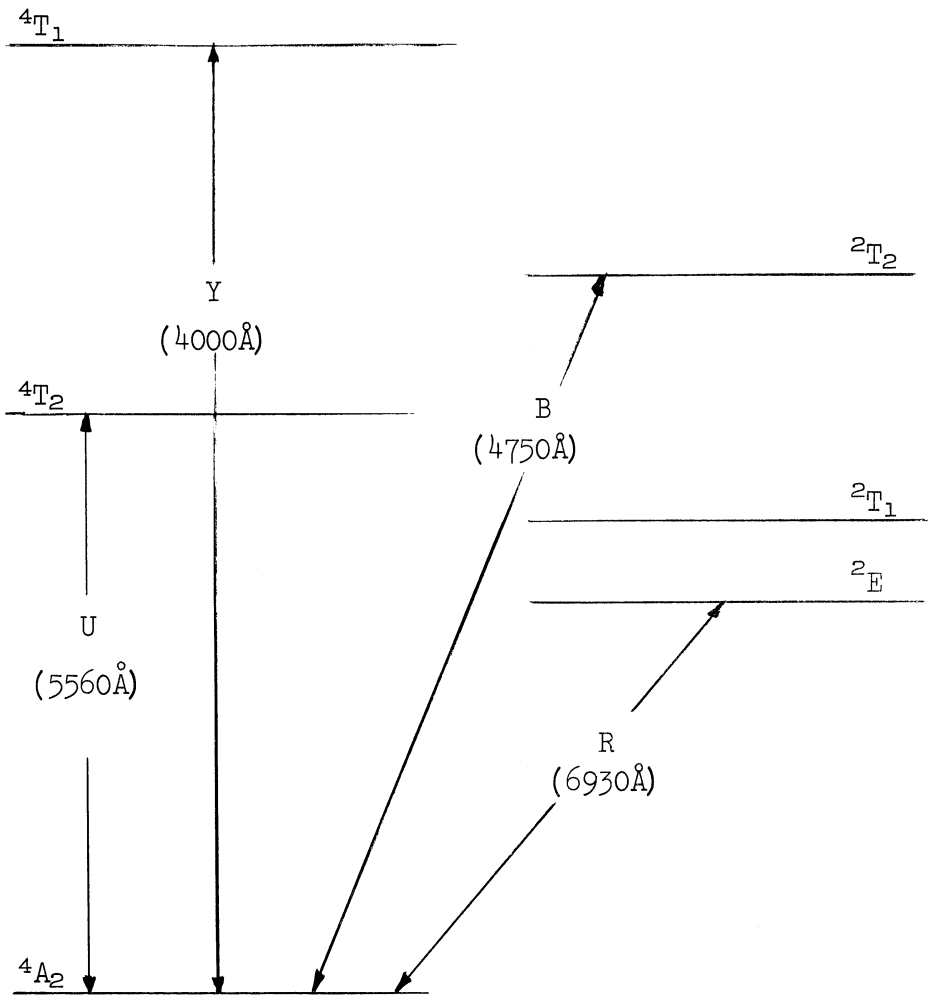

Fig. 3. Energy-level diagram for cubic field.

The numerical values given for the wavelengths of the emitted and/or absorbed radiation are for ruby. For the other two isoelectric ions, V^{2+} and Mn^{4+},

III. ENERGY-LEVEL DIAGRAM

Our next task is to analyze the effect of the six nearby oxygens when an impurity ion such as V^{2+}, Cr^{3+}, or Mn^{4+} is substituted for Al. These three ions are cited because each has the $3d^3$ configuration, so that energy-level diagrams of all three have many qualitative features in common. In most theoretical analyses, the assumption is made that the ion consists of an inert inner ion core (the argon core) and that the electronic properties of the ions are determined by the three electrons in the outer unfilled 3d shell. The validity of this assumption has been questioned recently, but for the present discussion we shall assume the existence of such inert inner filled electron shells.

Earlier, it was emphasized that the crystal structure of sapphire is complex. To make theoretical analysis somewhat tractable, it is generally assumed that the oxygens give rise to a crystalline electric field which has predominantly cubic symmetry but which also has a small component of trigonal symmetry. Such a crystalline electric field can arise if we first imagine that the oxygens are placed at the center of the faces of a cube surrounding the impurity ion, and then imagine a small distortion produced by stretching the cube along the body diagonal. If these assumptions are made, we can first take into account the effect of the cubic component of the crystalline electric field, and later consider the perturbation of the cubic-field energy levels by the small trigonal field.

The details of this quantum mechanical calculation is somewhat involved, but the general qualitative features of the energy-level diagram can be predicted readily from group theory. We are concerned with what is called the crystal-field spectra, i.e., the spectrum which arises from electrons making transitions within the 3d shell. For a cubic field, the energy-level diagram would be as shown in Fig. 3:[5]

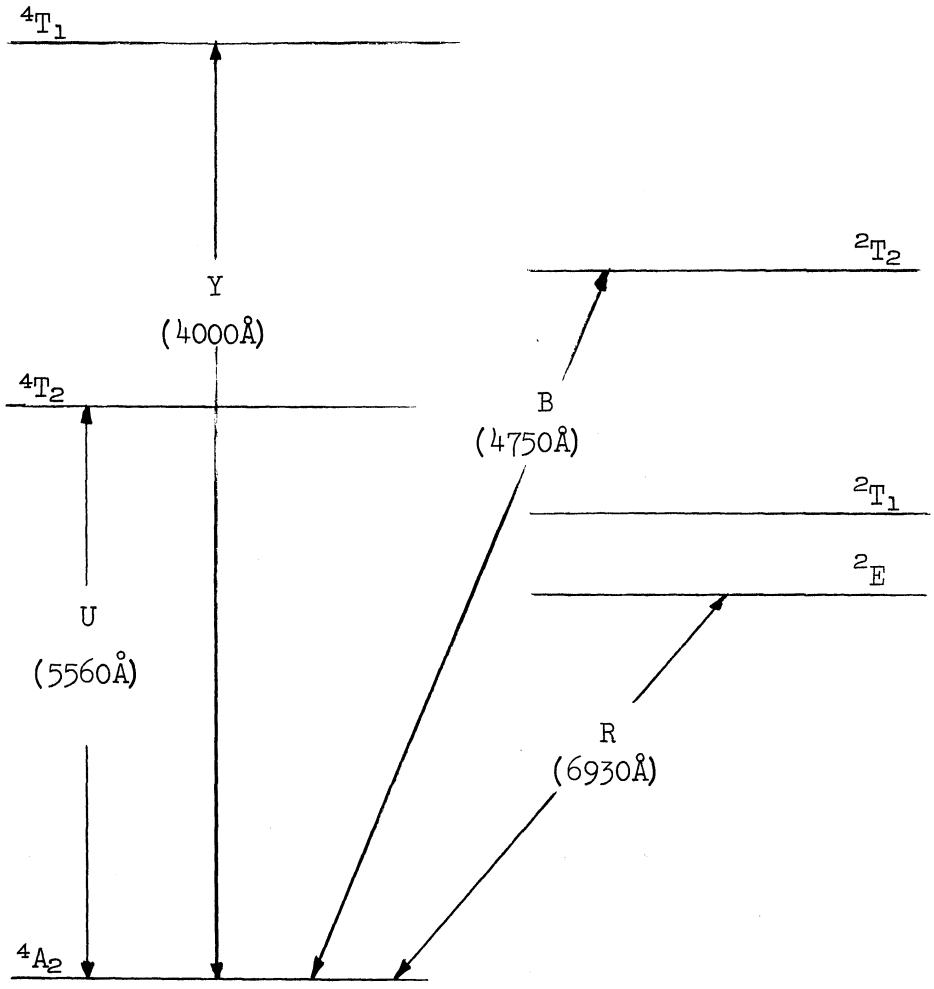

Fig. 3. Energy-level diagram for cubic field.

The numerical values given for the wavelengths of the emitted and/or absorbed radiation are for ruby. For the other two isoelectric ions, V^{2+} and Mn^{4+},

the wavelengths would be slightly different.

If we next take the trigonal crystalline electric field into account,[6] each of the indicated levels will split into two or more levels. The ^2E level will split into two levels; the separation in ruby, for example, is about 29 cm^{-1}, as shown in Fig. 4.

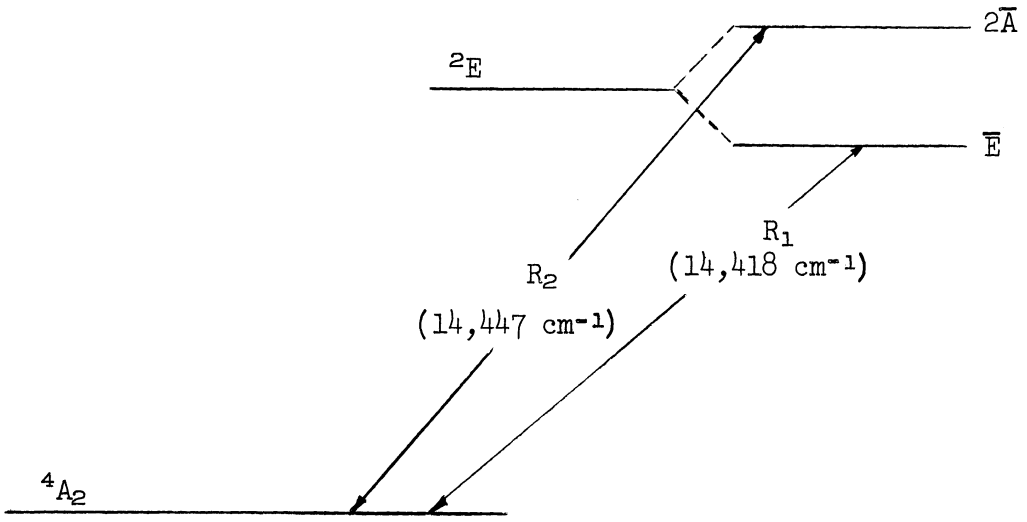

Fig. 4. Split in ^2E level by trigonal field.

This results in the splitting of the R line into two components, referred to in the literature as the R_1 and R_2 lines. The former is the ruby laser line.

The ground state also splits, as indicated in Fig. 5.

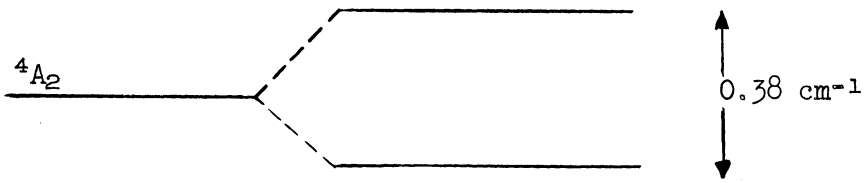

Fig. 5. Split in ground level.

The separation of the levels in this case is very small, only about 1/100 that of the ^2E state. But this very small splitting is important in the ruby maser.

IV. PROPERTIES OF OTHER $3d^3$ IONS

In the preceding section a few of the properties of Cr^{3+} in sapphire were described. The next question that arises is whether or not it is possible to fabricate other materials which have similar properties. To answer this question, a brief discussion of V^{2+} and Mn^{4+} will be presented. The results for Mn^{4+} were published very recently by S. Geschwind and others at the Bell Telephone Laboratories.[7] These results along with properties for V^{2+} and Cr^{3+} are summarized in Fig. 6.

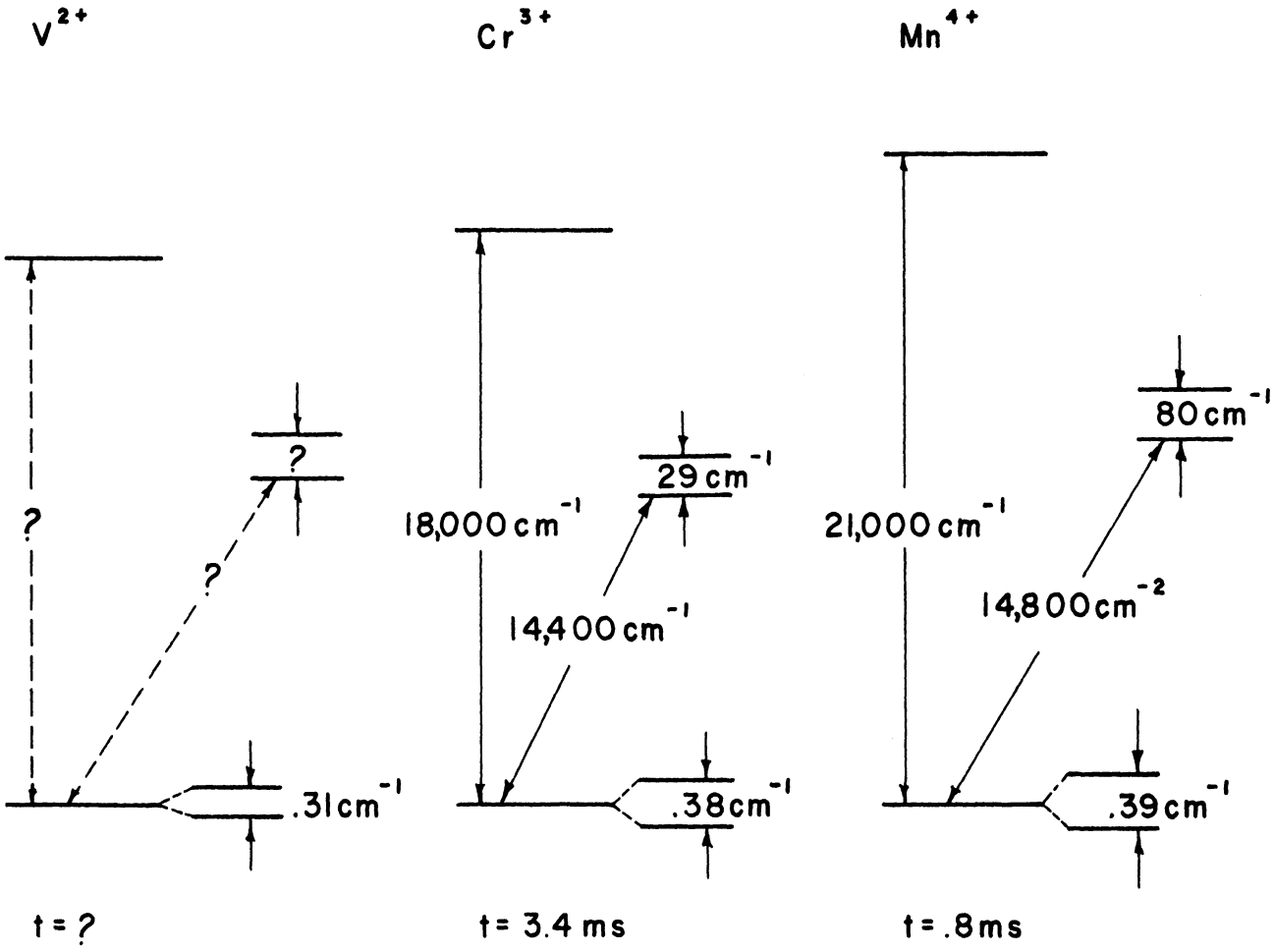

Fig. 6. Properties of V^{2+}, Cr^{3+}, and Mn^{4+}.

The measured values of Mn^{4+} are:

$$R_2 = 14{,}866 \text{ cm}^{-1} \ (79°K)$$

$$R_1 = 14{,}786$$

$$2D = -.3914$$

$$g_{||} \sim g_{\perp} = 1.9937$$

$$|A_{||}| = |A_{\perp}| = 70.0 \times 10^{-4} \text{ cm}^{-1}$$

There are several interesting facts to note. In the first place, the R_1 lines are very nearly equal. Another very remarkable fact is that the results for Mn^{4+} in sapphire are very close to those of Mn^{4+} in lithium titanate. In a paper by Lorenz and Prener[8] the values $\lambda = 6790$Å (14,700 cm^{-1}) and $t = 1.1$ ms are reported. The values for the ground-state splitting are not known, because the measurements were made on a powder. The very close agreement of the numerical values for sapphire and lithium titanate, despite the apparent differences in the host crystal material, stems from the fact that coordination for Mn^{4+} is octahedral; i.e., in both cases the Mn^{4+} ion is bonded to six nearby oxygens.

The work on V^{2+} in sapphire was started in our laboratory when it was noticed that V^{2+} is produced by X-rays.[9] Our experiments showed that normally vanadium in sapphire is present as V^{3+}, but that after irradiation, part of this converted to V^{2+}. The chemical impurity responsible for the stabilization of V^{2+} is not yet known. For Mn^{4+} in both sapphire and lithium tetanate, the presence of Mg impurity is needed.

Vanadium is a favorable system to investigate because it is essentially 100% V^{51}, and because its nuclear magnetic moment is rather large, due to

the fact that vanadium has an odd-proton-even-neutron nucleus. The nuclear magnetic moment can then be used as a signature to identify vanadium, and for this reason vanadium can be quite easily identified in the different oxidation states in sapphire.

With these preliminary remarks, let us return to the ruby energy-level diagrams given in Section III. As mentioned before, the paramagnetic ion in ruby is Cr^{3+}, whose electron shell structure is $1s^2 2s^2 2p^6 3s^2 3p^6 3d^3$. The three 3d electrons in the last unfilled shell are the electrons responsible for the interesting microwave and optical properties of Cr^{3+}. (It should be noted that V^{2+} and Mn^{4+} have the same electron shell structure, so that the comments about to be made are applicable to the three ions V^{2+}, Cr^{3+}, and Mn^{4+}.)

It was mentioned earlier that the chromium ions, occupying the Al substitutional sites, are surrounded by six oxygens. The question we now wish to answer is: What effect will these oxygens have upon the Cr^{3+} energy levels? Since the actual arrangement of the oxygens is quite complex, to make the analysis more tractable we shall first assume that the effects of the oxygens come predominantly from the octahedral arrangement of the oxygens. In other words, for the first step in the analysis we shall assume that, with the Cr^{3+} ion at the origin of the coordinate system, the oxygens are located along the coordinate axes at the same distance from the origin. Later we shall consider the effects of a small distortion along the body diagonal.

Perhaps the graphical representation in Fig. 7 will make the physical problem clearer.

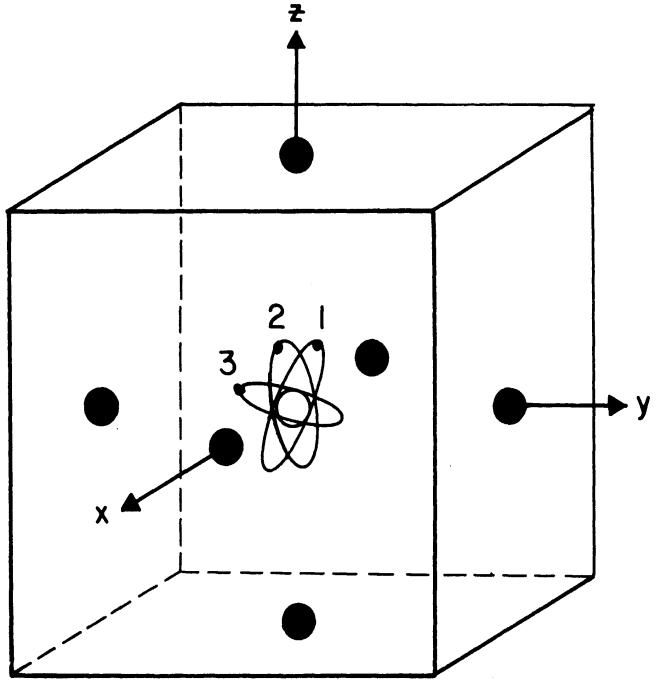

Fig. 7. Octahedral coordination.

Electrons 1, 2, and 3 are moving in the spherically symmetric coulomb field of +6 e. Each electron has orbital and spin angular momentum li and si respectively. There are mutual coulomb repulsive forces among the electrons, and the negative charges located along the coordinate axes will also have an important influence on the motion of the electrons.

The problem indicated here is a complicated one; consequently it will be necessary for us to make a series of approximations. In order to avoid the complexities of theoretical arguments, we shall first consider the case of a single 3d electron, and shall then show how additional factors have to be brought into the analyses as we proceed to the $3d^2$ and the $3d^3$ cases.

The case of the single 3d electron will be dealt with in great detail in order to bring out many features of the theoretical techniques. The single

3d electron is in the central spherical symmetric coulomb field, but its orbital motion is profoundly affected by the oxygens surrounding it. Furthermore, the electron has orbital and spin angular momentum, so that the coupling of these vectors will affect the electron energy level. The Schroedinger equation we need to solve is

$$H\psi = E\psi \tag{4-1}$$

with

$$\mathcal{H} \equiv -\frac{\hbar^2}{2m}\nabla^2 + V(r) + F_c(x^4+y^4+z^4-\frac{3}{5}r^4) + F_t(xy+yz+zx) + \lambda \ell \cdot s \tag{4-2a}$$

The full trigonal part of the Hamiltonian up to fourth power is[10]

$$\begin{aligned} V_{tr} = {} & F_t(xy+yz+zx) + F_t'[xyz(x+y+z) - \frac{1}{7}r^2(xy+yz+zx)] \\ & + F_t''(x+y+z) + F_t''' xyz + F_t''''[x^3+y^3+z^3-\frac{3}{5}r^2(x+y+z)] \end{aligned} \tag{4-2b}$$

if the approximation is made that the symmetry of the Al^{3+} or Cr^{3+} site is C_{3v}. This is equivalent to neglecting the angle of 4°22' shown in Fig. 2. In the following discussion we restrict ourselves to the form (4-2a) for the sake of simplicity. However, one important characteristic of (4-2b) must be kept in mind, namely, that it has no center of inversion. This is important when selection rules for electric dipole transitions are examined.

There are three steps to the Schroedinger equation, as follows:

I. $-\frac{\hbar^2}{2m}\nabla^2 + V(r) + F_c(x^4+y^4+z^4-\frac{3}{5}r^4)$

II. $-\frac{\hbar^2}{2m}\nabla^2 + V(r) + F_c(x^4+y^4+z^4-\frac{3}{5}r^4) + F_t(xy+yz+zx)$

III. $-\frac{\hbar^2}{2m}\nabla^2 + V(r) + F_c(x^4+y^4+z^4-\frac{3}{5}r^4) + F_t(xy+yz+z\mathbf{x}) + \lambda \ell \cdot s$

The purpose of Step I will be to show how the symmetry properties of the Hamiltonian can be exploited to construct wave functions, and also to point out the physical reasons for the importance of group theory in attacking these problems. Consider then the first three terms in (4-2a), i.e.,

$$\mathcal{H}_o \equiv -\frac{\hbar^2}{2m}\nabla^2 + V(r) + F_c(x^4+y^4+z^4-\frac{3}{5}r^4) \qquad (4\text{-}3)$$

We notice that the first two terms are invariant under all rotations, finite or infinitesimal. Consequently, as is well known, if the last term were absent, the solution of the Schroedinger equation could be represented by the spherical harmonics. The corresponding energy levels are called the s, p, d, etc., states. The mathematical significance of this remark is that the wave functions belonging to a particular energy level can be represented by polynomials of x, y, and z which transform among themselves under infinitesimal rotations. For example, the wave functions for the d-electron can be represented either by the set of spherical harmonics of degree 2—Y_2^m, m = 0, ±1, ±2—or by the polynomials xy, yz, zx, x^2-y^2, $3z^2-r^2$.

But what happens if the symmetry of the Hamiltonian is lower? For example, in (4-3), the Hamiltonian is invariant under the simple substitution of ±x, ±y, ±z among themselves, but not under infinitesimal rotations. In the latter case,

$$\begin{aligned} x &\longrightarrow x - \epsilon y \\ y &\longrightarrow y + \epsilon y \end{aligned} \qquad (4\text{-}4)$$

and polynomials in mixed powers of x and y are generated.

However, the Hamiltonian is invariant under a group of transformations called the cubic group. This is the group of operations that carry a cube into itself. Let us see how we can make use of the Hamiltonians invariance under the cubic group to generate wave functions belonging to the same energy level. For this, we need to recall that if ψ is a wave function belonging to the energy level E of

$$H\psi = E\psi \tag{4-1}$$

and if R_g is one of a group of transformations that leaves the Hamiltonian unchanged, i.e.,

$$R_g(H\psi) = H(R_g\psi) \tag{4-5}$$

then the set of functions $R_g\psi$ generated by the group of operations R_g are also solutions belonging to the same energy level E. To illustrate the physical significance of this result, let us examine the effect of the cubic crystalline electric field upon the 3d electrons. As mentioned earlier, the 3d wave functions can be represented by the five linearly independent monomials of the second degree: xy, yz, zx, x^2-y^2, and $3z^2-r^2$. Consequently, let us suppose that

$$f(r)xy \tag{4-6a}$$

is a solution of (4-1) belonging to E. Since f(r) is a function independent of the angle, in order to exhibit the angular dependence hereafter we shall write simply

$$xy \tag{4-6b}$$

instead of f(r)xy. According to the comment made earlier, if R_g is an opera-

tion of the group then other solutions can be generated by the operation. For example, (4-3) does not change if the substitution

$$\begin{aligned} x &\longrightarrow x \\ y &\longrightarrow z \\ z &\longrightarrow -y \end{aligned} \qquad (4\text{-}7a)$$

is carried out. Geometrically, this corresponds to a 90° rotation about the x-axis. Carrying out this substitution on (4-6b) we obtain

$$xz \qquad (4\text{-}6c)$$

Another possible substitution is

$$\begin{aligned} x &\longrightarrow z \\ y &\longrightarrow y \\ z &\longrightarrow x \end{aligned} \qquad (4\text{-}7b)$$

Geometrically, this represents a reflection on a diagonal plane passing through the y-axis. Applied to (4-6b) this operation yields

$$yz \qquad (4\text{-}6d)$$

which along with xy and zx belong to the same energy level E. Also, it is clear that for the rest of the substitutions that carry a cube into itself, the functions xy, yz, and zx, will transform among themselves, but that at no time will they transform into x^2-y^2 and $3z^2-r^2$. But since these last two polynomials will transform among themselves, they belong to another energy level.

V. TRIGONAL FIELD AND SPIN-ORBIT COUPLING

In the last section it was shown how symmetry properties can be used to show that the 3d electron will split into two energy levels, with 2- and 3-fold degeneracy respectively. In order to bring out other properties, we shall consider the trigonal case in detail. A detailed discussion of this case is possible because there are only six operations involved.

As mentioned earlier, the six oxygens in sapphire form a distorted cube. This can be realized by distorting the cube along one of the body diagonals. If this is done along the [111] body diagonal (see Fig. 8), the additional term $F_t(xy+yz+zx)$ shown in (4-2a) appears in the Hamiltonian. What effect will this term have upon the energy levels? In particular, we shall consider the effect of such a distortion upon the energy level associated with the functions xy, yz, and zx, or some suitable linear combination of these functions.

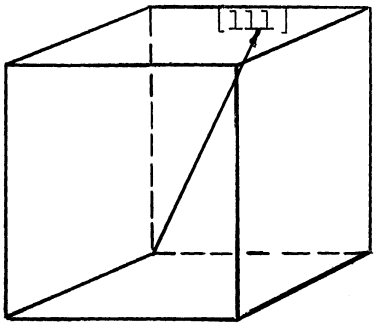

Fig. 8. Cube with [111] body diagonal.

According to the above comments, we need to look for the group of substitutions or operations that leaves the Hamiltonian unchanged. Clearly the

Hamiltonian

$$\mathcal{H} \equiv -\frac{\hbar^2}{2m}\nabla^2 + V(r) + F_c(x^4+y^4+z^4-\frac{3}{5}r^4) + F_t(xy+yz+zx) \qquad (5\text{-}1)$$

will be invariant for substitutions that leave $F_t(xy+yz+zx)$ unchanged; and these will be:

$$E: \quad \begin{matrix} x \longrightarrow x \\ y \longrightarrow y \\ z \longrightarrow z \end{matrix} \qquad (5\text{-}2a)$$

$$C_3^{(1)}: \quad \begin{matrix} x \longrightarrow y \\ y \longrightarrow z \\ z \longrightarrow x \end{matrix} \qquad C_3^{(2)}: \quad \begin{matrix} x \longrightarrow z \\ y \longrightarrow x \\ z \longrightarrow y \end{matrix} \qquad (5\text{-}2b)$$

$$\sigma_v^{(1)}: \quad \begin{matrix} x \longrightarrow x \\ y \longrightarrow z \\ z \longrightarrow y \end{matrix} \qquad \sigma_v^{(2)}: \quad \begin{matrix} x \longrightarrow z \\ y \longrightarrow y \\ z \longrightarrow x \end{matrix} \qquad \sigma_v^{(3)}: \quad \begin{matrix} x \longrightarrow y \\ y \longrightarrow x \\ z \longrightarrow z \end{matrix} \qquad (5\text{-}2c)$$

Substitution (5-2a) is the identity operation; substitutions (5-2b) represent 120° and 240° rotations about the [lll] body diagonal, and substitutions (5-2c) represent reflections in the three face diagonal planes.

From the set of functions xy, yz, and zx we note that the function

$$xy + yz + zx \qquad (5\text{-}3)$$

can be constructed. Clearly, this function transforms always into itself under the operations indicated in (5-2). Physically this means that one of the three functions will split off due to this trigonal field. To construct the remaining two linearly independent functions consider the geometrical procedure shown in Fig. 9a.

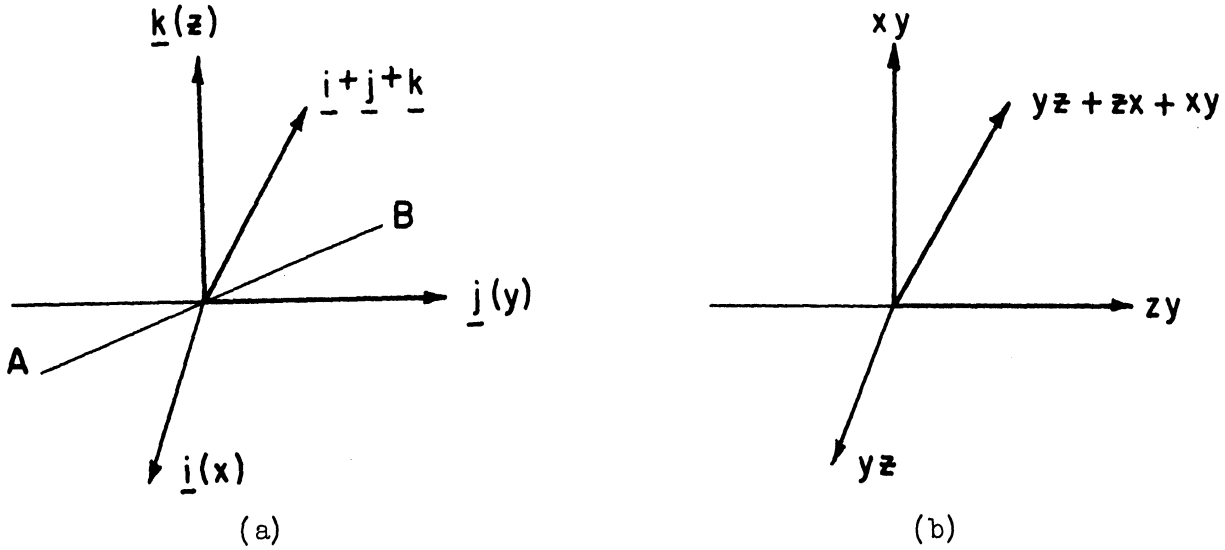

Fig. 9. Geometric constructions of linearly independent functions (simplified).

The plane normal to the vector $\underline{i}+\underline{j}+\underline{k}$ intersects the xy plane along AB, so that a vector in this direction can be written

$$-\underline{i} + \underline{j} \tag{5-4}$$

Referring to Fig. 9b, this suggests the corresponding function

$$-yz + zx \tag{5-5}$$

The vector normal to $-\underline{i}+\underline{j}$ and $\underline{i}+\underline{j}+\underline{k}$ is given by

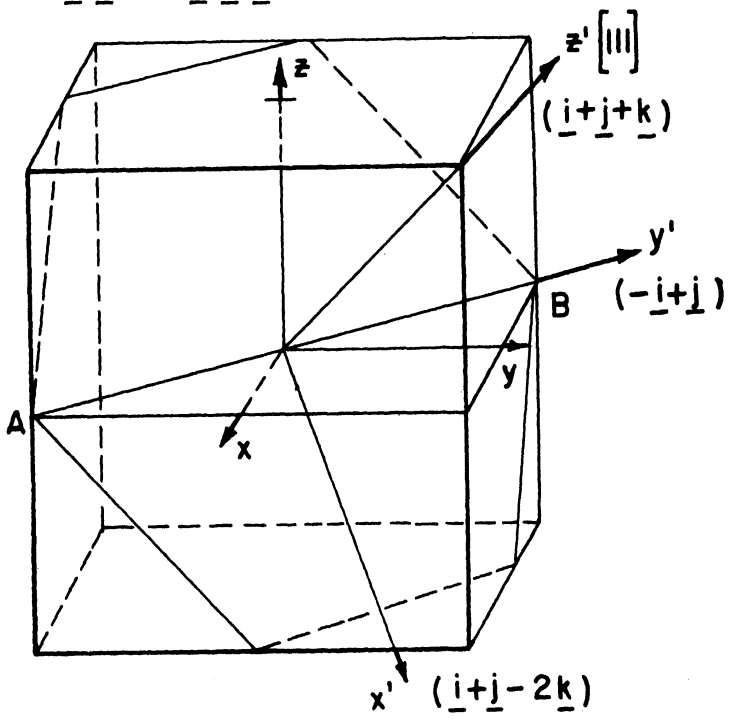

Fig. 10. Geometric constructions of linearly independent functions.

$$\begin{vmatrix} \underline{i} & \underline{j} & \underline{k} \\ -1 & 1 & 0 \\ 1 & 1 & 1 \end{vmatrix} = \underline{i} + \underline{j} - 2\underline{k} \qquad (5\text{-}6)$$

so that the combination

$$yz + zx - 2xy \qquad (5\text{-}7)$$

is suggested. We shall now verify that the functions of (5-5) and (5-7) transform among themselves for the substitutions (5-2) and we shall furthermore construct the matrices representing the operations of (5-2). If we let

$$\begin{aligned} f_1 &\equiv -yz + zx \\ f_2 &\equiv yz + zx - 2xy \end{aligned} \qquad (5\text{-}8)$$

then E carries f_1 into f_1 and f_2 into f_2. Consequently the representative matrix is

$$M(E) = \begin{pmatrix} 1 & 0 \\ 0 & 1 \end{pmatrix} \qquad (5\text{-}9)$$

Consider next $C_3^{(1)}$. In this case

$$\begin{aligned} f_1 &\longrightarrow -zx + xy = -\frac{1}{2} f_1 - \frac{1}{2} f_2 \\ f_2 &\longrightarrow zx + xy - 2yz = \frac{3}{2} f_1 - \frac{1}{2} f_2 \end{aligned} \qquad (5\text{-}10)$$

so that the matrix representation is

$$M\left(C_3^{(1)}\right) = \begin{pmatrix} -\frac{1}{2} & -\frac{1}{2} \\ \frac{3}{2} & -\frac{1}{2} \end{pmatrix} \qquad (5\text{-}11)$$

Similarly,

$$C_3^{(2)}: \quad f_1 \longrightarrow -xy+yz = -\frac{1}{2} f_1 + \frac{1}{2} f_2$$
$$f_2 \longrightarrow xy+yz-2zx = -\frac{3}{2} f_1 - \frac{1}{2} f_2$$
$$M\left(C_3^{(2)}\right) = \begin{pmatrix} -\frac{1}{2} & \frac{1}{2} \\ -\frac{3}{2} & -\frac{1}{2} \end{pmatrix} \quad (5\text{-}12a)$$

$$\sigma_v^{(1)}: \quad f_1 \longrightarrow -zy+yx = \frac{1}{2} f_1 - \frac{1}{2} f_2$$
$$f_2 \longrightarrow zy+yx-2xz = -\frac{3}{2} f_1 - \frac{1}{2} f_2$$
$$M\left(\sigma_v^{(1)}\right) = \begin{pmatrix} \frac{1}{2} & -\frac{1}{2} \\ -\frac{3}{2} & -\frac{1}{2} \end{pmatrix} \quad (5\text{-}12b)$$

$$\sigma_v^{(2)}: \quad f_1 \longrightarrow -xy+xz = \frac{1}{2} f_1 + \frac{1}{2} f_2$$
$$f_2 \longrightarrow xy+xz-2yz = \frac{3}{2} f_1 - \frac{1}{2} f_2$$
$$M\left(\sigma_v^{(2)}\right) = \begin{pmatrix} \frac{1}{2} & \frac{1}{2} \\ \frac{3}{2} & -\frac{1}{2} \end{pmatrix} \quad (5\text{-}12c)$$

$$\sigma_v^{(3)}: \quad f_1 \longrightarrow -xz+yz = -f_1$$
$$f_2 \longrightarrow xz+yz-2xy = f_2$$
$$M\left(\sigma_v^{(3)}\right) = \begin{pmatrix} -1 & 0 \\ 0 & 1 \end{pmatrix} \quad (5\text{-}12d)$$

Earlier we showed that when a suitable linear combination of xy, yz, and zx, namely

$$xy + yz + zx \qquad (5\text{-}3)$$

is taken, this function is such that it always transforms into itself under the operations of (5-2). The following question now arises: Is it possible to construct some linear combination of f_1 and f_2 of (5-8)—say g_1 and g_2—such that g_1 will always transform into itself and g_2 into itself? The answer to this question is no; it is provided by group theory and stems from the fact that the set of numbers obtained by taking the diagonal sum of the matrices is identical to the row of numbers in the group character table.

The character table for the C_{3v} group, with which we are concerned here, is as follows:

	E	$2C_3$	$3\sigma_v$
A_1	1	1	1
A_2	1	1	-1
E	2	-1	0

The symbols appearing at the top of the column represent the symmetry operations, and the numbers in the column below give the trace or the diagonal sum of the representative matrix. The numbers under E give the dimensionality for the so-called irreducible representations A_1, A_2, and E. (The maxtrix representing the symmetry operations A_1 and A_2 are 1-x-1 matrices, whereas those for E are 2-x-2 matrices.)

Clearly, then,

$$xy + yz + zx \tag{5-3}$$

transforms like A_1.

If, next, the last term in (4-2a) is taken into account, the transformation properties of the spin functions have to be considered. The appropriate character table is the one for the double C_{3v} group, which is as follows:

	E	R	$2C_3$	$2C_3R$	$3\sigma_v$	$3\sigma_vR$
A_1	1	1	1	1	1	1
A_2	1	1	1	1	-1	-1
E	2	2	-1	-1	0	0
$\overline{E}$	2	-2	1	-1	0	0
$2\overline{A}$	1	-1	-1	1	i	-i
	1	-1	-1	1	-i	i

It can be shown that the spin functions for S = 1/2 transforms like $\bar{E}$. Figure 11 shows how the energy levels split upon introducing the perturbations in (4-2a) in succession in the indicated order.

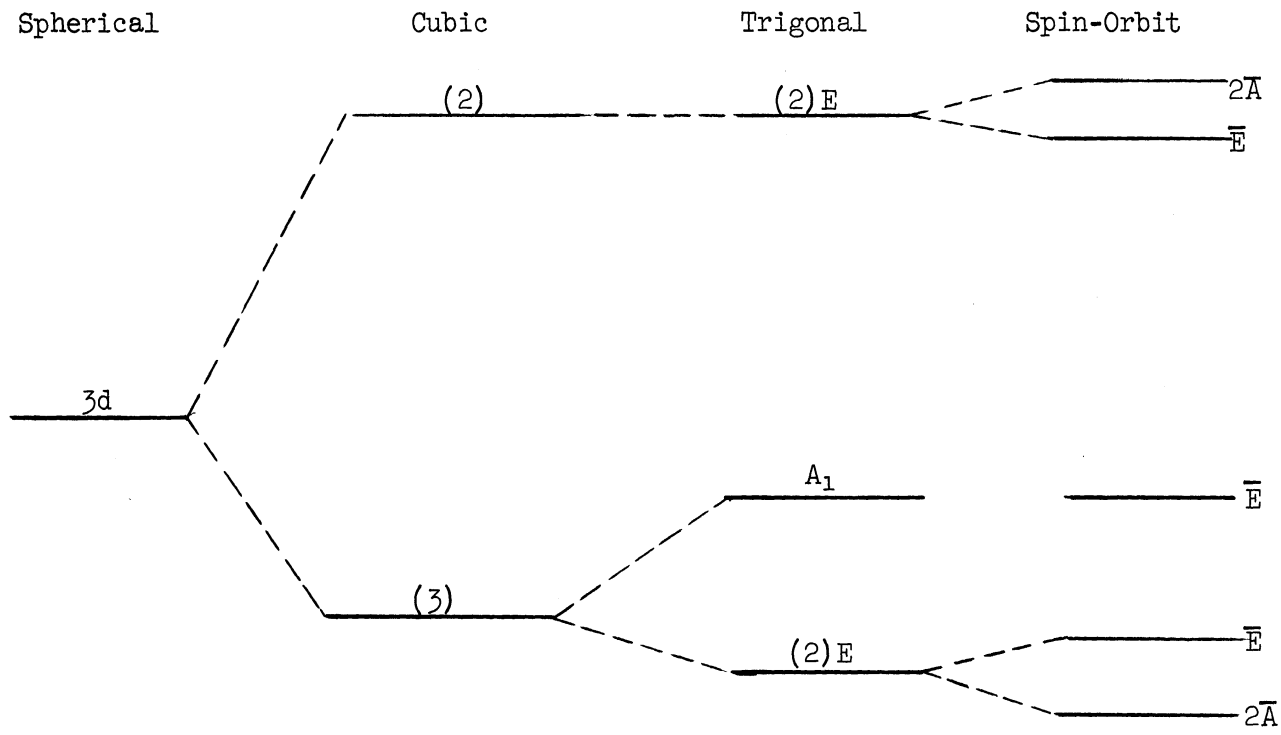

Fig. 11. Split in energy levels upon introduction of perturbations.

VI. CHARACTER TABLE

In the previous section, we mentioned such terms as character table, irreducible representations, etc., without adequate explanation. Here we shall discuss these concepts in greater detail, with particular reference to the cubic group. A clear-cut understanding of the character table is necessary before we can proceed to the two-electron $3d^2$ and three-electron $3d^3$ configurations. We shall present a discussion of what is meant by the character table, point out some of the important properties, and show how this table can be used. Perhaps it should be emphasized that the character table is somewhat like the multiplication table; if we know how to use the table, we can use it to work out multiplication problems!

Consider, then, the group character table for the cubic group:

	E	$8C_3$	$3C_2$	$6C_2'$	$6C_4$
A_1	1	1	1	1	1
A_2	1	1	1	-1	-1
E	2	-1	2	0	0
T_1	3	0	-1	-1	1
T_2	3	0	-1	1	-1

The symbols across the top of the table represent the different classes of symmetry operations and the number in front of the symbols gives the number of operations belonging to that class. A "class" of operations is a set of similar operations and can often be obtained more or less intuitively. For

example, for the group of operations that carry a sphere into a sphere, all rotations of a given angle independent of the axis of rotation belong to the same class. For the cubic group, there are the set of rotations about the body diagonals. The two rotations of 120° and 240° about a body diagonal will carry a cube into a cube. Since there is a total of four body diagonals, we might intuitively guess that all eight such operations belong to the same class. In the above table, the rotations about the body diagonals are in the class C_3. As another example, consider C_2, the class of 180° rotations about the coordinate axes. Since there are three axes, we should expect three operations in class C_2, as indicated in the table. Class C_2' comprises the set of 180° rotations about the face diagonals, and C_4 the class of 90° rotations about the coordinate axes.

Mathematically, the set of similar operations belonging to a given class is generated by the similarity transformation

$$R_C' = R_g R_C R_g^{-1} \tag{6-1}$$

If all symmetry operations R_g belonging to the group are used, a set of distinct operations R_C' will be generated. This is the set belonging to the class C.

For the cubic group, there are five classes, and the total number of symmetry operations is

$$1 + 8 + 3 + 6 + 6 = 24 \tag{6-2}$$

The symbols A_1, A_2, E_1, T_1, T_2 are the different irreducible representations of the cubic group. In order to see what is meant by this, consider a

set of polynomials of degree ℓ. There are, as is well known, $2\ell+1$ linearly independent such polynomials. Suppose these polynomials are represented by $\phi_1, \phi_2 \cdots \phi_i \cdots \phi_n$ in which $n = 2\ell+1$. If, now, some operation R_g of the cubic group—and these operations are simple linear substitutions—is applied to any one of the functions $\phi_i(x,y,z)$, the new function will be a polynomial of x,y,z of the same degree ℓ; therefore the new function can be written as a linear combination of the original set of functions. Thus

$$R_g(\phi_i) = \sum M_{ij}(R_g)\phi_j \tag{6-3}$$

and the operation R_g, operating on the set $\{\phi\}$, can be represented by the matrix

$$M(R_g) \tag{6-4}$$

The dimension of this matrix is clearly $(2\ell+1) \times (2\ell+1)$. Also, since there are 24 operations in the cubic group there will be 24 such matrices, one corresponding to each operation R_g. This set of matrices is said to be a representation of the cubic group because the symmetry operations of the group and the matrix representing the operation can be set into one-to-one correspondence; i.e., if R_i, R_j, and R_k are any three operations such that

$$R_i R_j = R_k \tag{6-5a}$$

and if

$$\begin{aligned} R_i &\longleftrightarrow M(R_i) \\ R_j &\longleftrightarrow M(R_j) \\ R_k &\longleftrightarrow M(R_k) \end{aligned} \tag{6-5b}$$

then

$$M(R_i)M(R_j) = M(R_k) \tag{6-5c}$$

This group of matrices may have one of two possible forms. It is possible that all the matrices in the set will simultaneously have the form

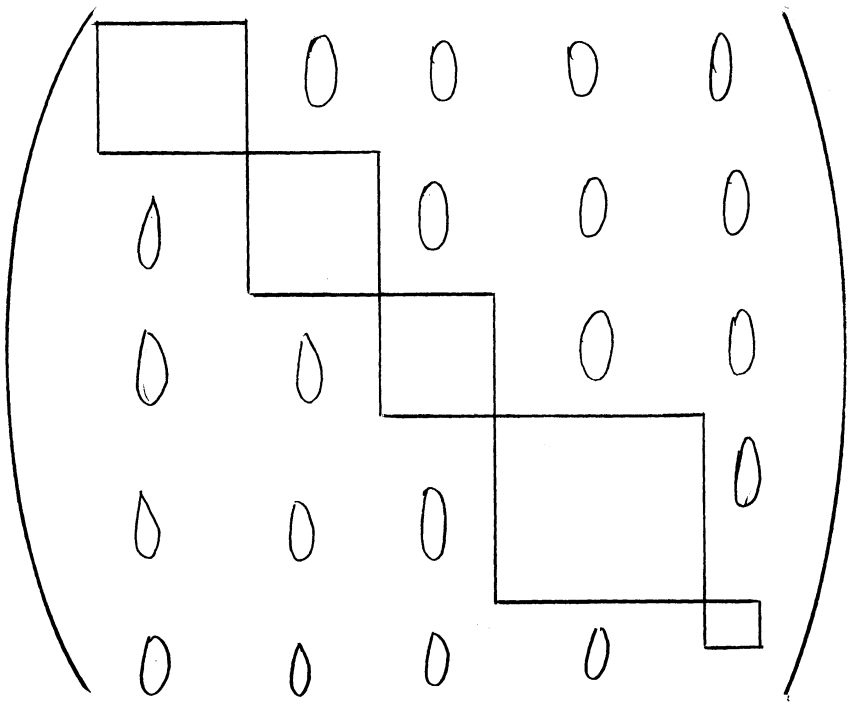

(6-6)

or can be put into it. In this form the non-zero blocks occur along the diagonal only. If the matrices have or can be put into this form, the group is said to be reducible; if not, it is said to be irreducible. For example, for the 3d electron case discussed earlier, $\ell = 2$, the linearly independent functions are xy, yz, zx, x^2-y^2, and $3z^2-r^2$, so that 24 operations of the cubic group will generate 24 5-x-5 matrices. Furthermore, each of the 24 matrices will have the form

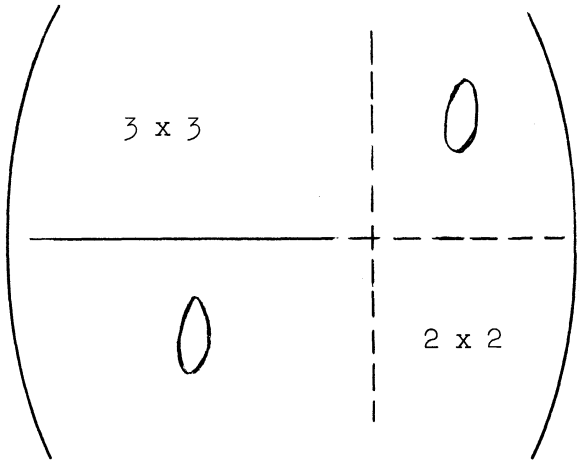

(6-7)

Thus the 24 5-x-5 matrices constitute a reducible representation of the cubic group.

Suppose, now, we consider the group of 24 matrices generated by R_g operating on the set xy, yz, and zx. The matrices will be 3-x-3, as shown earlier. It will be seen that all the matrices cannot be partitioned into the form (6-6). The next question is: By taking a suitable linearly independent, linear combination of xy, yz, and zx, is it possible to generate a set of matrices, all of which will have one of the forms in (6-8)?

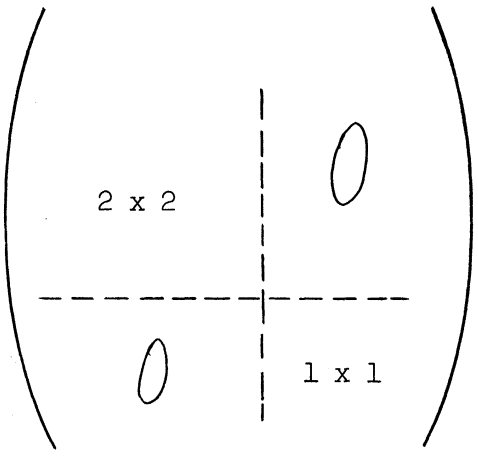

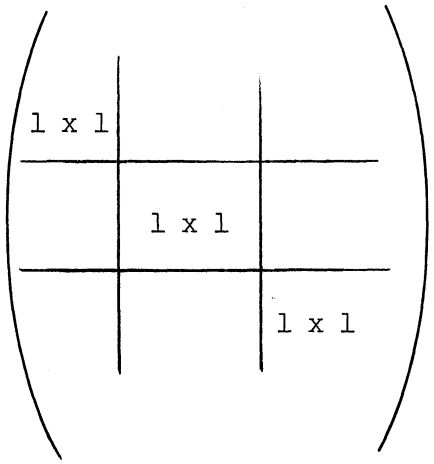

(6-8)

Group theory guarantees us that this is impossible. The set of numbers obtained by taking the diagonal sum of the representative matrices will always

be identical to the set T_2.

The symbols A_1, A_2, E_1, T_1, and T_2 stand for a set of matrices that are in one-to-one correspondence with the symmetry operations of the cubic group. These five sets of 24 matrices are irreducible in that the matrices of each set cannot all be put into the form (6-6) simultaneously. Furthermore, group theory assures us that whatever its dimension, any set of 24 matrices which represents the cubic group operations can be decomposed or reduced to a linear combination of the five irreducible representations. For example, for polynomials of degree 100, there will be 201 linearly independent polynomials; the cubic operations will generate a set of 24 matrices of rank 201. But the rank of the highest sub-matrix cannot be more than three.

However, if we were to select a set of matrices from the original 24 such that the selected set satisfies the group property, then this set could possibly be reducible. For example, consider the rotations about a body diagonal. If the axis of rotation is the (111) direction, then

$$\text{E:}\quad \begin{array}{ll} x \longrightarrow x & xy \longrightarrow xy \\ y \longrightarrow y & yz \longrightarrow yz \\ z \longrightarrow z & zx \longrightarrow zx \end{array} \qquad M(E) = \begin{pmatrix} 1 & 0 & 0 \\ 0 & 1 & 0 \\ 0 & 0 & 1 \end{pmatrix} \tag{6-9a}$$

$$C_3^{(1)}:\quad \begin{array}{ll} x \longrightarrow y & xy \longrightarrow yz \\ y \longrightarrow z & yz \longrightarrow zx \\ z \longrightarrow x & zx \longrightarrow xy \end{array} \qquad M\left(C_3^{(1)}\right) = \begin{pmatrix} 0 & 1 & 0 \\ 0 & 0 & 1 \\ 1 & 0 & 0 \end{pmatrix} \tag{6-9b}$$

$$C_3^{(2)}: \quad \begin{array}{ll} x \longrightarrow z & xy \longrightarrow zx \\ y \longrightarrow x & yz \longrightarrow xy \\ z \longrightarrow y & zx \longrightarrow yz \end{array} \qquad M\left(C_3^{(2)}\right) = \begin{pmatrix} 0 & 0 & 1 \\ 1 & 0 & 0 \\ 0 & 1 & 0 \end{pmatrix} \tag{6-9c}$$

$$M\left(C_3^{(1)}\right) M\left(C_3^{(2)}\right) = \begin{pmatrix} 1 & 0 & 0 \\ 0 & 1 & 0 \\ 0 & 0 & 1 \end{pmatrix} = M(E) \tag{6-9d}$$

The above symmetry operations constitute the group C_3, whose character table is as follows:

	E	$2C_3$	
A	1	1	
E	2	-1	
xy,yz,zx	3	0	= A+E

Mathematically, this means that if an appropriate linear combination of xy, yz, and zx is taken, the three matrices can be reduced. As indicated earlier, the appropriate linear combinations are

$$f_0 = xy + yz + zx$$

$$f_1 = -yz + zx$$

$$f_2 = yz + zx - zxy$$

$$C_3^{(1)} f_0 \longrightarrow f_0$$

$$C_3^{(1)} f_1 \longrightarrow -zx + xy = -\frac{1}{2} f_1 - \frac{1}{2} f_2$$

$$C_3^{(1)} f_2 \longrightarrow zx + xy - 2yz = \frac{3}{2} f_1 - \frac{1}{2} f_2$$

so that

$$M\left(C_3^{(1)}\right) = \left(\begin{array}{c|cc} 1 & 0 & 0 \\ \hline 0 & -\frac{1}{2} & -\frac{1}{2} \\ 0 & \frac{3}{2} & -\frac{1}{2} \end{array}\right) \tag{6-10}$$

and for $C_3^{(2)}$ we obtain

$$M\left(C_3^{(2)}\right) = \left(\begin{array}{c|cc} 1 & 0 & 0 \\ \hline 0 & -\frac{1}{2} & \frac{1}{2} \\ 0 & -\frac{3}{2} & -\frac{1}{2} \end{array}\right) \tag{6-11}$$

Since

$$M(E) = \left(\begin{array}{c|cc} 1 & 0 & 0 \\ \hline 0 & 1 & 0 \\ 0 & 0 & 1 \end{array}\right) \tag{6-9a}$$

all three matrices can be partitioned as indicated by the dotted lines.

The characters, or the traces, satisfy the vertical and horizontal orthogonality relations. Let

$$\chi(C_i, \Gamma) \tag{6-12}$$

represent the character, or the trace, of the matrix which represents operation R_g in class C_i for the irreducible representation Γ. Then the vertical orthogonality relation states that

$$\sum_{\Gamma} \chi(C_i,\Gamma)\chi(C_j,\Gamma) = \frac{G}{n(C_i)} \delta_{ij} \tag{6-13}$$

in which G is the order of the group, or the number of symmetry operations of the group, and $n(C_i)$ represents the number of symmetry operations in class C_i. For example, if the numbers in the column $3C_2$ are multiplied by the corresponding numbers in $6C_4$ and added, we find

$$1 \cdot 1 + 1(-1) + 2(0) + (-1)(1) + (-1)(-1) = 0 \qquad (6\text{-}14)$$

On the other hand, taking the sum of the squares of the characters in $3C_2$, we find

$$1^2 + 1^2 + 2^2 + (-1)^2 + (-1)^2 = 8 \qquad (6\text{-}15)$$

which is $24/3$. This orthogonality relation applied to the class E gives

$$1^2 + 1^2 + 2^2 + 3^2 + 3^2 = 24 \qquad (6\text{-}16)$$

which states that the sum of the squares of the degrees of the irreducible representations is equal to the order of the group.

The horizontal orthogonality relation states that

$$\sum_i n(C_i)\chi(C_i,\Gamma_\alpha)\chi(C_i,\Gamma_\beta) = G\delta_{\alpha\beta} \qquad (6\text{-}17)$$

For example, if we take the representations A_2 and T_2 we find

$$1(1)(3) + 8(1)(0) + 3(1)(-1) + 6(-1)(1) + 6(-1)(-1) = 0 \qquad (6\text{-}18)$$

On the other hand, taking the square of T_2, we find

$$1.3^2 + 8.0^2 + 3(-1)^2 + 6(1)^2 + 6(-1)^2 = 24 \qquad (6\text{-}19)$$

This theorem is important in determining the irreducible components of a reducible representation. Suppose that $\chi(C_i D)$ is the character of the matrix of an operation in class C_i for some representation D of the cubic group. If the latter is reducible, its characters are given by the sum of the irreducible components. Thus, if $a(\Gamma)$ represents the number of times the irreducible representation Γ is contained in D, then

$$\chi(C_i,D) = \sum_{\alpha} a(\Gamma_\alpha)\chi(C_i,\Gamma_\alpha) \tag{6-20}$$

If we multiply this equation by $n(C_i)\chi(C_i,\Gamma_\beta)$ and sum over classes, we obtain

$$\sum_i n(C_i)\chi(C_i,D)\chi(C_i,\Gamma_\beta) = \sum_{\alpha,i} n(C_i)\chi(C_i,\Gamma_\beta)a(\Gamma_\alpha)\chi(C_i,\Gamma_\alpha)$$

$$= \sum_{\alpha} G\delta_{\alpha\beta}\, a(\Gamma_\alpha) = Ga(\Gamma_\beta)$$

therefore

$$a(\Gamma_\beta) = \frac{1}{G}\sum_i n(C_i)\chi(C_i,D)\chi(C_i,\Gamma_\beta) \tag{6-21}$$

In many instances, the irreducible representations can be determined by inspection.

Another important theorem is concerned with the reduction of a product representation. For example, this problem will arise when we consider the two- and three-electron cases. Since the wave functions will be products of wave functions of the individual electrons, we shall be concerned with the transformation properties of such product functions. The theorem simply states that

$$\chi(C_i,\Gamma_\alpha\Gamma_\beta) = \chi(C_i,\Gamma_\alpha)\chi(C_i,\Gamma_\beta) \tag{6-22}$$

and the reduction of this is carried out by the recipe stated earlier. This theorem is useful in determining the condition under which certain integrals can be expected to vanish. In the calculation of the energy levels, we need the integrals

$$\int \bar{\psi}_i V \psi_j d\tau \tag{6-23}$$

The perturbation potential is invariant under the symmetry operation, and so in the case of the cubic group it belongs to the identity representation A_1. Now it can be verified that

$$A_1\Gamma_i = \Gamma_i \tag{6-24}$$

where Γ_i is A_1, A_2, E_1, T_1, or T_2. Furthermore, it can be shown that $\Gamma_i\Gamma_j$ for $i \neq j$ does not contain A_1. Now $V\psi_j$ contains Γ_j but the integral will contain A_1 only if $i = j$; furthermore, the integral will be automatically zero if A_1 is not contained in the product representation. This, then, tells us that in the perturbation calculation we need to calculate only those integrals which connect states belonging to the same representation.

The theorem given in (6-22) is also useful in determining the selection rules for electric dipole transitions. For this the relevant integral is

$$\int \bar{\psi}_i \underline{r} \psi_j d\tau \tag{6-25}$$

in which i and j are the two states involved in the transition. Now $\underline{r}$ transforms like T_1 so that the integral will be zero, unless the product of ψ_i and ψ_j (or more precisely, $\Gamma_i\Gamma_j$) contains T_1. Using the cubic group character

table, we find

$$
\begin{aligned}
A_2T_1 &= T_2 \\
A_2E &= E \\
A_2T_2 &= T_1 \\
ET_1 &= T_1 + T_2 \\
ET_2 &= T_1 + T_2 \\
A_2^2 &= A_1 \\
E_2 &= A_1 + A_2 + E \\
T_1^2 &= A_1 + E + T_1 + T_2 \\
T_2^2 &= A_1 + E + T_1 + T_2 \\
T_1T_2 &= A_2 + E + T_1 + T_2
\end{aligned}
\qquad (6\text{-}26)
$$

The allowed transitions then are

$$
\begin{aligned}
A_2 &\longleftrightarrow T_2 \\
E &\longleftrightarrow T_1 \\
E &\longleftrightarrow T_2 \\
T_1 &\longleftrightarrow T_1 \\
T_2 &\longleftrightarrow T_2 \\
T_1 &\longleftrightarrow T_2
\end{aligned}
\qquad (6\text{-}27)
$$

We see, then, that the levels E and T_2 brought about by the splitting of the 3d levels can give rise to an allowed transition, despite the fact that $\Delta\ell = 0$!

Of course this is true for the cubic group O, which has no center of symmetry. For the cubic group O_h, the levels derived from the 3d orbitals be-

long to the even (gerade) representations E_g and T_{2g}, whereas $\underline{r}$ transforms according to the odd (ungerade) representation T_{1u}, so that integrals of the form

$$\int \bar{\psi}_{i(E_g)} \underline{r} \psi_{j(T_{2g})} d\tau$$

vanish identically and electric dipole transitions are not allowed between states of these levels.

VII. THE $3d^2$ CONFIGURATION

Earlier we indicated that the 3d-electron energy level is split into levels belonging to the cubic irreducible representations E and T_2. In our notation henceforth we shall speak of the t_2 or the e electron depending upon whether the electron occupies one of the T_2 or E orbitals. Since there are three T_2 and two E orbitals, it is clear that there can be all together $2 \times 3 = 6$ electrons occupying the T_2 orbitals, and $2 \times 2 = 4$ electrons occupying the E orbitals. Consequently, we may speak of the t_2 and the e subshells of the d-electron shell. As in atomic spectroscopy, we shall consider next the possible electron configuration arising from two equivalent t_2 electrons.

The basic Schroedinger equation

$$H\psi = E\psi \tag{4-1}$$

we wish to solve is such that

$$H \equiv H_1 + H_2 + \frac{e^2}{r_{12}} \tag{7-1}$$

in which

$$H_i = -\frac{\hbar^2}{2m} \nabla^2 + V(r_i) + F_c(x_i^4+y_i^4+z_i^4 - \frac{3}{5} r_i^4) \tag{7-2}$$

The method of attack is to expand the solution in terms of product functions of the two electrons. For the t_2^2 configuration, there are nine product functions obtained by multiplying the set $(xy)_1,(yz)_1,(zx)_1$ into $(xy)_2,(yz)_2$, $(zx)_2$. The indices 1 and 2 refer to the two t_2 electrons. Earlier, the

symmetry properties of the Hamiltonian were exploited to obtain information about the nature of energy levels and wave functions. The Hamiltonian (7-1) is invariant under the operations of the cubic group, so that some of the previous arguments can be used.

However, we note that the Hamiltonian exhibits an additional symmetry property of being invariant when the indices 1 and 2 are permuted. This means that the solutions of (4-1) must constitute the basis functions for the symmetric group S_2. For this group, there are only two operations: the identity operation, represented by the permutation (1) (2), and the operation exchanging the indices 1 and 2, represented by (12). Clearly, then, there are only two irreducible representations, and the character table is as follows:

	(1^2) (1)(2)	(2) (12) ← Class	
S	1	1	
A	1	-1	
	9	3	= 6S + 3A

This table shows that the irreducible representations are one-dimensional, i.e., the basis functions are such that each transforms into itself or into its negative upon permutation of the indices 1 and 2. These are the familiar symmetric and antisymmetric representations. Consider now the effect of these operations upon the nine product functions:

$$
\begin{array}{lll}
(yz)_1(yz)_2 & (zx)_1(yz)_2 & (xy)_1(yz)_2 \\
(yz)_1(zx)_2 & (zx)_1(zx)_2 & (xy)_1(zx)_2 \\
(yz)_1(xy)_2 & (zx)_1(xy)_2 & (xy)_1(xy)_2
\end{array} \qquad (7\text{-}3)
$$

The two permutations are represented by 9-x-9 matrices. The character, or the trace, is simply equal to the number of functions that are not affected by the permutations. Consequently for the class (1^2) the character is 9, since none of the functions change when left alone. For the permutation (12) only three functions—$(yz)_1(yz)_2$, $(zx)_1(zx)_2$, and $(xy)_1(xy)_2$—transform into themselves. Consequently the character for class (2) is 3. By inspection (there is no need here to appeal to the general theorem enunciated earlier!) it is seen that the reducible representation contains six symmetric and three antisymmetric irreducible representations. Since these representations are one-dimensional, the nine functions of (7-3) can be grouped into six symmetric and three antisymmetric functions. The symmetric functions are

$$
\begin{array}{ll}
(yz)_1(yz)_2 & (yz)_1(zx)_2 + (yz)_2(zx)_1 \\
(zx)_1(zx)_2 & (yz)_1(xy)_2 + (yz)_2(xy)_1 \\
(xy)_1(xy)_2 & (zx)_1(xy)_2 + (zx)_2(xy)_1
\end{array} \qquad (7\text{-}4)
$$

and the antisymmetric functions are

$$
\begin{array}{l}
(yz)_1(zx)_2 - (yz)_2(zx)_1 \\
(zx)_1(xy)_2 - (zx)_2(xy)_1 \\
(xy)_1(yz)_2 - (xy)_2(yz)_1
\end{array} \qquad (7\text{-}5)
$$

Next consider transformations induced by the operations of the cubic group. For (7-4) we shall obtain 24 6-x-6 matrices and for (7-5) 24 3-x-3 matrices. Our task is to decompose these into a sum of irreducible representations. The calculation of the characters would be rather tedious if we had to carry out the linear substitutions mentioned earlier. Fortunately, however, by using the result

$$\chi(R,S) = \frac{1}{2}\left\{[\chi(R)]^2 + \chi(R^2)\right\} \tag{7-6a}$$

and

$$\chi(R,A) = \frac{1}{2}\left\{[\chi(R)]^2 - \chi(R^2)\right\} \tag{7-6b}$$

the necessary decomposition can be readily carried through (see, for example, Ref. 12, p. 134). From the cubic character table we have

	E	$8C_3$	$3C_2$	$6C_2'$	$6C_4$
T_2	3	0	-1	1	-1
T_2^2	9	0	1	1	1
$\chi(R^2)$	3	0	3	3	-1

To the characters of T_2^2, we need to add or subtract those of $\chi(R^2)$. In so doing, we note that

$$E^2 = E$$

$$C_3^2 = C_3$$

$$C_2^2 = E$$

$$C_2'^2 = E$$

$$C_4^2 = C_2^2$$

giving the set of numbers indicated in the row $\chi(R^2)$. Consequently, characters for the symmetric and antisymmetric representations are

	E	$8C_3$	$3C_2$	$6C_2'$	$6C_4$
S	6	0	2	2	0
A	3	0	-1	-1	1

so that

$$S = A_1 + E + T_2 \tag{7-7}$$

and

$$A = T_1 \tag{7-8}$$

As a check, we note that

$$(T_2)^2 = A_1 + E + T_1 + T_2 = S + A \tag{7-9}$$

According to Paul's principle the overall wave function, including both orbit and spin, must be antisymmetric in the indices 1 and 2. Therefore if the orbital function is symmetric, the spin functions must be antisymmetric, and vice versa. The symmetric and antisymmetric spin functions have spins 1 and 0, respectively. Consequently, we obtain the allowed states

$$^1A_1 + {}^1E + {}^1T_2 \tag{7-10a}$$

and

$$^3T_1 \tag{7-11a}$$

in agreement with the result obtained by other procedures.

For future use, we shall restate our results in terms of Young tableaux (see Refs. 12 and 13). Using this notation we have shown that

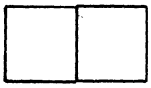

$= {}^1A_1 + {}^1E + {}^1T_2$ (7-10b)

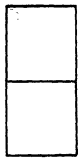

$= {}^3T_1$ (7-11b)

We shall need these results to determine the allowed states for the $3d^3$ configurations.

VIII. THE $3d^3$ CONFIGURATION

The aim of this section will be to present a number of arguments to make the Orgel-Sugano-Tanabe diagram of Cr^{3+} understandable. As has been pointed out already, the cubic crystalline electric field will lead to the splitting of free ion energy levels. The Orgel-Sugano-Tanabe diagrams show how the energy-level splittings are affected by the strength of the crystalline field, as shown in Fig. 12.

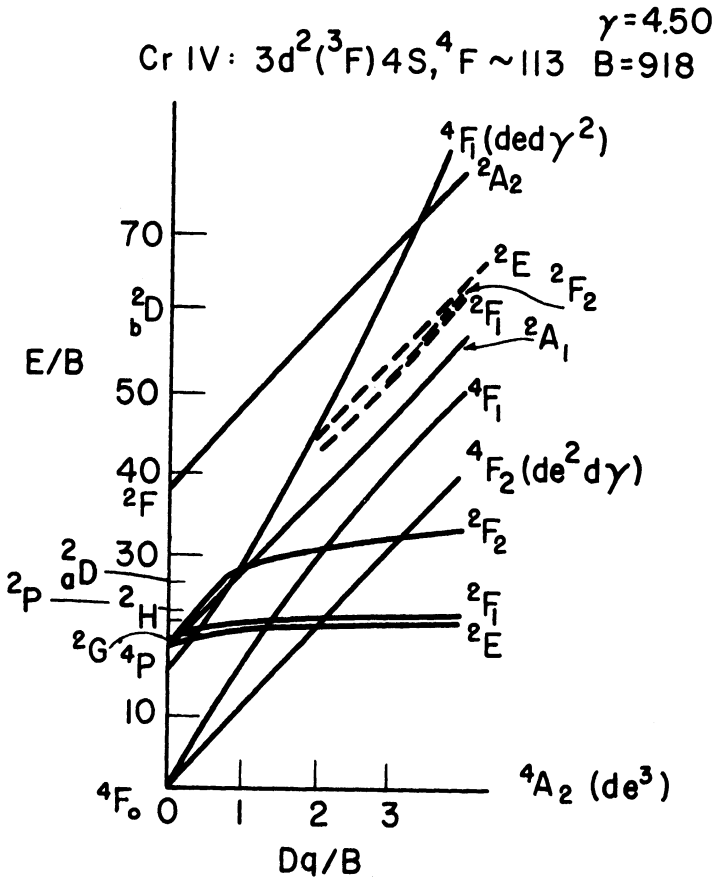

Fig. 12. Splitting of states of the $3d^3$ configuration by an octahedral field (Ref. 5, Fig. 2).

To develop the qualitative ideas, on the basis of symmetry arguments we shall first consider the case of weak crystalline field and then the case of the

strong crystalline electric field.

To carry out this program we shall make frequent reference to the group character table and to the reduction of reducibility representations. For the sake of convenience the group character table, the characters of the reducibility representation, and their irreducible components are presented in the following cubic character table:

	E	$8C_3$	$3C_2$	$6C_2'$	$6C_4$	
A_1	1	1	1	1	1	
A_2	1	1	1	-1	-1	
E	2	-1	2	0	0	
T_1	3	0	-1	-1	1	
T_2	3	0	-1	1	-1	
P	3	0	-1	-1	1	T_1
D	5	-1	1	1	-1	$E+T_2$
F	7	1	-1	-1	-1	$A_2+T_1+T_2$
G	9	0	1	1	1	$A_1+E+T_1+T_2$
H	11	-1	-1	-1	1	$E+2T_1+T_2$
$A_2 \times A_2$	1	1	1	1	1	A_1
$A_2 \times E$	2	-1	2	0	0	E
$A_2 \times T_1$	3	0	-1	1	-1	T_2
$A_2 \times T_2$	3	0	-1	-1	1	T_1
$E \times E$	4	1	4	0	0	A_1+A_2+E
$E \times T_1$	6	0	-2	0	0	T_1+T_2
$E \times T_2$	6	0	-2	0	0	T_1+T_2
$T_1 \times T_1$	9	0	1	1	1	$A_1+E+T_1+T_2$
$T_1 \times T_2$	9	0	1	-1	-1	$A_2+E+T_1+T_2$
$T_2 \times T_2$	9	0	1	1	1	$A_1+E+T_1+T_2$

The terms for the $3d^3$ electron configuration (see, for example, Ref. 12, p. 423) are ^2P, $(^2D)^2$, ^2F, ^2G, ^2H, ^4D, and ^4F. According to the Atomic Energy Tables,[6,14] these levels are arranged as follows:

^2F - - - - -36490

^2H - - - - -21078

a^2D - - - - -20218

^2G - - - - -15064

^2P - - - - -14185

^4P - - - - -14072

^4F - - - - -0

(The numerical indicates the term value for the lowest J value of the multiplet.)

When this 3-electron system is placed in an electric field having cubic symmetry, the above atomic energy levels will split, as indicated by the character table. For example, since

$$F = A_2 + T_2 + T_1$$

the ^4F ground state will split into three levels, as shown in Fig. 13. The splitting will be similar for other levels. The complete splitting scheme of the terms arising from the $3d^3$ configuration is given in Fig. 14.

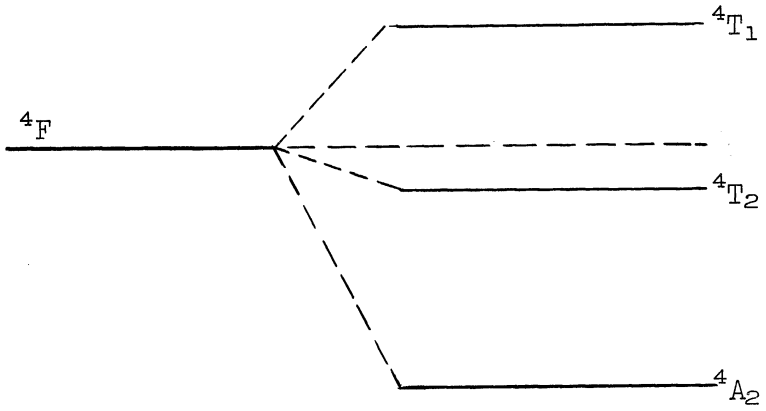

Fig. 13. Splitting of ^4F ground states.

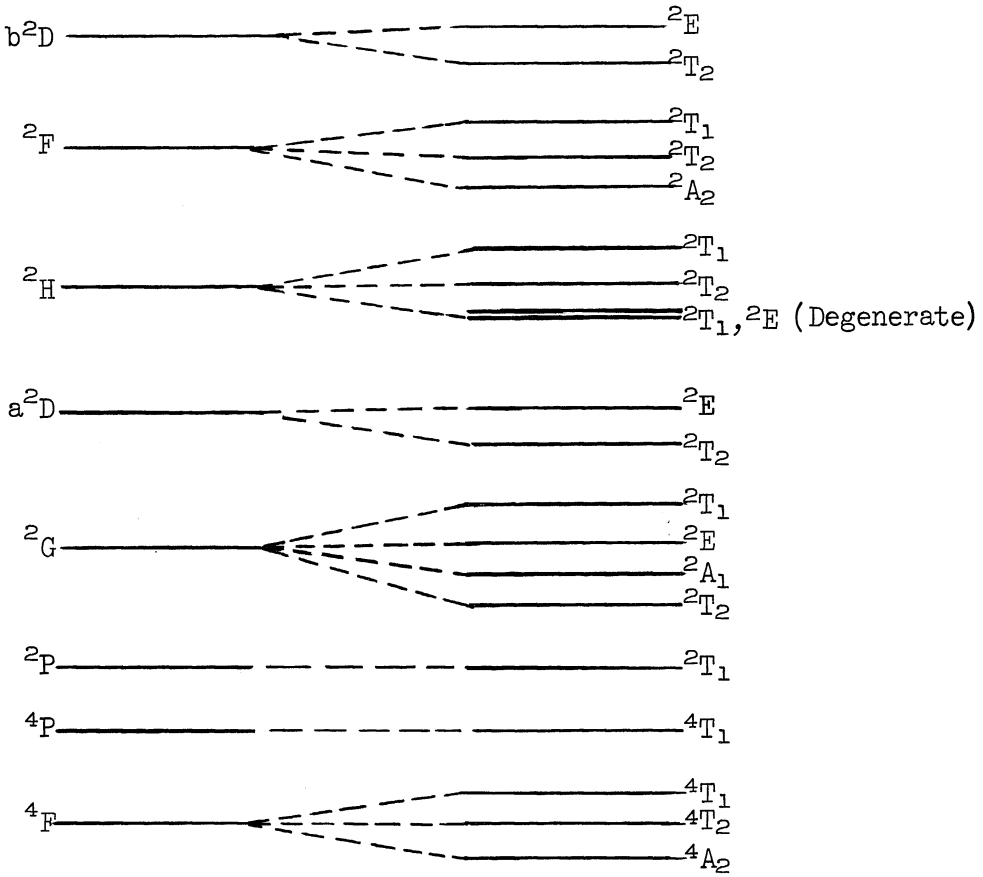

Fig. 14. Complete splitting scheme of the terms arising from the $3d^3$ configuration.

Group theory does not give the sequence of terms shown in Fig. 14. However, provided the constant b_4 is positive, detailed calculations of the sequence can be obtained from pages 13 and 17 of Ref. 15.

The scheme gives an explanation of the left-hand side of the OST diagram. It should perhaps be noted that Sugano and Tanabe[5] have indicated the splittings only of states ^4F, ^4P, ^2G, and ^2F.

Consider next the right-hand side of Fig. 14. To understand how these levels came about, let us first recall an earlier remark that the effect of the cubic crystalline field is to remove the equivalency of some of the d-electrons. In a spherically symmetric electric field and d-shell can accommodate as many as ten equivalent electrons. On the other hand, in a cubic field six electrons will be affected differently from the remaining four, so that often the terms t_2-subshell and e-subshell are introduced. The electrons in the t_2-subshell will be equivalent to one another, but not to those in the e-subshell. It is easy to see, then, that the possible electron configurations are

$$(t_2)^3,\ (t_2)^2e,\ t_2(e)^2,\ (e)^3$$

The right superscript, as in atomic spectroscopy, represents the number of electrons with the indicated orbital. For example, $t_2(e)^2$ means that there is one electron occupying the t_2 level, and two electrons occupying the e levels. We shall discuss the allowed states associated with each configuration.

Consider first the configuration t_2^3. The Hamiltonian will be invariant under the permutation of the indices 1, 2, and 3, so that the wave functions

must constitute the basis for the irreducible representations of the symmetric group S_3. This group consists of six permutations, belonging to three classes as indicated below:

Classes	(1^3)	(2,1)	(3)
Permutation	E	(12) (13) (23)	(123) (132)

There are, accordingly, three irreducible representations of degrees 1, 2, and 1, respectively. These representations will be denoted by the symbols [3], [2,1], and $[1^3]$ respectively. The group character table (see, for example, Ref. 12) is

	(1^3)	3(2,1)	2(3)
[3]	1	1	1
[2,1]	2	0	-1
$[1^3]$	1	-1	1
t_2^3	27	9	3

The characters of the reducible representation t_2^3 given in this table are obtained by noting how the three electron wave functions transform under permutations of the group S_3. As mentioned earlier, the t_2 wave functions are given by

$$\xi = (yz)$$

$$\eta = (zx)$$

$$\zeta = (xy)$$

The 3-electron wave functions are given by the product of 1-electron wave function. Since the wave function for each electron can be any one of the three functions indicated above, these are $3^3 = 27$ product functions, so that the character for the identity operation, E, is 27. Consider next the character for the permutation of class (2,1), and in particular consider the permutation (12). The character for this operation and consequently for the class (2,1) is given by the number of functions that are not changed by the permutation. This will occur if the orbital part for electrons 1 and 2 is the same. A typical function is, say,

$$\xi(1) \times \xi(2) \times \eta(3)$$

The orbital of electrons 1 and 2 can be one of the three functions, and electron 3 can also, independently, have any one of the three orbitals. Consequently, the number of product functions remaining unchanged by the permutation (12) is 9, which means that the character for this class is 9. Finally, the character for class (3) is the number of functions that are not affected by the permutation (123) or (132). Clearly, there are only three such functions, given by

$$\xi(1) \times \xi(2) \times \xi(3), \quad \eta(1) \times \eta(2) \times \eta(3), \quad \zeta(1) \times \zeta(2) \times \zeta(3)$$

and hence the character is 3. Using the theorem enunciated earlier, we find that

$$(t_2)^3 = 10\,[3] + 8\,[2,1] + [1^3]$$

or, in terms of Young's tableaux,

$(t_2)^3$ = 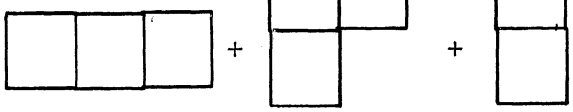 + + 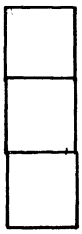

(10) (8) (1)

The dimensionality of the representation given by each shape is given by the numbers underneath. The representation [3] or 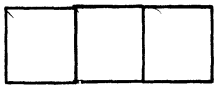 , for which the orbital part is totally symmetric, is forbidden by Pauli's principle. Or to use the language of tableau calculus, in order for the total wave function to satisfy Pauli's principle, the tableau representing the spin part must be the transpose of the orbital part. Furthermore, since the electron has only two possible spin orientations, the electron spin tableau must not have more than two rows. Thus, of the three shapes

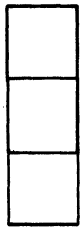 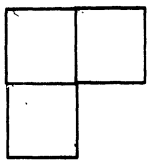 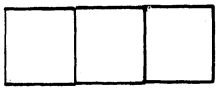

the first one is forbidden for the electron spin, which leaves

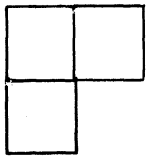 and 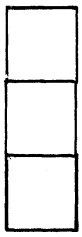

as the only allowed orbital tableaux. Now

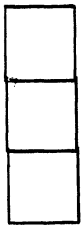

belongs to $^4A_2$ of the cubic irreducible representation.

This can be seen as follows. The tableau represents the totally antisymmetric space function and is given by

$$\psi_a = N \sum_P \delta_p P[(xy)_1(yz)_2(zx)_3] = N \begin{vmatrix} (xy)_1(xy)_2(xy)_3 \\ (yz)_1(yz)_2(yz)_3 \\ (zx)_1(zx)_2(zx)_3 \end{vmatrix}$$

where

$$\delta_p = \begin{cases} +1 \text{ for an even permutation} \\ -1 \text{ for an odd permutation} \end{cases}$$

Selecting now one operation out of each class of the cubic group and operating on the ψ_a, we get:

	Operation	Result	Character
E:	$\begin{pmatrix} x \longrightarrow y \\ y \longrightarrow y \\ z \longrightarrow z \end{pmatrix}$	$E\psi_a = \psi_a$	1
C_3:	$\begin{pmatrix} x \longrightarrow y \\ y \longrightarrow z \\ z \longrightarrow x \end{pmatrix}$	$C_3\psi_a = \psi_a$	1
C_2:	$\begin{pmatrix} x \longrightarrow -x \\ y \longrightarrow -y \\ z \longrightarrow z \end{pmatrix}$	$C_2\psi_a = \psi_a$	1
C_2':	$\begin{pmatrix} x \longrightarrow y \\ y \longrightarrow x \\ z \longrightarrow -z \end{pmatrix}$	$C_2'\psi_a = -\psi_a$	-1
C_4:	$\begin{pmatrix} x \longrightarrow y \\ y \longrightarrow -x \\ z \longrightarrow z \end{pmatrix}$	$C_4\psi_a = -\psi_a$	-1

These are the characters of the irreducible representation A_2.

The irreducible cubic representations contained in the other tableaux can be readily obtained as follows. The outer product gives

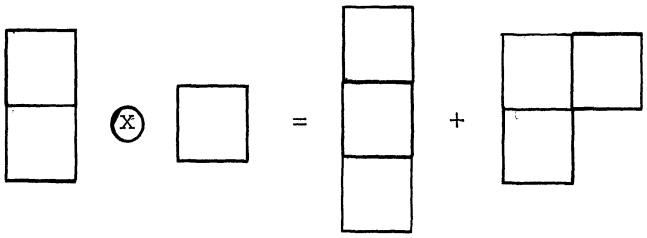

Now

belongs to T_2

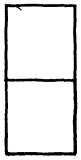

belongs to $^3T_1$

and furthermore

$$T_1 + T_2 = A_2 + E + T_1 + T_2$$

so that

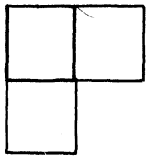

$$= {}^2E + {}^2T_1 + {}^2T_2$$

Collecting our results, we have shown that the allowed configurations of t_2^3 are

$$t_2^3 = {}^4A_2 + {}^2E + {}^2T_1 + {}^2T_2$$

This is in agreement with Bethe's result, which is obtained by a very different procedure.

The states for the configuration $(t_2)^2 e$ can be obtained easily by noting that

$$(t_2)^2 = {}^3T_1 + {}^1A_1 + {}^1E_1 + {}^1T_2$$

and by making use of the results for product representations. Thus, the addition of an e-electron to the state ${}^3T_1$ leads to

$$({}^3T_1)\ (E) = {}^2T_1 + {}^2T_2 + {}^4T_1 + {}^4T_2$$

The others are

$$({}^1A_1)\ (E) = {}^2E$$

$$({}^1E_1)\ (E) = {}^2A_1 + {}^2A_2 + {}^2E$$

$$({}^1T_2)\ (E) = {}^2T_1 + {}^2T_2$$

Carrying through a similar analysis for $t_2(e)^2$ we find that

$$t_2(e)^2 = {}^4T_1 + {}^2T_1 + {}^2T_2 + {}^2T_1 + {}^2T_2$$

And finally for e^3, the single state

$$e^3 = {}^2E$$

In summary we have found that the states arising for the weak-field case are as follows:

	$^4A_2$	$^4T_1$	$^4T_2$	$^2A_1$	$^2A_2$	^2E	$^2T_1$	$^2T_2$
^4F	1	1	1					
^4P		1						
^2P							1	
^2G				1		1	1	1
$^2(^2D)$						2		2
^2H						1	2	1
^2F					1		1	1
Total	1	2	1	1	1	4	5	5

From the strong-field analysis we obtain:

$(t_2)^3$	1					1	1	1
$(t_2)^2e$		1	1	1	1	2	2	2
$t_2(e)^2$		1					2	2
$(e)^3$						1		
Total	1	2	1	1	1	4	5	5

The two totals agree, as they should. Each of the states $^4A_2$, $^4T_2$, $^2A_1$ and $^2A_2$ occur only once. These are the states indicated by the straight lines connecting the left- and right-hand sides of the OST diagram. Since there are two $^4T_1$ states, the associated energy levels are given by the solution of a 2-x-2 determinant. Furthermore, according to well known results in quantum mechanics, the energy states of different symmetry do not interact, but those of the same symmetry tend to repel. Consequently, on the left-hand side, the two $^4T_1$ states should start out parallel to each other, but the separa-

tion should increase with increasing strength of the crystalline electric field.

The energy levels for the ^2E, $^2T_1$, and $^2T_2$ states are obtained by solving 4-x-4 (for ^2E) and 5-x-5 (for $^2T_1$ and $^2T_2$) determinants.

We shall now analyze the energy levels in greater detail. The term values for the d^3 configuration are given in Ref. 11, pp. 206 and 233 (see also Ref. 16). These values are:

^4F	$-15B$
^4P	0
^2G	$-11B + 3C$
$^2P, ^2H$	$-6B + 3C$
a^2D	$5B + 5C - \sqrt{193B^2 + 8BC + 4C^2}$
^2F	$9B + 3C$
b^2D	$5B + 5C + \sqrt{193B^2 + 8BC + 4C^2}$

Comparison of these results with the experimental spectrum given earlier shows very clearly the inadequacy of even the atomic theory. If the term values for the ^4F, ^4P, and ^2G states are used, the following numerical values are obtained:

$$B = 917.36 \text{ cm}^{-1}$$

$$C = 3678.67 \text{ cm}^{-1}$$

and

$$\gamma = \frac{C}{B} = 4.01$$

On the other hand, Sugano and Tanabe[5] have used

$$B = 918 \text{ cm}^{-1}$$

and

$$\gamma = \frac{C}{B} = 4.50$$

for their analysis.

For the octahedral coordination, the crystalline field energy of the t_2 and e orbitals are -4Dq and 6Dq respectively. These values are chosen by taking the separation of t_2 and e to be 10Dq, with the center of gravity at zero (or in matrix language, the trace of the cubic field energy matrix is taken to be zero.) Thus

$$3E(t_2) + 2E(e) = 0$$

$$E(e) - E(t_2 = 10Dq$$

therefore

$$E(e) = 6Dq, \quad E(t_2) = -4Dq$$

Then the crystalline field energies for the $(t_2)^n (e)^{3-n}$ configurations are given by

$$E(t_2^n e^{3-n}) = (-4Dq)n + (3-n)(6Dq)$$

so that we obtain:

n	Configuration	Crystalline Energy
3	$(t_2)^3$	-12Dq
2	$(t_2)^2 e$	- 2Dq
1	$t_2(e)^2$	+ 8Dq
0	$(e)^3$	18Dq

This means that for very large values of Dq (i.e., for a large crystalline field) the terms arising from the above configurations will cluster about the values indicated in the last column.

REFERENCES

1. R. Findley, "Telephone a Star is the Story of Communication Satellites." National Geographic Magazine 21, 638 (1962).

2. W. K. Victor, R. Stevens, and S. W. Golomb, "Radar Exploration of Venus." JPL Tech. Report No. 32-132.

3. R.W.G. Wyckoff, "Crystal Structures." Interscience Pub., Inc., New York.

4. P. P. Ewald and C. Hermann, Strukturbericht Vol. I (1913-1924), Akademische Verlogsgesellschaft M.B.H./Leipzig.

5. S. Sugano and Y. Tanabe, "Absorption Spectra of Cr^{3+} in Al_2O_3." J. Phys. Soc. Japan 13, 880 (1958).

6. J. S. Griffith, "Transition Metal Ions." Cambridge Univ. Press (1961).

7. S. Geschwind, P. Kisliuk, M. P. Klein, J. P. Remeika and D. L. Wood, "Sharp-Line Fluorescence, Electron Paramagnetic Resonance, and Thermoluminesence of Mn^{4+} in α-Al_2O_3." Phys. Rev. 126, 1684 (1962).

8. M. R. Lorenz and T. S. Prener, "Effect of Crystal Structure Upon the Luminesence of Manganese-Activated Lithium Titanate." J. Ch. Phys. 25, 013 (1956).

9. J. Lambe and C. Kikuchi, "Spin Resonance of V^{2+}, V^{3+}, V^{4+} in α-Al_2O_3." Phys. Rev. 118, 71 (1960).

10. Y. Tanabe and H. Kamimura, "On the Absorption Spectra of Complex Ions." J. Phys. Soc. Japan 13, 394 (1958).

11. E. V. Condon and G. H. Shortley, "The Theory of Atomic Spectra." Cambridge Univ. Press (1959).

12. M. Hamermesh, "Group Theory and its Application to Physical Problems," Addison-Wesley Pub. Co., Inc., 1962.

13. D. E. Rutherford, "Substitutional Analysis." Edinburgh Univ. Press, (1948).

14. C. E. Moore, "Atomic Energy Levels." Circular No. 467 of the National Bureau of Standards.

15. Seminar notes by Dr. H. Watanabe (Fall 1962) Nuclear Engineering, The University of Michigan.

16. G. Racah, Phys. Rev. 62, 438 (1942).

PART II

X-RAY PRODUCED V^{+2} FROM VO^{+2} IN SINGLE CRYSTALS OF ZINC AMMONIUM SULFATE—$ZnSO_4(NH_4)_2SO_4 \cdot 6H_2O$

by

Robert Borcherts

Foreword

The purpose of this report is to present the results, to date, of a set of electron spin resonance experiments on:

(a) VO^{+2} and V^{+2} in single crystals of zinc ammonium sulfate, and

(b) X-ray irradiated VO^{+2} in single crystals of zinc ammonium sulfate, magnesium ammonium sulfate, and zinc potassium sulfate.

Conclusions

Upon X-ray irradiation of the single crystals containing VO^{+2} it was found that the X-ray, or the subsequent energetic electron that it produces, breaks the VO bond, removing the oxygen from the VO^{+2} site and leaving V^{+2} behind.

Since the V^{+2} produced by irradiation and the crystalline field surrounding it is identical (as far as EPR measurements can determine) to that found in single crystals of "grown" V^{+2} in zinc ammonium sulfate, the oxygen must be at a distance so removed that the crystalline field is unaffected by its presence.

Figure 1 shows the EPR spectrum along the K_2 axis for the VO^{+2} crystal, the irradiated VO^{+2} crystal, and the V^{+2} crystal, depicting the results quite vividly.

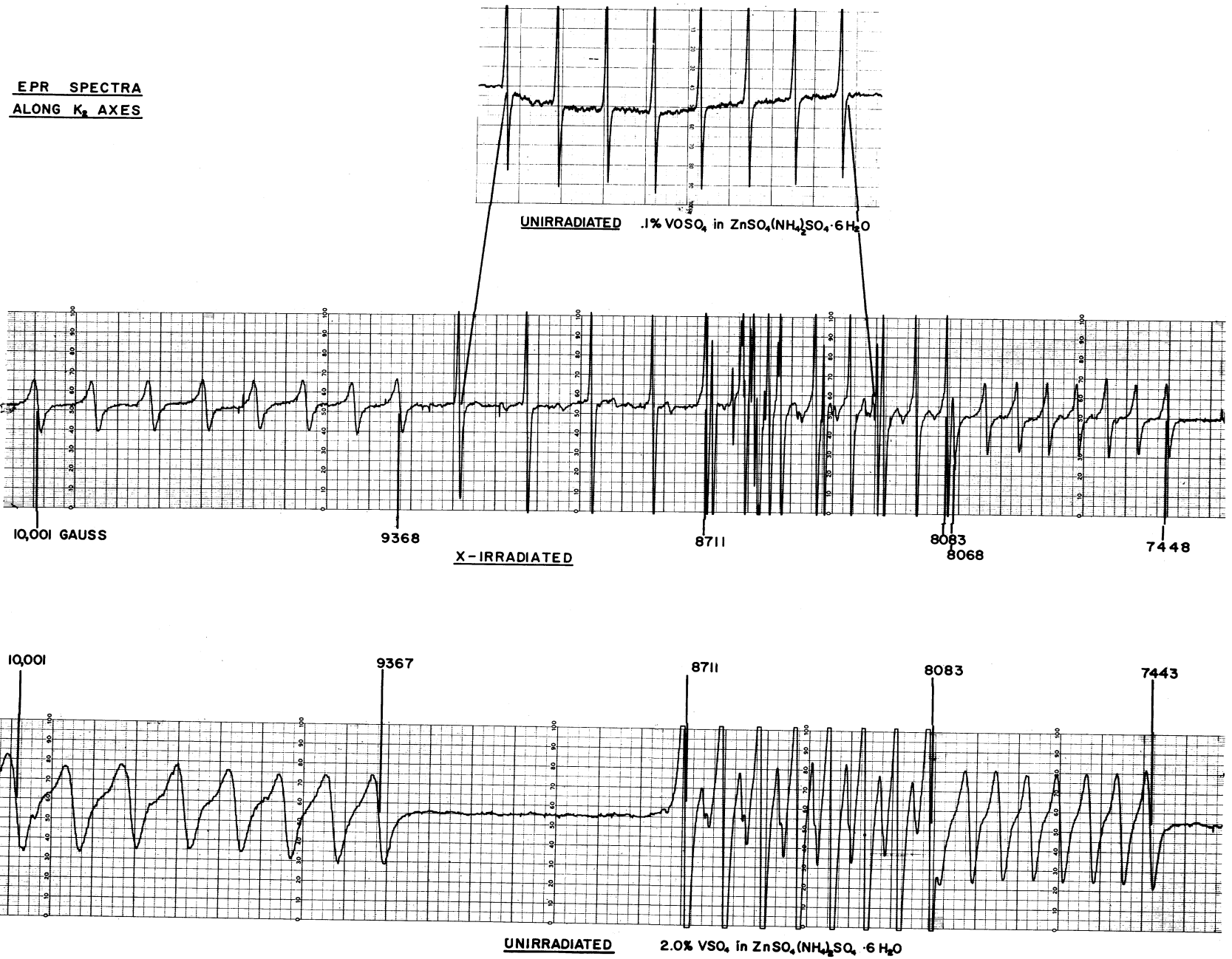

Fig. 1. EPR spectra along K_2 axes.

I. BACKGROUND

The first successful application of microwave techniques to the study of the centimeter and millimeter range of energy level separation was by Zavoisky[1] in 1945. Since then the study of electron spin resonance spectra of various ions in crystalline and non-crystalline solids has made a major contribution to knowledge in the field of solid state physics.

One ion of particular interest is that of vanadium. The +2, +3, and +4 spin states of V^{51} (abundance 99.76%, I = 7/2) have electronic spins of 3/2, 1, and 1/2 respectively. Consequently the electron spin resonance signature of each oxidation state is readily recognized—in non-cubic crystalline fields by the number and angular dependence of the fine structure groups as well as by the separation of the hyperfine structure, and in cubic crystalline fields by the separation of the hyperfine structure (see Figs. 2 and 3).

In 1950, Bleaney, Ingram, and Scovil[2] reported on the EPR spectrum of V^{+2} in $ZnSO_4(NH_4)_2SO_4 \cdot 6H_2O$, the same host crystal used in this set of experiments. In this crystal the six water molecules form a distorted octahedron surrounding the V^{+2} ion, producing a rhombic crystalline field. As a result the 2S+1 degenerate ground state splits into two spin doublets, $M_S = \pm 3/2$ and $M_S = \pm 1/2$ respectively, separated by 2D. Applying a magnetic field splits the remaining degeneracy and application of microwave energy at a frequency ν gives rise to three fine-structure groups at $g \cong 2$, corresponding to the selection rule $\Delta M = \pm 1$. Because of the 7/2 value of the nuclear spin of V^{51}, each of the fine-structure groups are composed of eight lines (2I+1) with a

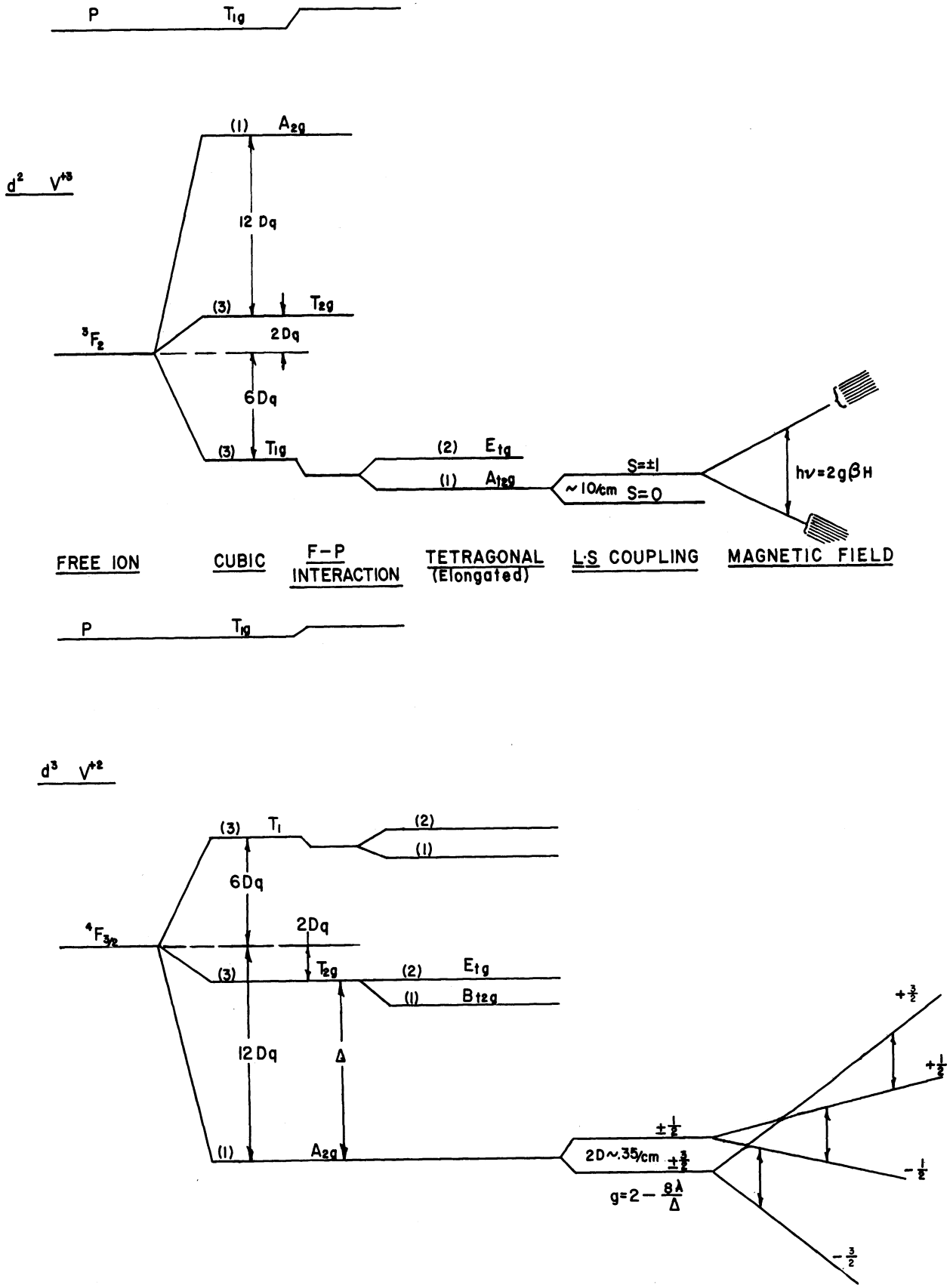

Fig. 2. V^{+3} and V^{+2} energy levels.

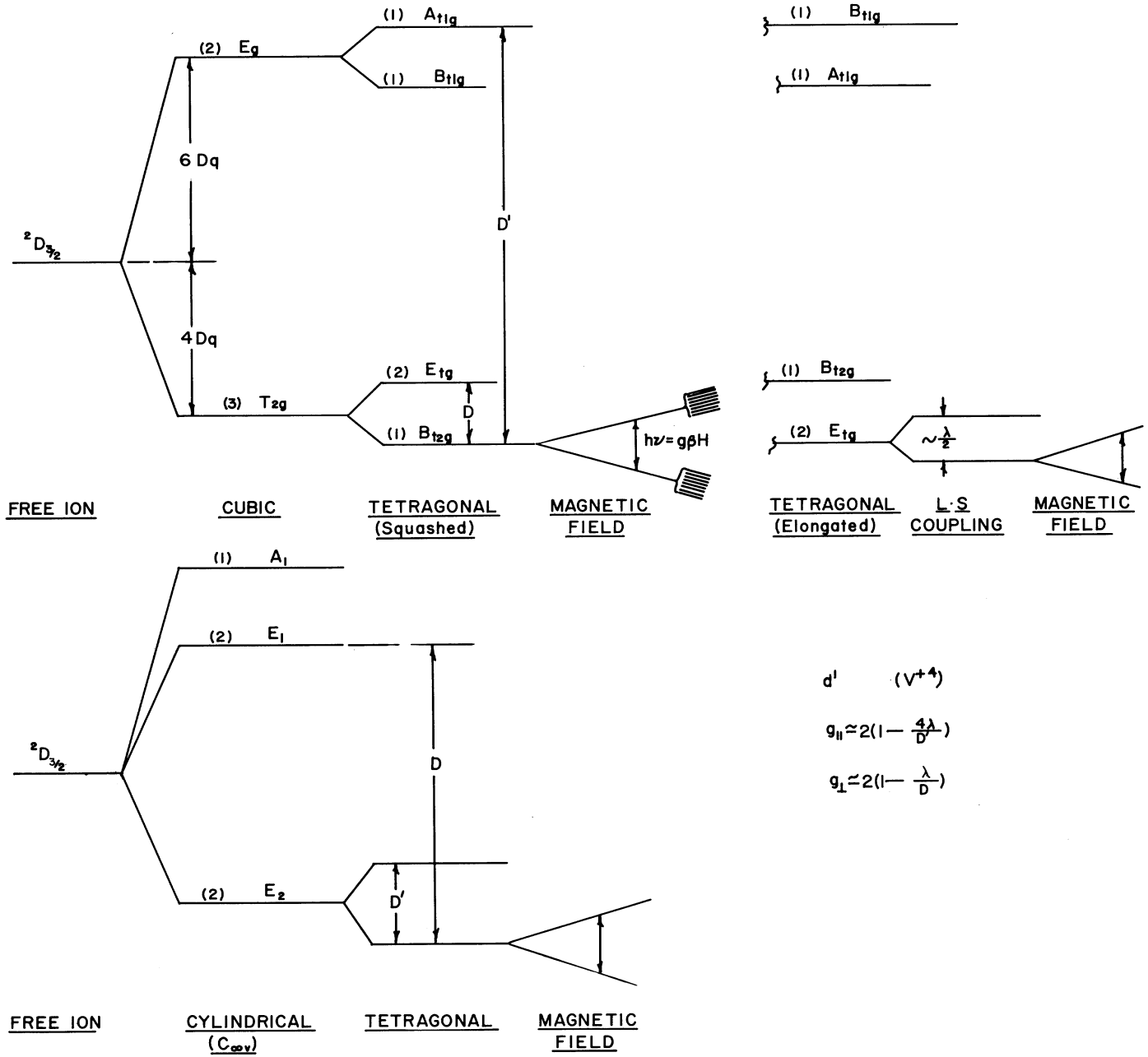

Fig. 3. V^{+4} and VO^{+2} energy levels.

separation of approximately 90 gauss.

In 1958, Zverev and Prokhorov[3] and later Lambe, Ager, and Kikuchi[4] reported on V^{+3} in sapphire (α-Al_2O_3). And in 1960, Lambe and Kikuchi[5] found a small amount of V^{+4} in Al_2O_3. They were also able to show that by X-ray irradiation or gamma irradiation some V^{+2} is produced. Also in 1960, Gerritsen and Lewis[6] and Zverev and Prokhorov[7] reported on V^{+4} in rutile (TiO_2).

In sapphire six oxygens surround each aluminum site in a distorted octahedron, giving rise to a trigonal crystalline electric field. If V^{+3} is substituted for the Al^{+3} ion, the trigonal component of the crystalline field splits the T_2 energy level into a doublet E and a singlet B. This splitting, acting through the $\underline{L}\cdot\underline{S}$ coupling, causes the ground state to split into a lower spin singlet $M_S = 0$ and an upper spin doublet $M_S = \pm 1$, separated by ~10/cm. An applied magnetic field causes the $M_S = \pm 1$ level to split and as a result a forbidden electron spin resonance transition corresponding to $\Delta M = \pm 2$ can be observed at a magnetic field of $H = h\nu/2g\beta$. Since the ground state is separated by ~10/cm the relaxation time of this transition is so short that in order to observe the spin resonance transitions the experiments must be performed at very low temperatures—approximately 4.2°K. If the temperature is too low, less than 2°K, the $M_S = \pm 1$ state becomes so depopulated that no signal is observed at all!

In rutile, six oxygen atoms surround the Ti^{+4} site in a distorted octahedron, producing an orthorhombic crystalline electric field. Since V^{+4} has only one 3d electron and thus a spin of 1/2, when it is substituted for the Ti^{+4} ion only one fine structure group corresponding to a $\Delta M = \pm 1$ transition

is observed. However, if tetragonal symmetry is present the relaxation time may be long or short depending on whether or not the tetragonal symmetry is "squashed" or "elongated" (see Fig. 3). For rutile the tetragonal field appears to be elongated since the experiment has to be performed at liquid nitrogen temperatures (77°K) in order to observe the EPR spectrum. The observed hyperfine spectra is very anisotropic, having a separation of 157 gauss along the z-axis and 35 gauss and 48 gauss along the x- and y-axes respectively. The g-values (g_x = 1.915; g_y = 1.913; g_z = 1.956) reflect the rhombic symmetry of the crystalline field.

Although the "valence state" of vanadium in the vanadyl radical VO^{+2} is also +4, the strong cylindrical crystalline field formed by the vanadium and the oxygen produces an energy level structure quite different from that of V^{+4} in a cubic field[8] (see Fig. 3).

The first electron spin resonance spectrum of the vanadyl radical (VO^{+2}) was reported by Garifianov and Kozyrev[9] in a frozen aqueous solution and later by Pake and Sands[10] in aqueous, acetone, and ether solutions; by O'Reilly[11] in vanadyl etioporphyrin dissolved in benzene and high viscosity oil; by Faber and Rogers[12] in various adsorbers (charcoal, Dowex-59, IR-4B and IR-100); and by Roberts, Koski, and Caughey[13] in some vanadyl porphyrins. As mentioned above, the VO^{+2} radical produces a very strong cylindrical of axial field so that it matters little what other kind of field surrounds the VO^{+2}. This is evidenced by the similar spectra found by these investigators.[9-13] The results of these investigations are that the $g_\perp$ and $g_{||}$ values are 1.98-1.99 and 1.88-1.93 respectively, and that there is a hyperfine splitting of 160-

200 gauss parallel to the z-axis and of 60-85 gauss perpendicular to the z- or VO^{+2}-axis. The variation in these values is suggested to be due to the extent of covalent bonding between the vanadyl ion and the surrounding ligands.[12] Because the samples used in all these investigations were either powders or solutions, the EPR spectrum, is either an average of the randomly oriented VO^{+2} radicals in the frozen or powdered samples (see Fig. 4a), or a time-averaged spectrum as a result of the motion of the VO^{+2} in solutions.

Thus, because of the need for EPR information on oriented VO^{+2} and because of the success of Lambe and Kikuchi[5] and Wertz, Auzins, Griffiths, and Orten[14] in producing the various oxidation states of vanadium, the experiments reported here were undertaken. Underlying these immediate reasons is perhaps a deeper one—that of a systematic study of the solid state chemistry of vanadium.

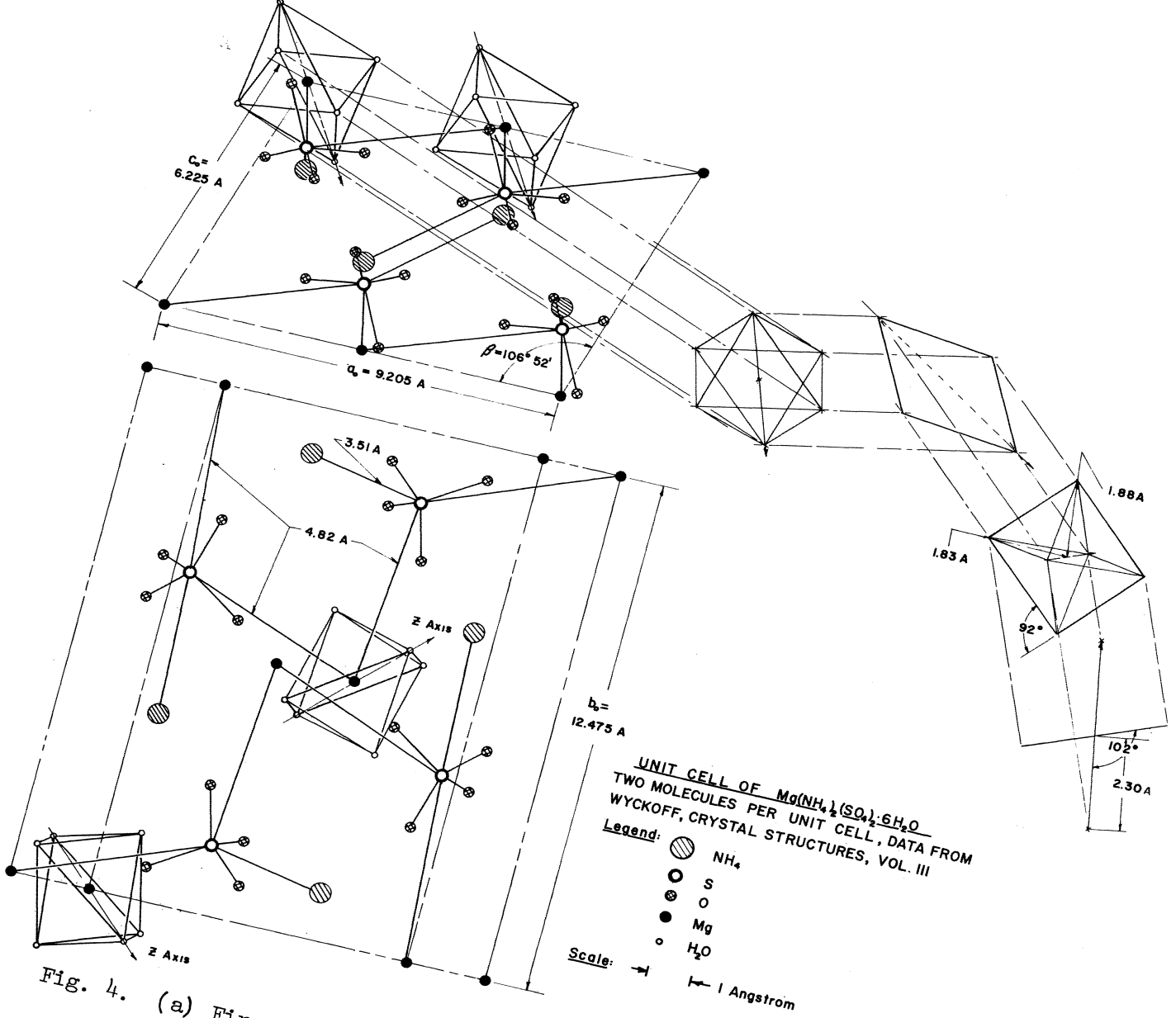

Fig. 4. (a) First derivative of crushed crystal absorption spectrum; (b) Plot of $\sin\theta \left[\frac{d\theta}{dH}\right]_M$ for 0.1% $VOSO_4$ in $Zn(NH_4)_2(SO_4)_2 \cdot 6H_2O$.

II. EXPERIMENTAL METHODS

A. CRYSTAL GROWTH

Single crystals of 0.05, 0.1, 0.5, and 1.0% (vanadium to zinc) concentrations of $ZnSO_4(NH_4)_2SO_4 \cdot 6H_2O$ were grown from a water solution into which reagent grade $ZnSO_4 \cdot 7H_2O$, $(NH_4)_2 \cdot SO_4$ and $VOSO_4 \cdot 2H_2O$ were added in the prescribed amounts. Light blue crystals up to 3-4 mm in length were usually obtainable in 1-2 days. Zinc potassium sulfate and magnesium ammonium sulfate crystals containing 1.0% VO^{+2} were also grown by this method.

In contrast to the ease of growing the vanadyl crystals, the growth of the 1.0% and 2.0% vanadous ammonium sulfate crystals required a greater degree of skill due to the rapidity at which V^{+2} becomes oxidized. Cathodic reduction of the vanadyl solution, in which the cathode and the anode are separated by a porcelain cup, followed by evaporation at 5°C in a carbon dioxide atmosphere was the method used to grow these crystals.

B. CRYSTAL STRUCTURE AND ORIENTATION

Figure 5 shows the two molecules contained in the unit cell of $MgSO_4(NH_4)_2SO_4 \cdot 6H_2O$. The position of the atoms is taken from the data in Wykcoff.[15] The octahedron of water molecules surrounding the divalent metal ions forms the crystalline electric field which determines the constants in the spin Hamiltonian. That is, the data obtained from paramagnetic ions placed in these positions directly reflects the environment and the interaction of the electrons with the environment. Measurements of EPR experiments

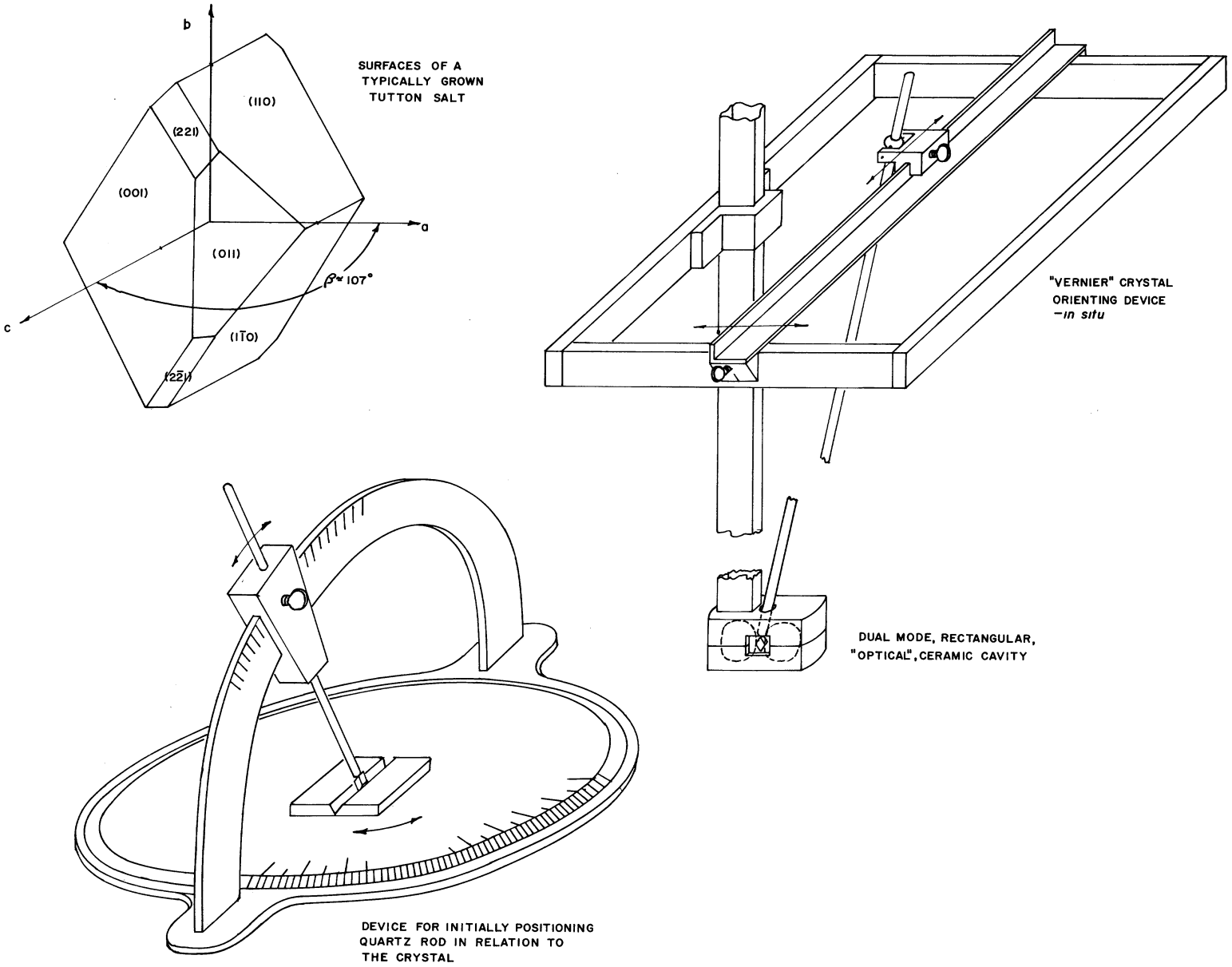

Fig. 5. Unit cell of $Mg(NH_4)_2(SO_4)_2 \cdot 6H_2O$.

can be made with great precision so that very minute changes in the environment can be observed.

As shown in Fig. 6 these double sulfates or Tutton salts grow with well recognized faces[16] so that orientation of the crystal in the cavity becomes a task accomplished with relative ease. Figure 6 also shows the device used for positioning the 22-inch quartz rod to the crystal to within a degree or two of the desired orientation. After placing the crystal in the cavity the final adjustments of the crystal orientation are made by moving the quartz rod until the desired spin resonance spectrum is observed on the recorder. The experimental data that can be recorded are: (a) the magnetic field at resonance, (b) the angle of the magnetic field to some axis, (c) the frequency of the klystron, (d) the first derivative of the line shape as presented on the recorder, and (e) the angle that the c-axis makes with the horizontal. The angle that the c-axis of the crystal makes with the horizontal is observed through the optical hole in the side of the cavity by means of a surveyors transit.

C. EPR EXPERIMENTAL SETUP

Electron spin resonance spectra and magnetic field measurements were made at room temperature with a Varian V-4500 EPR Spectrometer and a Varian Model F-8 Fluxmeter connected to a Berkeley 7580 Transfer Oscillator and a Berkeley 7370 Universal Eput and Timer. Both X- and K-band klystrons (~10 kmc and ~24 kmc respectively) were used. The K-band klystron was needed for the V^{+2} measurements since the zero field splitting is 9.8 kmc.[5] Both cavities were a silvered ceramic so that 100 kc modulation of the DC magnetic field could

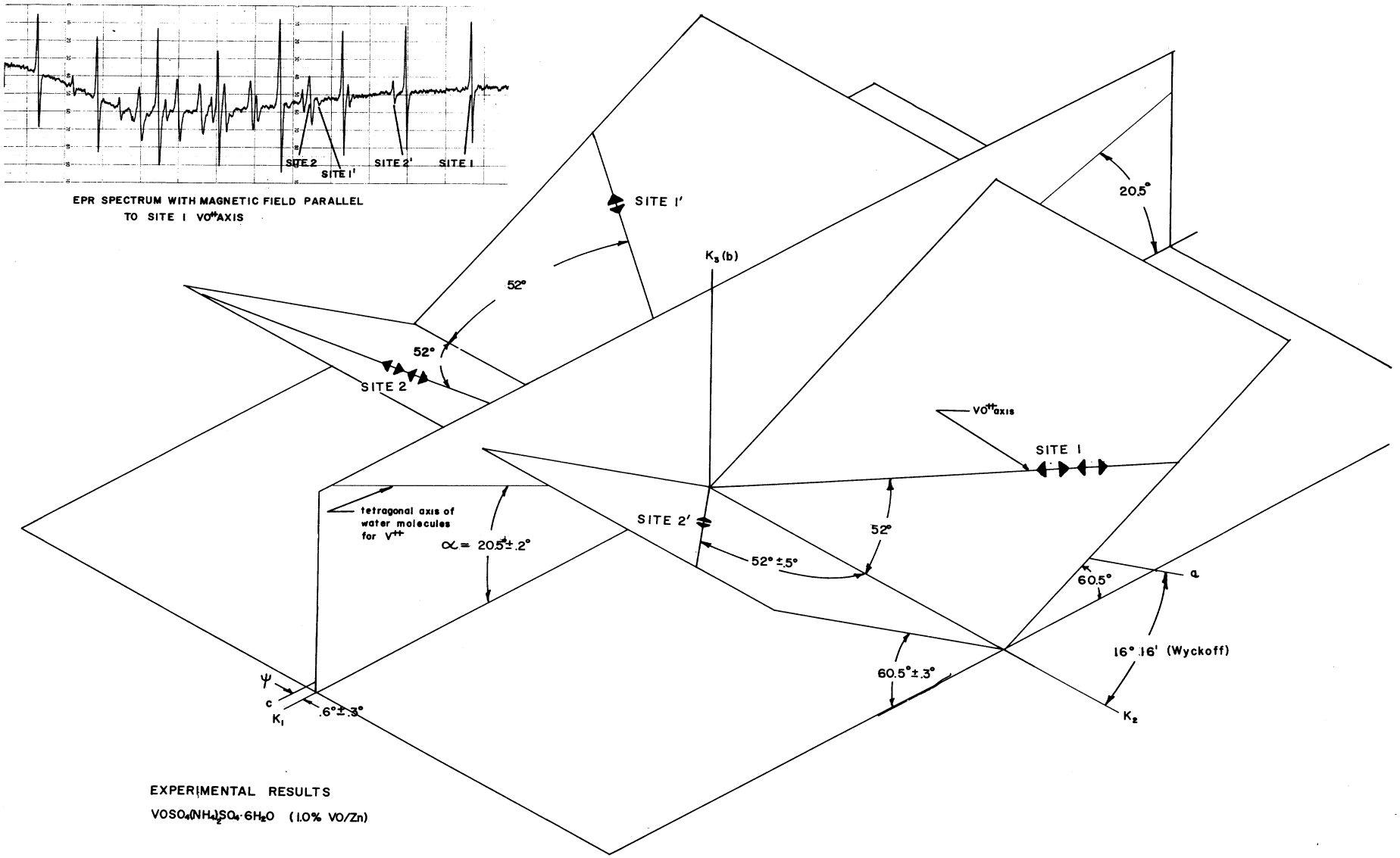

Fig. 6. Faces of Tutton crystal; orienting devices.

be employed. X-ray irradiations were made for approximately 15 minutes in the white beam of a GE X-ray machine operated at 45 kvp-40 ma with the crystal approximately 1 inch from the tungsten target. Magnetic field measurements could be made accurate to 0.2 gauss and 0.1 gauss for K- and X-band frequencies respectively. Klystron frequency measurements of 5 Mc/sec and 0.5 Mc/sec accuracy for K- and X-bands respectively gives a lower limit of ±0.0005 on the error of the g-value.

III. EXPERIMENTAL RESULTS

A. VO^{+2} CRYSTALS

From the spin resonance measurements of the VO^{+2} crystals the following axial spin Hamiltonian* constants were calculated:

	Present Work	Other Results (Powder)		
$g_{\parallel}$	= 1.9328 ± 5	1.947[13]	1.948[11]	1.88 - 1.93[12]
$g_{\perp}$	= 1.9802 ± 5	1.988	1.987	1.978 - 1.989
$\|A\|$	= 0.01824 ± 2/cm	0.0158	0.0159	0.0158 - 0.0184
$\|B\|$	= 0.007162 ± 5/cm	0.0054	0.0052	0.0061 - 0.0075
$\|Q'\|$	= 0.00024 ± 5/cm			

The VO^{+2} radical enters the crystal with the VO^{+2} axis in one of four different directions, as shown in Fig. 7. A pair of VO^{+2} axes lying in the same plane belong to the same type of sites (the crystal has two molecules per unit cell), and the lower concentration position (10%) has slightly different g-values ($g_{\parallel} = 1.9314 \pm 5$, $g_{\perp} = 1.9812 \pm 5$) and a line width of 4.7 gauss compared with 5.7 gauss for the 40% position. No variation in intensity ratio was noted for crystals of different VO/Zn concentration.

---

* $$\mathcal{H}_{axial} = g_{\parallel}\beta H_z S_z + g_{\perp}\beta[H_x S_x + H_y S_y] + A I_z S_z$$
$$+ B(I_x S_x + I_y S_y) + Q'[I_z^2 - \tfrac{1}{3} I(I+1)]$$

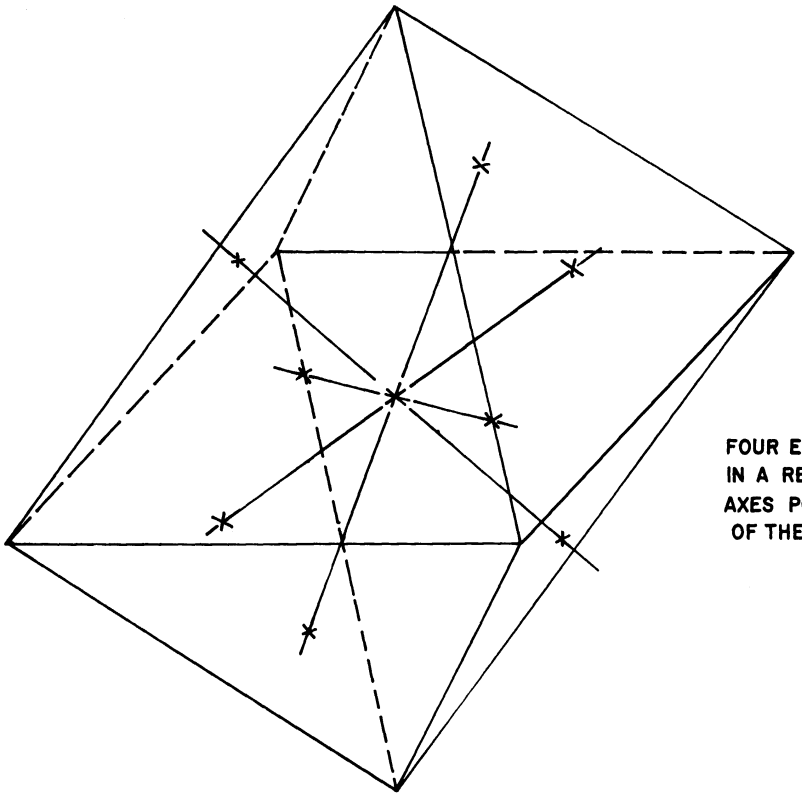

FOUR EQUIVALENT VO^{+2} POSITIONS IN A REGULAR OCTAHEDRON, THE VO^{+2} AXES POINT TOWARDS THE CENTROIDS OF THE TRIANGULAR FACES

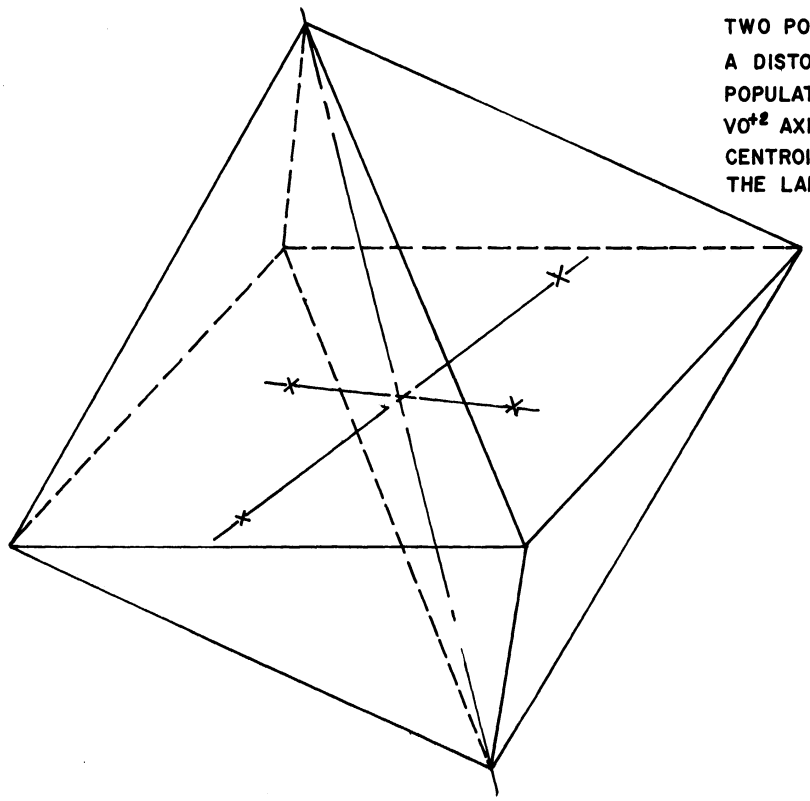

TWO POSITIONS OF VO^{+2} AXES IN A DISTORTED OCTAHEDRON. THE MOST POPULATED POSITION IS WHERE THE VO^{+2} AXIS POINTS TOWARD THE CENTROID OF THE TRIANGLE WITH THE LARGEST AREA.

Fig. 7. Experimental positions of axes in $VO(NH_4)_2(SO_4)_2 \cdot 6H_2O$ (1% VO/Zn).

The angle between the plane formed by the K_1K_3 axis (see Fig. 7) and the c-axis was found to be 0.6° ± 0.3°. A similar measurement for the V^{+2} crystals could not be made since it was found that the yz-plane of the one site made an angle of ~6° with the yz-axis of the other site.

1. Discussion

The axial spin Hamiltonian constants ($g_\perp$, $g_{||}$, $|A|$, $|B|$, and $|Q'|$) obtained from measurements at 0 and 90° fit the angular part between 0 and 90° to a remarkable degree, as shown in Table I. In Fig. 7 the z-axis for the analysis of the data is the VO^{+2} axis; in fact, it is the location of the z-axis and the result of $g_\perp > g_{||}$ (see Fig. 3) that indicates the vanadyl radical is present as an entity in the crystal and that its axis is oriented in the directions shown.

One can attempt to explain why there are four directions for the VO^{+2} radical and only two molecules per unit cell on the following basis. The VO^{+2} ion is expected to enter an octahedron of water molecules in one of four equivalent directions (see Fig. 8) in order to achieve minimum energy. However, in the Tutton crystal the water molecules do not form a regular octahedron or even one with axial symmetry, but rather one with considerable rhombic asymmetry. This is seen from the X-ray data and from the V^{+2} EPR data presented in Section III-C. This rhombic symmetry makes the four positions of the VO^{+2} ion non-equivalent and ordered in energy. That is, one of the positions (40% - see Fig. 7) is energetically more favorable, another (10% - see Fig. 7) is energetically less favorable, and the remaining two positions are so energetically unfavorable that the small population of these

TABLE I

COMPARISON OF EXPERIMENTAL AND CALCULATED VALUES OF MAGNETIC FIELD FOR $\Delta M=\pm 1$, $\Delta m=0$ TRANSITIONS IN $VOSO_4(NH_4)_2SO_4 \cdot 6H_2O$ WITH

$A = 0.01824$/cm $\quad g_{\parallel} = 1.9328$

$B = 0.007162$/cm $\quad g_{\perp} = 1.9802$

$Q' = 0.00024$/cm $\quad \nu = 9.2669$ KMc

		$m=\frac{7}{2}$	$m=\frac{5}{2}$	$m=\frac{3}{2}$	$m=\frac{1}{2}$	$m=-\frac{1}{2}$	$m=-\frac{3}{2}$	$m=-\frac{5}{2}$	$m=-\frac{7}{2}$
$\theta = 0°$	EXP	2713.9	2910.7	3109.8	3310.0	3512.4	3716.6	3922.8	4130.2
	CALC	2714.0 (−.1)	2910.8 (−.1)	3109.5 (.3)	3310.0 (.0)	3512.3 (.1)	3716.5 (.1)	3922.6 (.2)	4130.5 (−.3)
$\theta = 20°$	EXP	2736.0	2924.7	3114.0	3304.3	3495.9	3687.9	3880.9	
	CALC	2733.4 (2.6)	2922.8 (1.9)	3113.0 (1.0)	3304.1 (.2)	3496.0 (−.1)	3688.9 (−1.0)	3882.9 (−2.0)	4077.8
$\theta = 40°$	EXP	2803.8	2967.9	3130.9	3291.9	3452.1	3611.6	3769.6	3929.0
	CALC	2805.0 (−1.2)	2967.2 (.7)	3131.6 (−.7)	3292.5 (−.6)	3452.3 (−.2)	3611.4 (.2)	3770.1 (−.5)	3928.9 (.1)
$\theta = 60°$	EXP	2912.9	3037.3	3157.7		3394.0	3512.0	3629.9	3749.3
	CALC	2912.0 (.9)	3037.3 (.0)	3158.7 (1.0)	3278.2	3395.6 (−1.6)	3512.2 (−.2)	3630.1 (−.2)	3750.2 (−.9)
$\theta = 80°$	EXP	3031.8		3179.7	3257.8			3522.9	3621.9
	CALC	3032.8 (−1.0)	3104.8	3179.8 (−.1)	3258.3 (−.5)	3341.0	3420.0	3522.2 (.7)	3622.1 (−.2)
$\theta = 90°$	EXP	3059.2	3115.5	3180.0	3252.0	3330.8	3415.7	3507.0	3604.0
	CALC	3059.9 (−.7)	3116.7 (−1.2)	3180.9 (−.9)	3252.1 (−.1)	3330.5 (.3)	3415.2 (.5)	3506.3 (.7)	3603.5 (.5)

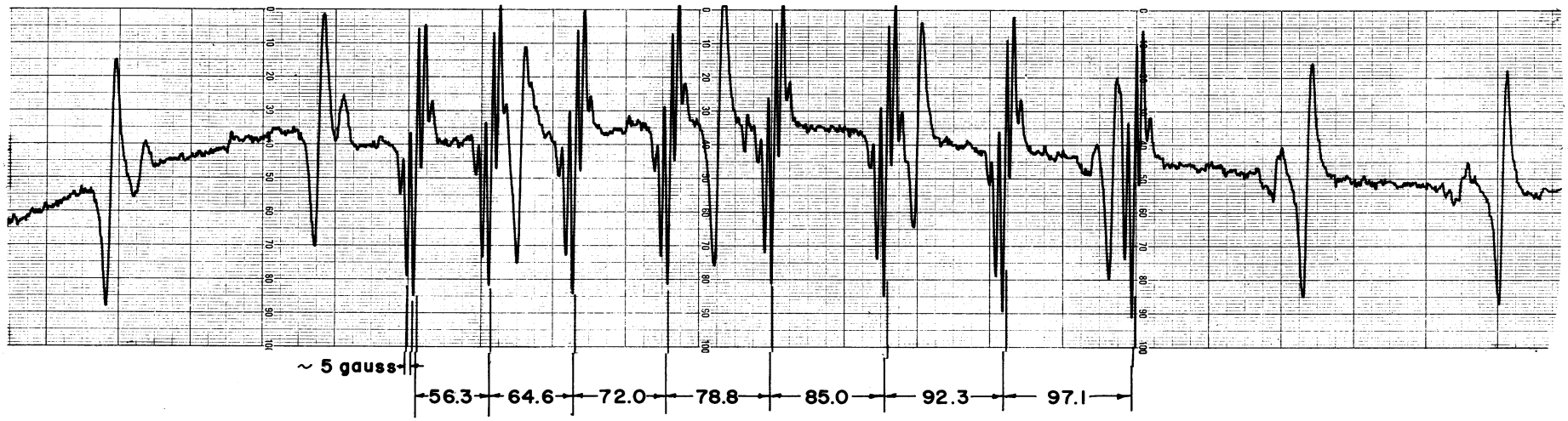

EPR SPECTRUM OF .1% $VOSO_4$ in $Zn(NH_4)_2(SO_4)_2 \cdot 6H_2O$ WITH MAGNETIC FIELD ALONG "TETRAGONAL" AXIS

Fig. 8. VO^{+2} axes in regular and distorted octahedra.

positions are unobservable by EPR techniques. The assignment of a 10% position and a 40% position to one of the two types of sites can be made by looking at the positions of the VO^{+2} ions in the water octahedra and noting the energetically favored position. This assignment is then <u>not</u> arbitrary to the extent that the X-ray data are assumed to be correct and that the VO^{+2} ion distorts the water octahedra a negligible amount.

One interesting result lies in the value of $|Q'|$. Though evaluated at 90° where its effect is of the order of one gauss, the term involving $|Q'|$ increases to 4 gauss at 60°. And since the difference between calculated and experimental values, as shown by Table I, is of the order of one gauss, this value for $|Q'|$ should be quite close to being correct. Now $|Q'|$ is related to the quadrupole moment of the nucleus, Q, by the relation

$$Q' = \frac{3eQ}{4I(I+1)} \frac{\partial^2 V}{\partial z^2}$$

where

$$\frac{\partial^2 V}{\partial z^2} = \left(\frac{\partial^2 V}{\partial z^2}\right)_{crystal} + < 1/r^3 >_{electron}$$

Evaluating this expression for V^{51}, ($eQ = 0.2 \times 10^{-24}$ cm^2)[18]

$$\left(\frac{\partial^2 V}{\partial z^2}\right)_{crystal} + < 1/r^3 >_{electron} = 3 \times 10^{22}/cm^3$$

The value of $< 1/r^3 >$, if evaluated by the expression

$$< 1/r^3 > = \frac{b}{\frac{4}{5}\gamma\beta_n\beta}$$

where

$$b = (A-B)/3$$

and

$$\gamma = \mu_n/\beta_n I$$

is $1.3 \times 10^{25}/cm^3$. Thus it appears as if $(\partial^2 V/\partial z^2)_{crystal}$ is of opposite sign to $< 1/r^3 >$ and equal in magnitude to three places!

Another interesting experimental result is the splitting of each of the resonances into five separate resonances when the magnetic field is in the direction of the tetragonal axis of the surrounding water molecules (see Fig. 9). This splitting, approximately 4 gauss, may provide some information on the molecular orbital wave function of the vanadyl ion and the surrounding water molecules.

B. VO^{+2} POWDER

The EPR spectrum obtained from the powder formed by crushing the VO^{+2} crystals gives the same qualitative spectrum (see Fig. 4a) that is reported in Refs. 9-13. One should be able to explain this spectrum quantitatively from the spin Hamiltonian constants of the single crystal. Since the resulting crystal spectrum shows only axial symmetry, the spectrum is dependent only on θ, the angle between the magnetic field and the VO^{+2} axis. Thus, for a given magnetic field, only those crystals or crystallites whose VO^{+2} axes are at an angle θ to the magnetic field such that $H = H_m(\theta)$ will contribute

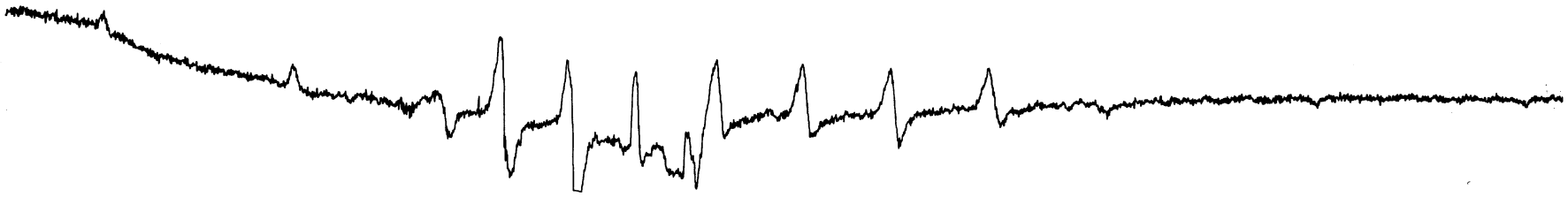

FIRST DERIVATIVE OF CRUSHED CRYSTAL ABSORPTION SPECTRUM

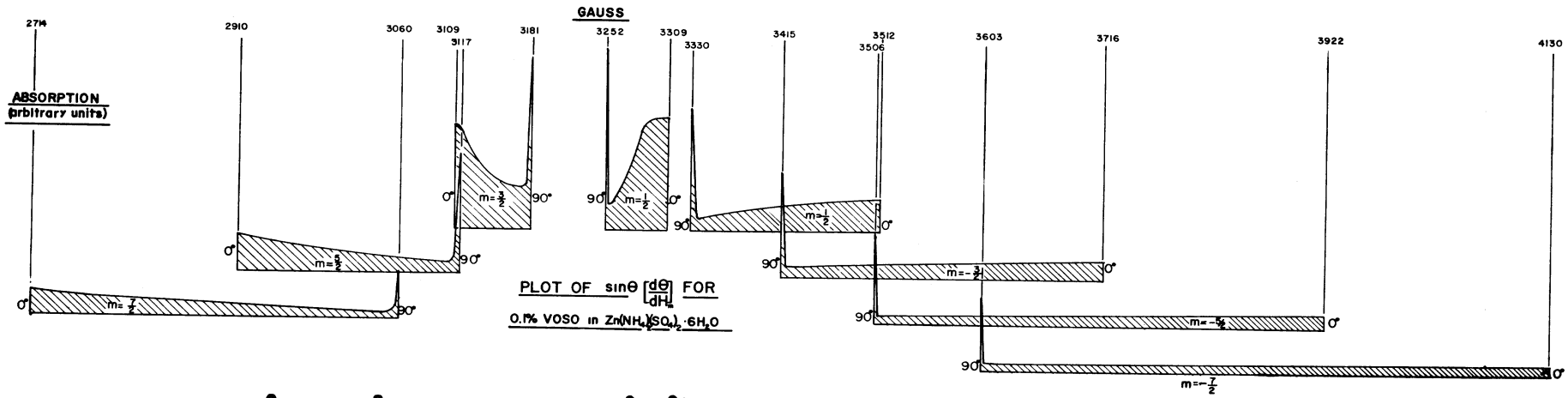

$$H_m = \frac{h\nu}{g\beta} - \frac{K}{g\beta}m - \frac{B^2}{4g^2\beta^2 H_e}\left(1+\frac{A^2}{K^2}\right)\left(I(I+1)-m^2\right) - \frac{m^2}{2g^2\beta^2 H_e}\left(\frac{A^2-B^2}{K}\right)^2\left(\frac{g_{11}g_{\perp}}{g^2}\right)^2 \sin^2\theta\cos^2\theta + 2m(Q')^2\frac{\sin^2\theta\cos^2\theta}{Kg}\left(\frac{ABg_{\perp}g_{11}}{K^2g^2}\right)^2\left(4I(I+1)-8m^2-1\right)$$
$$- m\left(2I(I+1)-2m^2-1\right)(Q')^2\frac{\sin^4\theta}{2K}\left(\frac{Bg_{\perp}}{Kg}\right)^4$$

A = 0.01824/cm g_{11} = 1.9328
B = 0.007162/cm $g_{\perp}$ = 1.9802
Q' = 0.00024/cm ν = 9.2669 KMc

Fig. 9. EPR spectrum of 0.1% $VOSO_4$ in $Zn(NH_4)_2(SO_4)_2 \cdot 6H_2O$ with magnetic field along "tetragonal" axis.

to the absorption.* Because of the axial symmetry, the number lying at this angle is proportional to the solid angle $\sin\theta\, d\theta$. Thus the number of VO^{+2} ions contributing to paramagnetic resonance between magnetic field H and H+dH is

$$\sum_{m=7/2}^{-7/2} \sin\theta \left| \frac{d\theta}{dH_m(\theta)} \right|$$

where the sum is over the eight values of I, the nuclear spin.

Figure 4b shows a plot of such an equation evaluated for the spin Hamiltonian parameters for a single crystal containing VO^{+2}. Note that in this figure the experimental curve is the first derivative of the absorption curve and that it shows the effect of the finite width of the resonances. The sharp peaking of the calculated curve corresponds to those VO^{+2} oriented at 90° and corresponds also to a $(\cos\theta)^{-1}$ dependence. From the powder spectrum,

---

*

$$H_m(\theta) = \frac{h\nu}{g\beta} - \frac{K}{g\beta} m - \frac{B^2}{4g^2\beta^2 H_o}\left[1 + \left(\frac{A}{K}\right)^2\right]\left[I(I+1) - m^2\right]$$

$$- \frac{m^2}{2g^2\beta^2 H_o}\left(\frac{A^2-B^2}{K}\right)^2\left(\frac{g_{\parallel}g_{\perp}}{g^2}\right)^2 \sin^2\theta\cos^2\theta + 2\frac{(Q')^2\sin^2\theta\cos^2\theta}{K^5 g^5\beta}$$

$$\times A^2B^2g_{\parallel}^2g_{\perp}^2 m[4I(I+1) - 8m^2 - 1] - \frac{1}{2}(Q')^2\frac{\sin^4\theta}{K^3g\beta}\left(\frac{Bg_{\perp}}{Kg}\right)^4$$

$$\times [2I(I+1) - 2m^2 - 1]m$$

where

$$K^2g^2 = g_{\parallel}^2A^2\cos^2\theta + g_{\perp}^2B^2\sin^2\theta$$

$$g^2 = g_{\parallel}^2\cos^2\theta + g_{\perp}^2\sin^2\theta$$

$$H_o = h\nu/g\beta$$

the separation of the two extreme peaks corresponds to $7|A|/g_{\parallel}\beta$, and if one neglects the quadrupole contribution, the separation of the two extreme lines in the central part of the spectrum is $7|B|/g_{\perp}\beta$ so that $|A|$, $|B|$, $g_{\parallel}$, and $g_{\perp}$ can be obtained from a powder sample—to the accuracy limited by the width of the peaks.

C. V^{+2} AND IRRADIATED VO^{+2} CRYSTALS

Operation at K-band frequencies gave the following values for the rhombic spin Hamiltonian constants (see Appendix B):

	V^{+2} (Grown)	V^{+2} (Irradiated VO^{+2})	V^{+2} (Reference 2)
g_z	1.9718 ± 5	1.9719 ± 5	1.951 ± 2
$g_x = g_y$	1.9750 ± 5	1.9745 ± 5	
$\|D\|$	0.15603 ± 5/cm	0.15609 ± 5	0.158 ± 10
$\|E\|$	0.02297 ± 5/cm	0.02303 ± 5	0.049 ± 40
$\|A\|$	0.008270 ± 5/cm	0.008270 ± 5/cm	0.0088
*ψ	2° ± 3.0°	3° ± 1.0°	2°
*α	20.5° ± 0.5°	20.5° ± 0.5°	22°

For the V^{+2} produced by X-ray irradiation in the three different Tutton salts, the following rhombic spin Hamiltonian constans were calculated:

*α and ψ locate the z-axis with respect to the ac-plane and the c-axis (see Fig. 7).

	$Zn(NH_4)_2(SO_4)_2 \cdot 6H_2O$	$Mg(NH_4)_2(SO_4)_2 \cdot 6H_2O$	$ZnK_2(SO_4)_2 \cdot 6H_2O$
g_z	1.9718 ± 5	1.9720 ± 5	1.9722 ± 5
$g_x = g_y$	1.9745 ± 5	1.9733 ± 5	1.9750 ± 5
$\|D\|$	0.15609 ± 5/cm	0.15795 ± 5 (+1.2%)	0.15246 ± 5 (-2.3%)
$\|E\|$	0.02303 ± 5/cm	0.02456 ± 5 (-6.6%)	0.02746 ± 5 (+19.2%)
$\|A\|$	0.008270 ± 5/cm	0.008270 ± 5/cm	0.008270 ± 5/cm
ψ	3° ± 1°	1° ± 1°	11° ± 2°
α	20.5° ± 0.5°	20.0° ± 0.5°	14.7° ± 0.5°

The angle that the K_1K_3 plane makes with the c-axis could not be determined since the zy-plane of the one site makes an angle of 6° with the zy-plane of the other site.

1. Discussion

As seen by the close agreement of the V^{+2} (grown) and V^{+2} (irradiated VO^{+2}) spin Hamiltonian constants, and the angle α, one can assume that when the oxygen moves away from the VO^{+2} site leaving V^{+2} behind, it is removed far enough so that its influence on the crystalline field is no longer felt. This is also implied by the data on the irradiated VO^{+2} in the Tutton salts where Mg is substituted for Zn and K for NH_4. That is, these ions, though several angstroms away from the V^{+2} site and its associated octahedron of water molecules, distort the octahedron by an amount that can be measured by the changes in the values of $|D|$, $|E|$, α, and ψ.*

*In experiments on Cu^{+2} in various Tutton salts, Bleaney, Penrose and Plumpton[19] noticed that the changes in the monovalent ion influence the angles α and ψ to a great extent. They also noticed large changes in the g-values (~1.0%) which were not observed in the present set of experiments.

If one performs a general coordinate rotation on the spin Hamiltonian for rhombic symmetry (in order to diagonalize the Zeeman term—Appendix A), it is seen that only when the magnetic field is along the x-, y-, or z-axes do the cross terms become zero, simplifying the spectrum and enabling one to make measurements that can be used to determine the spin Hamiltonian constants. For this reason no attempt was made to measure the angular part of the spectrum. An illustration of the effect of this mixing can be seen in Fig. 10. Note that in both the x- and y-directions the mixing and the resulting spread of the spectrum from the second site is so complete that it is almost unobservable.

The $|D|$ value can be calculated from the data along the z-axis and the $|E|$ value from that along the x- or y-axis. However, the plane of the zy-axis from the one site does not coincide with that from the second site. For this reason the center part of the spectrum in Fig. 1 showing the magnetic field along the K_2-axis is not a "pure" spectrum. The K_2-axis is approximately 5° from the x-axis of each of the two sites.

Note that the value of $|E|$ reported by Bleaney, Ingram and Scovil[2] is almost twice the value found in these experiments. Since they used the information along the z-direction to evaluate both $|D|$ and $|E|$, and $|E|$ enters as a second-order effect along this direction, it is thought that their value is not as correct as the value reported here.

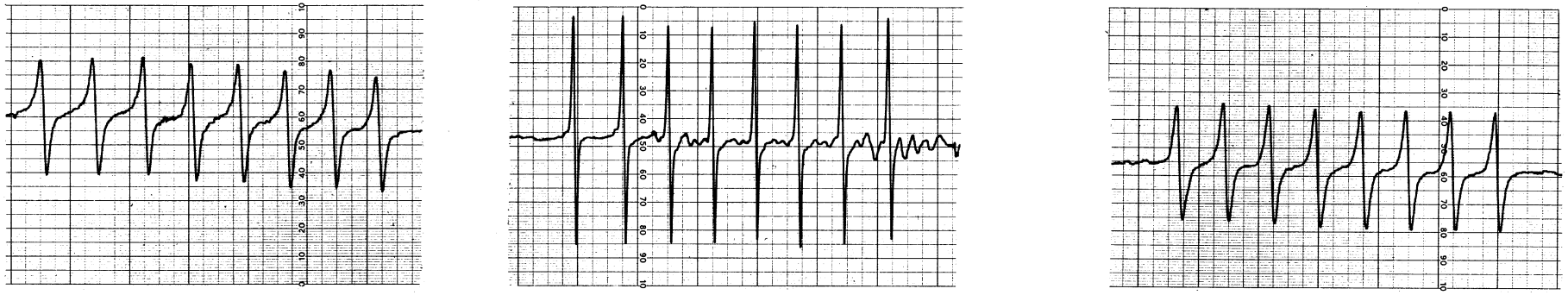

Fig. 10. Magnetic field parallel to Z axis, 1% V^{+2} in $Zn(NH_4)_2(SO_4)_2 \cdot 6H_2O$.

IV. FURTHER STUDY

The additional structure of the EPR absorption lines shown in Fig. 9 might yield some information about its origin if attacked with double resonance (ENDOR) techniques.

Furthermore, with ENDOR techniques the size of the quadrupole interaction, which may be present to some extent as suggested by EPR experiments, can be more accurately determined.

Since second-order effects indicate that A and D have the same sign, a low temperature experiment to indicate the relative intensity of the high and low field transitions should determine the absolute sign of D and thus A.

The growing of both V^{++} and VO^{++} in the same crystal, though the initial attempt has been unsuccessful, would serve as a very precise indicator that the environment of the V^{++} (grown) and the V^{++} (produced by X-ray irradiation) are identical.

Similar experiments should be carried out to determine the optical absorption spectrum for determination of the spin orbit coupling constant λ and to measure the production of V^{++} (irradiated) as a function of the radiation dose to the crystal.

APPENDIX A

CALCULATION OF ANGULAR VARIATION OF EPR RESONANCE IN RHOMBIC FIELD

In this appendix we wish to obtain formulae so that evaluation of the constants in the rhombic spin Hamiltonian can be made from experimental data.

We start with the general rhombic spin Hamiltonian

$$\begin{aligned}\mathcal{H}_{\text{rhombic}} &= \beta[g_z H_z S_z + g_x H_x S_x + g_y H_y S_y] + D[S_z^2 - \tfrac{1}{3} S(S+1)] \\ &+ E(S_x^2 - S_y^2) + AI_z S_z + BS_x I_x + CS_y I_y + Q'[I_z^2 - \tfrac{1}{3} I(I+1)] \\ &+ Q''[I_x^2 - I_y^2]\end{aligned}$$

and proceed to diagonalize the Hamiltonian in the Zeeman term and subsequently treat the off-diagonal elements as perturbations.

1. FINE STRUCTURE TERM

Since we would like to have $g_x H_x S_x + g_y H_y S_y + g_z H_z S_z = g S'_z H$ we proceed to make a coordinate transformation with the new set of coordinates x' y' z' related to x y z by the Eulerian angles θ, ϕ, and ψ,

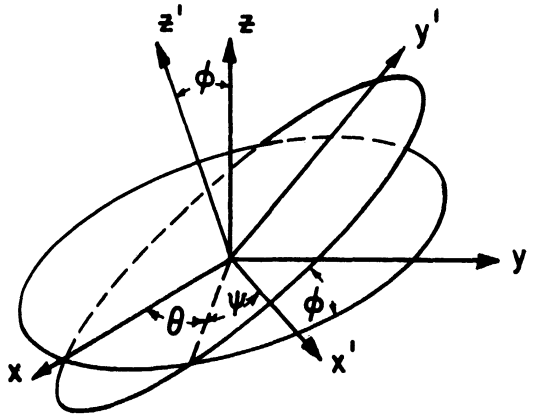

then S_x', S_y', and S_z' are related by the following:

$$S_x = (\cos\Theta\cos\psi - \sin\Theta\sin\psi\cos\phi)S_x' - (\cos\Theta\sin\psi + \sin\Theta\cos\psi\cos\phi)S_y' + \sin\Theta\sin\phi\, S_z'$$

$$S_y = (\sin\Theta\cos\psi + \cos\Theta\sin\psi\cos\phi)S_x' - (\sin\Theta\sin\psi + \cos\Theta\cos\psi\cos\phi)S_y' - \cos\Theta\sin\phi\, S_z'$$

$$S_z = \sin\phi\sin\psi\, S_x' + \sin\phi\cos\psi\, S_y' + \cos\phi\, S_z'$$

Now if

$$H_x = H\sin\Theta\cos\delta$$

$$H_y = H\sin\Theta\sin\delta$$

$$H_z = H\cos\Theta$$

and if we require

$$\cos\Theta = -(g_y/g_\perp)\sin\delta$$

$$\sin\Theta = (g_x/g_\perp)\cos\delta$$

$$\sin\phi = (g_\perp/g)\sin\Theta$$

$$\cos\phi = (g_z/g)\cos\Theta$$

where

$$g_\perp^2 = g_x^2\cos^2\delta + g_y^2\sin^2\delta$$

$$g^2 = g_{||}^2\cos^2\Theta + g_\perp^2\sin^2\Theta$$

then

$$g_zH_zS_z + g_xH_xS_x + g_yH_yS_y = gHS_z'$$

Thus the Zeeman term is diagonalized.

The axial and rhombic field terms become, respectively,

$$D[S_z^2 - \tfrac{1}{3}S(S+1)] = D\left\{\left(\frac{g_z}{g}\right)^2 \cos^2\Theta (S_z')^2 + \left(\frac{g_\perp}{2g}\right)^2 \sin^2\Theta (S_+'S_- + S_-'S_+') - \left(\frac{g_\perp}{2g}\right)^2 \sin^2\Theta [(S_+')^2 e^{2i\psi} + (S_-')^2 e^{-2i\psi}] - \frac{1}{3}S(S+1) + \frac{g_\perp g_\parallel}{2g^2} \sin\Theta \cos\Theta\, i e^{-i\psi}(S_z'S_-' + S_-'S_z')\right\}$$

$$E(S_y^2 - S_y^2) = E\left\{\frac{\sin^2\Theta}{g^2}(g_x^2\cos^2\delta - g_y^2\sin^2\delta)[(S_z')^2 - \tfrac{1}{4}(S_+'S_-' + S_-'S_+')]\right.$$

$$+ e^{i\psi}\left[-\frac{g_x g_y}{g_\perp g} \sin\Theta \sin\delta \cos\delta + \frac{i}{2}\frac{g_\parallel}{g^3} \sin\Theta \cos\Theta (g_x^2\cos^2\delta - g_y^2\sin^2\delta)\right](S_+'S_z' + S_z'S_+')$$

$$+ e^{i\psi}\left[-\frac{g_x g_y}{g_\perp g} \sin\Theta \sin\delta \cos\delta - \frac{i}{2}\frac{g_\parallel}{g^3} \sin\Theta \cos\Theta (g_x^2\cos^2\delta - g_y^2\sin^2\delta)\right](S_-'S_z' + S_z'S_-')$$

$$+ e^{2i\psi}\left[-\frac{1}{4}\left(1 - \frac{g_\parallel^2}{g^2}\cos^2\Theta\right)\left(\frac{g_x^2}{g_\perp^2}\cos^2\delta - \frac{g_y^2}{g_\perp^2}\sin^2\delta\right) - i\frac{g_x g_y g_\parallel}{g_\perp^2 g} \sin\delta \cos\delta \cos\Theta\right](S_+')^2$$

$$+ e^{-2i\psi}\left[-\frac{1}{4}\left(1 - \frac{g_\parallel^2}{g^2}\cos^2\Theta\right)\left(\frac{g_x^2}{g_\perp^2}\cos^2\delta - \frac{g_y^2}{g_\perp^2}\sin^2\delta\right) + i\frac{g_x g_y g_\parallel}{g_\perp^2 g} \sin\delta \cos\delta \cos\Theta\right](S_-')^2\Big\}$$

The diagonal terms of the fine structure part involving S_z, S_z^2, and $S_+'S_-'+S_-'S_+'$ evaluated for the states $|S\ M_s>$ with the selection rule $M \rightarrow M-1$ yields

$$\Delta E_o \equiv g\beta H_o M + (M - \tfrac{1}{2})\left(3\frac{g_{\parallel}^2}{g^2}\cos^2\Theta - 1\right)\left[D - 3E\left(\frac{g_x^2}{g_{\perp}^2}\cos^2\delta - \frac{g_y^2}{g_{\perp}^2}\sin^2\delta\right)\right]$$

The non-diagonal terms, i.e., the terms involving $(S_+')^2$, $(S_-')^2$, $(S_-'S_z'+S_z'S_-')$ and $(S_+'S_z'+S_z'S_+')$, can be evaluated by second-order perturbation theory (there are no first-order terms), give the following correction to the rhombic fine structure term:

$$\frac{4S(S+1)-24M(M-1)-9}{2g\beta H_o}\left\{\left[D - \frac{E}{g_{\perp}^2}(g_x^2\cos^2\delta - g_y^2\sin^2\delta)\right]^2 \frac{g_{\perp}^2 g_{\parallel}^2}{g^4}\sin^2\Theta\cos^2\Theta + E^2\sin^2\Theta\frac{g_x^2 g_y^2}{g_{\perp}^2 g^2}\sin^2 2\delta\right\} + \frac{2S(S+1)-6M(M-1)-3}{8g\beta H_o}\left\{\left[D\frac{g_{\perp}^2}{g^2}\sin^2\Theta + \frac{E}{g_{\perp}^2}(g_x^2\cos^2\delta - g_y^2\sin^2\delta)\left(1 + \frac{g_{\parallel}^2}{g^2}\cos^2\Theta\right)\right]^2 + \left[2E\frac{g_x g_y g_{\parallel}}{g_{\perp}^2 g}\cos\Theta\sin 2\delta\right]^2\right\}$$

2. HYPERFINE TERM

In attempting to carry out a similar procedure on the rhombic hyperfine terms the results become extremely complicated. Since the experimental results indicate little, if any, rhombic symmetry in the hyperfine terms for VO^{++} and none for V^{++}, we will assume that B = C and Q" = 0; i.e., we have

$$AI_zS_z + B(I_xS_x + I_yS_y) + Q''[I_z^2 - \tfrac{1}{3}I(I+1)] + \gamma\beta_n\underline{H}\cdot\underline{I}$$

Here we perform a rotation on the nuclear spin as we did previously on the electron spin, with the difference that where the rotation matrix for the angle ϕ was

$$\begin{pmatrix} 1 & 0 & 0 \\ 0 & \cos\phi & -\sin\phi \\ 0 & \sin\phi & \cos\phi \end{pmatrix}$$

it now becomes (for I_x, I_y and I_z):

$$\begin{pmatrix} 1 & 0 & 0 \\ 0 & \frac{A}{K}\cos\phi & -\frac{B}{K}\sin\phi \\ 0 & \frac{B}{K}\sin\phi & \frac{A}{K}\cos\phi \end{pmatrix}$$

where K is defined by setting the dterminant of this matrix equal to unity, i.e., $K^2 = A^2\cos^2\phi + B^2\sin^2\phi$. Since we have chosen axial symmetry in the hyperfine term we may arbitrarily choose $\psi = 0$. The hyperfine term then becomes

$$AI_zS_z + B(I_xS_x + I_yS_y) = KI'_zS'_z + BS'_xI'_x + \frac{AB}{K}S'_yI'_y + I'_zS'_y\left(\frac{A^2-B^2}{K}\right)\frac{g_\perp g_{\parallel}}{g^2}\sin\Theta\cos\Theta$$

The first term is the only one which is diagonal in M, m, and with the section rules $M \to M-1$, $\Delta m = 0$ its contribution to the separation of energy levels is Km. Evaluating the other terms by second-order perturbation theory (neglecting the terms of order Km with respect to $g\beta H$), we obtain

$$\frac{B^2}{4}\left(\frac{A^2+K^2}{K^2}\right)\frac{[I(I+1)-m^2]}{g\beta H} + B^2\left(\frac{A}{K}\right)\left(M - \frac{1}{2}\right)\frac{m}{g\beta H}$$

3. QUADRUPOLE TERM

Since the quadrupole term $Q'[I_z^2 - \frac{1}{3}I(I+1)]$ transforms similarly to the fine structure part, one can quickly obtain the quadrupole contribution to the

difference in energy levels as

$$(Q')^2 \left(\frac{AB}{K^2}\right)^2 \frac{g_\perp^2 g_\parallel^2}{g^2} \frac{\sin^2\Theta\cos^2\Theta}{2KM(M-1)} [4I(I+1) - 8m^2 - 1]$$

$$- (Q')^2 \left(\frac{B^2}{K^2} \frac{g_\perp^2}{g^2}\right)^2 \frac{\sin^4\Theta}{8KM(M-1)} [2I(I+1) - 2m^2 - 1]$$

These are also obtained by second-order perturbation theory and then by applying the selection rules $M \to M-1$, $\Delta m = 0$. Although there is a diagonal contribution of the quadrupole part to the energy level of the form

$$Q' \left\{ \frac{A^2}{K^2} \cos^2\phi\, m^2 + \frac{B^2}{2K^2} \sin^2\phi\, [I(I+1) - m^2] - \frac{1}{3} I(I+1) \right\}$$

it is the same for each value of M, so that the selection rule $\Delta m = 0$ results in cancellation of this term.

APPENDIX B

EXACT ENERGY LEVEL CALCULATIONS FOR V^{+2} ALONG x-, y-, AND z-AXES FOR RHOMBIC FIELD

Given the rhombic spin Hamiltonian with axial hyperfine term

$$\mathcal{H}_{\text{rhombic}} = \beta \underline{H} \cdot \underline{\underline{g}} \cdot \underline{S} + D[S_z^2 - \tfrac{1}{3} S(S+1)] + E(S_x^2 - S_y^2) + \underline{I} \cdot \underline{\underline{A}} \cdot \underline{S} ,$$

we obtain for the fine structure term for V^{+2} ($S = 3/2$) and for $\mathcal{H}$ parallel to z-axis

$$\mathcal{H}_z = g_z \beta H S_z + D[S_z^2 - \tfrac{1}{3} S(S+1)] + \frac{E}{2} [S_+^2 + S_-^2] .$$

Degenerate perturbation calculations lead to the following secular determinant:

M =	-3/2	-1/2	1/2	3/2
$-\frac{3}{2}$	$-\frac{3}{2} g_z \beta H + D - \lambda$		$\sqrt{3}\, E$	
$-\frac{1}{2}$		$-\frac{1}{2} g_{\parallel} \beta H - D - \lambda$		$\sqrt{3}\, E$
$\frac{1}{2}$	$\sqrt{3}\, E$		$\frac{1}{2} g_z \beta H - D - \lambda$	
$\frac{3}{2}$		$\sqrt{3}\, E$		$\frac{3}{2} g_z \beta H + D - \lambda$

This determinant may be solved for the following energy levels:

$$S_z = \frac{3}{2}; \quad \lambda_2^+ = \frac{1}{2} g_z\beta H + \sqrt{3E^2+(g_z\beta H+D)^2}$$

$$S_z = \frac{1}{2}; \quad \lambda_1^+ = -\frac{1}{2} g_z\beta H + \sqrt{3E^2+(g_z\beta H-D)^2}$$

$$S_z = -\frac{1}{2}; \quad \lambda_2^- = \frac{1}{2} g_z\beta H - \sqrt{3E^2+(g_z\beta H+D)^2}$$

$$S_z = -\frac{3}{2}; \quad \lambda_1^- = -\frac{1}{2} g_z\beta H - \sqrt{3E^2+(g_{11}\beta H-D)^2}$$

For the transitions M → M-1 the change in energy is:

$$E_{3/2,1/2} \equiv \lambda_2^+ - \lambda_1^+ = g_z\beta H_{3/2} + \sqrt{3E^2+(g_z\beta H_{3/2}+D)^2} - \sqrt{3E^2+(g_z\beta H_{3/2}-D)^2}$$

$$E_{1/2,-1/2} \equiv \lambda_1^+ - \lambda_2^- = -g_z\beta H_{1/2} + \sqrt{3E^2+(g_z\beta H_{1/2}-D)^2} + \sqrt{3E^2+(g_z\beta H_{1/2}+D)^2}$$

$$E_{-1/2,-3/2} \equiv \lambda_2^- - \lambda_1^- = g_z\beta H_{-1/2} - \sqrt{3E^2+(g_z\beta H_{-1/2}+D)^2} + \sqrt{3E^2+(g_z\beta H_{-1/2}-D)^2}$$

Making use of a Taylor's expansion for each of the square roots and solving for the magnetic field (in the major term) yields the following equation (to fourth order):

$$\text{(A)} \quad H_{3/2} = \frac{h\nu}{g_z\beta} - 2\left(\frac{D}{g_z\beta}\right) + \frac{3E^2D}{(g_z\beta)^3 H_{3/2}^2}\left[\frac{1}{1-\left(\frac{D}{g_z\beta H_{3/2}}\right)^2}\right]$$

$$- \frac{27}{4}\frac{E^4D}{(g_z\beta)^5}\frac{1}{(H_{3/2})^4}$$

$$\text{(B)} \quad H_{1/2} = \frac{h\nu}{g_z\beta} - \frac{3E^2}{(g_z\beta)^2 H_{1/2}}\left[\frac{1}{1-\left(\frac{D}{g_z\beta H_{1/2}}\right)^2}\right]$$

$$+ \frac{9}{4}\frac{E^4D}{(g_z\beta)^5 H_{1/2}^4}\left[1 + \frac{3D}{g_z\beta H} + \frac{3}{2}\left(\frac{E}{g_z\beta H_{1/2}}\right)^2\right]$$

$$(C)\quad H_{-1/2} = \frac{h\nu}{g_z\beta} + 2\left(\frac{D}{g_z\beta}\right) - \frac{3E^2D}{(g_z\beta)^3 H^2_{-1/2}}\left[\frac{1}{1-\left(\frac{D}{g_z\beta H_{-1/2}}\right)^2}\right]$$

$$+ \frac{27}{4}\frac{E^4D}{(g_z\beta)^5}\left(\frac{1}{H_{-1/2}}\right)^4$$

For the magnetic field parallel to the x-direction, the Zeeman term is not diagonal. To diagonalize, a coordinate rotation about the y-axis by 90° is performed, resulting in the fine structure spin Hamiltonian

$$\mathcal{H}'_x = g_x\beta H S'_z + D\left\{\frac{1}{4}\left[(S'_+)^2 + (S'_-)^2 + S'_+S'_- + S'_-S'_+\right] - \frac{5}{4}\right\}$$

$$+ E\left\{(S'_z)^2 + \frac{1}{4}\left[(S'_+)^2 + (S'_-)^2 - S'_-S'_+ - S'_+S'_-\right]\right\}$$

which leads to the following secular determinant:

M =	-3/2	-1/2	1/2	3/2
$-\frac{3}{2}$	$-\frac{3}{2}g_x\beta H$ $-(\frac{D-3E}{E})-\lambda$		$\sqrt{3}\,\frac{D+E}{2}$	
$-\frac{1}{2}$		$-\frac{1}{2}g_x\beta H$ $+(\frac{D-3E}{2})-\lambda$		$\sqrt{3}\,\frac{D+E}{2}$
$\frac{1}{2}$	$\sqrt{3}\,\frac{D+E}{2}$		$\frac{1}{2}g_x\beta H$ $+(\frac{D-3E}{2})-\lambda$	
$-\frac{3}{2}$		$\sqrt{3}\,\frac{D+E}{2}$		$\frac{3}{2}g_x\beta H$ $-(\frac{D-3E}{2})-\lambda$

This is the same secular determinant for $\vec{H}$ parallel to the z-axis with $g_x \rightarrow g_z$, $-(D-3E)/2 \rightarrow D$, and $(d+E)/2 \rightarrow E$. Thus with these changes, Equations (A), (B), and (C) also hold for the x-axis. Similarly, for the magnetic field parallel to the y-axis the following substitutions are made:

$$g_x \rightarrow g_z, \quad -\left(\frac{D+3E}{2}\right) \rightarrow D, \quad \text{and} \quad \frac{D-E}{2} \rightarrow E \ .$$

REFERENCES

1. E. J. Zavoisky, J. Phys. (USSR) 9, 211 (1945).

2. B. Bleaney, J.D.E. Ingram, and H.E.D. Scovil, Proc. Physical Soc. 64A, 601 (1951).

3. G. M. Zverev and A. M. Prokhorov, Soviet Phys. (JETP) 7, 1023 (1958).

4. J. Lambe, R. Ager, and C. Kikuchi, Bull. Am. Phys. Soc. 4, 261 (1959).

5. J. Lambe and C. Kikuchi, Phys. Rev. 118, 71 (1960).

6. H. J. Gerritsen and H. R. Lewis, Phys. Rev. 119, 1010 (1960).

7. G. M. Zverev and A. M. Prokhorov, Soviet Phys. (JETP) 12, 160 (1960).

8. M. B. Palma-Vittorelli, M. U. Palma, D. Palumbo, Nuovo Cimento 3, 718 (1956).

9. N. S. Garifianov and B. M. Kozyrev, Soviet Phys. (Doklady) 98, 929 (1954); see also B. M. Kozyrev, Disc. Faraday Soc. 19, 135 (1955).

10. G. E. Pake and R. H. Sands, Phys. Rev. 98m, 266A (1955).

11. D. E. O'Reilly, J. Chem. Phys. 29, 1188 (1958); 30, 591 (1959).

12. R. J. Faber and M. T. Rogers, J. Am. Chem. Soc. 81, 1849 (1959).

13. C. M. Roberts, W. S. Koski, and W. S. Caughey, J. Chem. Phys. 34, 591 (1961).

14. J. E. Wertz, D. Avzins, J.H.E. Griffiths, and J. W. Orten, Disc. Faraday Soc. 26, 66 (1958).

15. R. Wyckoff, Crystal Structures, 3, Table XF15, Interscience, New York.

16. A.E.H. Tutton, Crystalline Structure and Chemical Constitution, Macmillan and Co., London (1910).

17. C. N. Ballhausen and H. B. Gray, J. Inorg. Chem., 1, 111 (1962).

18. K. Murakawa, J. Physical Soc. of Japan 11, 422 (1956).

19. B. Bleaney, R. P. Penrose, and B.I.P. Plumpton, Proc. Royal Society, 198 A, 406 (1949).

PART III

Mn^{++} EPR RESULTS IN $A_{II}B_{VI}$ COMPOUNDS

by

G. H. Azarbayejani

I. INTRODUCTION

In earlier reports on ESR measurements in $A_{II}B_{VI}$ compounds doped with Mn[1,2,3] some interesting results on the ground state splitting factor 3a have been obtained. Further experiments which have been carried out pertaining to the cubic ground state splitting will be described here. In Section II crystal preparation and doping with impurities of CdTe and ZnTe will be considered. In Section III ESR measurements will be reported.

II. CRYSTAL PREPARATION[4]

CdTe and ZnTe crystals, which we have used in our experiments, are made from the elements in fused silica quartz tubes under vacuum and heated in R-F furnaces. The following steps are taken in preparing these crystals.

A. PREPARATION OF QUARTZ TUBES

All sample tubes are made of 10 mm (ID) tubing with 4-10 in. of added tubing. In one end, these tubes are closed in regular round shape, and in the other are connected to a quartz tube stub (see Fig. 1). The empty part is 4-10 in. long.

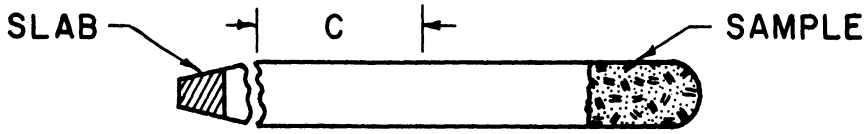

Fig. 1. Tube preparation.

The tubes are checked for leaks by using the vacuum station and Tesla coil. Good tubes are cleaned in the following sequence:

(1) Benzene rinse

(2) Acetone rinse

(3) Tapwater rinse with brushing at each stage

(4) Warm concentrated nitric acid bath for 2-4 hr

(5) Deionized water rinse (20 times)

(6) Drip drying by holding the tubes vertically with the open end down

(7) Heating the tube at quartz fusing temperature so that any foreign impurity remaining on the walls of the quartz tube will be fused into the quartz

(8) Cooling by air flow

(9) Closing the tube with a cork wrapped with glassine powder paper

(10) Labeling the tube prepared in this fashion with the letter "C," indicating that it is clean for use in crystal preparation.

B. PREPARATION OF SAMPLE

The following steps are taken for weighing the sample.

(1) Recording.—On a special data sheet the elements, properties, and weight of each are recorded. The base elements such as Cd and Te in CdTe should have a purity of 99.999%, whereas in the elements of intended impurity such as Mn or Cu it can be 99.99%.

(2) Treatment of the Elements.—Before weighing Cd and Zn, the metal bars are cut into pieces less than 10 mm long and are etched with concentrated nitric acid. Then they are rinsed thoroughly with deionized water, covered with high-purity metanol, agitated, drained, and allowed to dry on paper towels. Tellurium is usually used without etching but always in pieces so that its oxide content will be small.

(3) Weighing of the Elements.—The amount necessary for each element is calculated by desk calculator up to 7 figures and then, with use of the elements etched as described in paragraph (2), the weighing is carried out. The elements belonging to Group II^b (Cd, Zn) must be weighed before those belonging to Group III^b and Group VI; therefore for CdTe, Mn Cd is weighed first

and immediately added to the tube, with tellurium and Mn then weighed and added to the tube.

(4) Evacuation and Seal-Off of Sample.—The stube in Fig. 1 connects the tube to a vacuum station which has a fore pump for initial evacuation and a diffusion pump for further evacuation. After the desired vacuum is achieved the tube is heated in the "c" region to a length of 1—1-1/2 in. with about 2 in. above the top of the sample so that the walls of the tube collapse completely for a satisfactory seal-off.

(5) Reaction of Elements in R-F Furnaces.—To ensure a uniform distribution of the impurity ions in the compound the tube is placed vertically in a graphite cylinder. This graphite cylinder is placed along the axis of a vertical solenoid of 1/8-in. (ID) copper tube connected to a 20-KW Lepel R-F generator. The temperature is raised above the crystalline melting point and held there for several minutes; then the power is turned off, which in 5-10 minutes lowers the temperature to room temperature. The quartz tube of the sample is then inspected for cracks. If single crystals are desired, the polycrystalline obtained from the R-F furnace is annealed for several weeks under a temperature slightly lower than the melting point. The same technique is used for both ZnTe and CdTe doped with Mn.

III. ESR MEASUREMENTS

The first experiment on $A_{II}B_{VI}$ compounds, performed by Van Wieringen[5] on ZnS:Mn, raised a great demand for similar ESR experiments. Since then many other materials with structures close to cubic have been investigated. In Table I some of the recent ESR results on Mn^{++} which have been obtained in our laboratories or by other investigators are given.

TABLE I

Mn^{++} ESR EXPERIMENTAL RESULTS

Material	Crystalline Structure*	Coordination	a_o (A°)	C_o (A°)	g	3a $10^{-4}cm^{-1}$	D $10^{-4}cm^{-1}$	Ref.
MgO	R	6	4.24		2.0014	55	0	a
CaO	R	6	4.81		2.0009	17.7	0	b
αZnS	Z	4	5.43		2.0025	27.7	0	a
βZnO	W	4	3.24	5.18	2.0016	6	-216.9	c
ZnSe(P)	Z	4	5.67		2.010	-	-	d
ZnTe	Z	4	6.12		2.005	88.9	-	a
CdS	W	4	4.13	6.64	2.003	4.2	8.2	c
CdSe	W	4	4.30	7.01	2.005	47	?	a
CdTe	Z	4	6.88		2.007	83.1	-	a

*W stands for wurtzite (BZnS), R for rock salt (NaCl), and Z for zincblende (ZnS) structure.

Refs.

a. Results of our laboratories.
b. Shuskes, Phys. Rev. 127, 1529 (1962).
c. Dorain, Phys. Rev. 112, 1058 (1958).
d. Matsumara, J. Phys. Soc. Japan 14, 108 (1959).

According to Watanabe[6]

$$3a \propto (Dq)^2 \tag{1}$$

$$Dq \propto \overline{r^4}/\overline{R^5} \tag{2}$$

where r is the position of an electron with respect to a paramagnetic ion and R is the position of the nearest neighbors of paramagnetic ions. This theory was originally developed for ions in an octahedral field produced in crystals with the structure of NaCl. In Table I, MgO and CaO have this structure, and if we assume that $\overline{r^4}$ of Eq. (2) remains the same for both materials we have:

$$\left(\frac{a_{MgO}}{a_{CaO}}\right)_T = \left(\frac{R_{CaO}}{R_{MgO}}\right)^{10} = \left(\frac{a_{o\,CaO}}{a_{o\,MgO}}\right)^{10} = \left(\frac{4.81}{4.24}\right)^{10} \approx 3.4 \tag{3a}$$

The experimental results (Table I) gives

$$\left(\frac{a_{MgO}}{a_{CaO}}\right)_E = \frac{55}{17.1} = 3.1 \tag{3b}$$

Also

$$\left(\frac{a_{MgO}}{a_{ZnS}}\right)_E = 2.0 \tag{4a}$$

where

$$\left(\frac{a_{MgO}}{a_{ZnS}}\right)_T = 3.03 \tag{4b}$$

and

E = experimental

T = theoretical

Comparison of a_{ZnTe} and a_{ZnS} gives

$$\left(\frac{a_{ZnS}}{a_{ZnTe}}\right)_E = 0.312 \tag{5a}$$

where

$$\left(\frac{a_{ZnS}}{a_{ZnTe}}\right)_T = 3 \tag{5b}$$

Also

$$\left(\frac{a_{ZnTe}}{a_{CdTe}}\right)_E = 1.07 \tag{6a}$$

where

$$\left(\frac{a_{ZnTe}}{a_{CdTe}}\right)_T = 1.75 \tag{6b}$$

Equations (4a) and (4b) reveal a sharp discrepancy (as much as 35%) between experimental result and theoretical prediction and indicate a great need for testing other materials having a cubic field. This is why many studies have been carried out so far. As reflected by Eqs. (5a), (5b), (6a), and (6b) the discrepancy of 35% in MgO and ZnS is raised by 1000% in the case of ZnS and ZnTe, and by 75% in the case of ZnTe and CdTe. This demonstrates that although crystalline field theory gives a satisfactory result in light $A_{II}B_{VI}$ compounds and especially in octahedral coordination such as CaO and MgO, it fails to account for heavier compounds belonging to this group, especially those in tetrahedral coordination. In the following sections the experiments carried out on ZnTe and CdTe doped with Mn will be considered.

A. EXPERIMENTAL METHOD

The measurements at 300, 78, and 4.2°K were carried out in an X-band

(9.2-9.4 kmc/sec) magnetic resonance spectrometer. The ZnTe single crystals containing 0.1% MnTe were prepared as discussed in Section II-B. Being brittle and of low resistivity, the ZnTe single crystals are very difficult to cleave and orient properly. Therefore we had to select many samples and design a new cavity which permitted the simultaneous and orthogonal rotation of both DC magnetic field and crystal in the cavity. This cavity is shown in Fig. 2. The teflon pulley and nylon string are used particularly to facilitate the rotation of the crystal at low temperatures. With this device we were able to orient the crystal as well as find the temperature dependence of the ESR parameters in ZnTe and other similar materials. Considering that cubic ZnS and ZnTe have exactly the same crystalline structure and that the maximum splitting between the fine structure components of Mn^{++} ESR spectrum in the cubic ZnS occurs when the magnetic field and [001] axis are coincident,[7] one simply looks for the maximum separation in the spectrum of Mn^{++} as a function of angles θ' and ϕ'. These are the angles through which the DC magnetic field and crystal in the cavity are rotated from arbitrary positions. After maximum splitting is achieved and hence the location of one of the crystalline axes is determined further rotations regarding this axis are made to ensure the correct assignment of the axis. Before making an ESR measurement, it is of great importance to ensure that the piece of crystal is not polycrystalline or twin. Metallurgical microscopes with magnification ranging from 3 to 100 have been used for closer inspection of the faces, which are not shiny. After this stage X-ray photographs from both powdered and solid pieces of crystal are made to identify the structure as well as the singularity of the

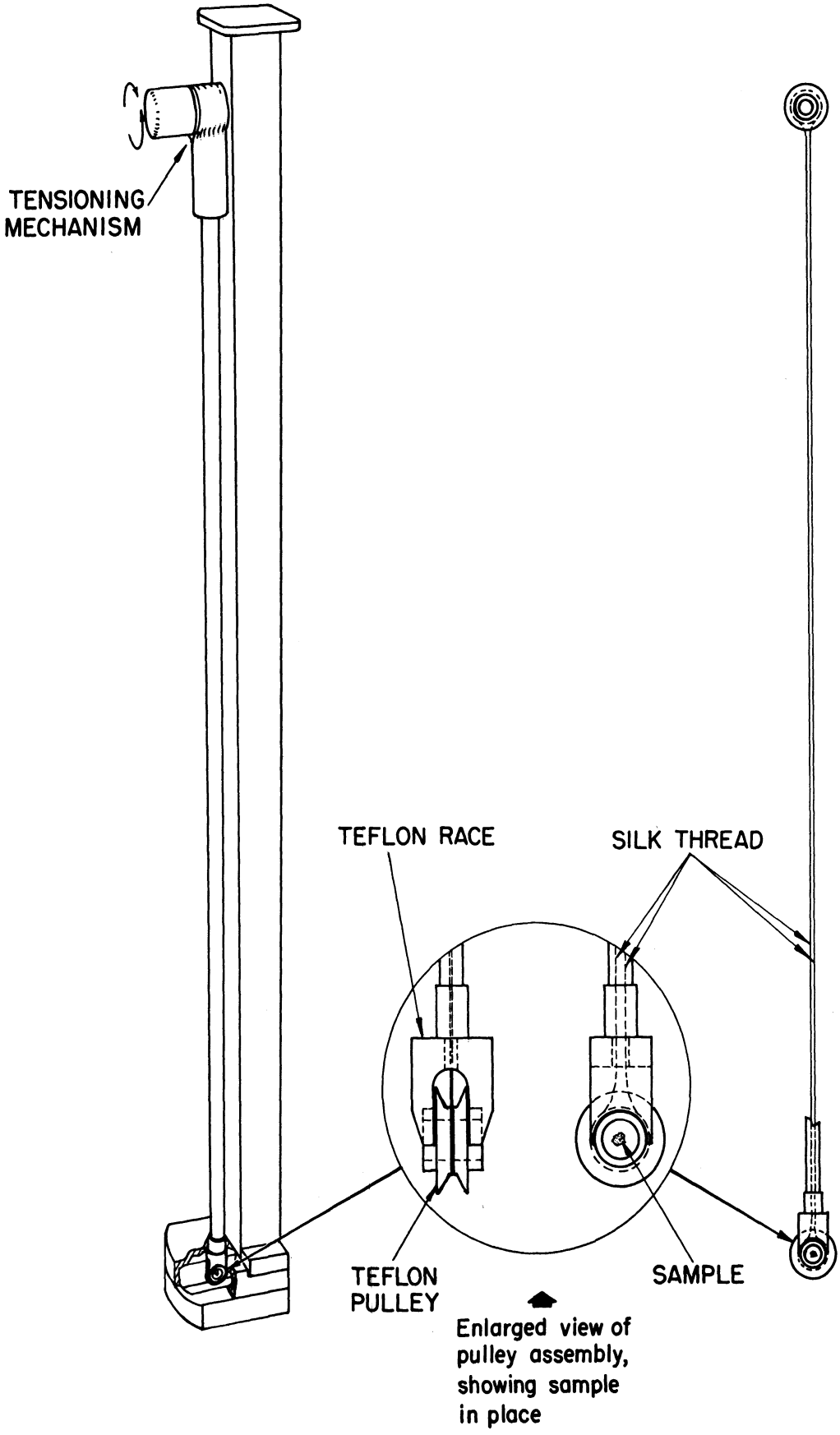

Fig. 2. Rotating sample holder and resonance cavity used for measurements.

crystal. These steps are very important in the measurement of cubic field parameters because the structure of the crystal depends a lot on the method by which they are prepared. Fortunately, in the case of the tellurides of Zn and Cd the structure is zincblende alone. For the selenides of these elements, however, structures of sphalerite (cubic ZnS) and of wurtzite (hexagonal ZnS) are observed, and sometimes it is possible for both structures to be present. A proton magnetometer and Hillard-Packard frequency counter have been used to obtain the line positions. A hydrazyl marker is used for g measurements due to the fact that in each measurement there might be slight shifts in klystron frequency, which is an especially important factor for temperature-dependence measurements.

B. EXPERIMENTAL RESULTS

1. ZnTe:Mn

In Fig. 3 the spectrum at 300°K is shown. At the top is the spectrum corresponding to $\theta = 0$, and at the bottom the spectrum corresponding to $\theta = 30°$. (θ is the angle between [001] and the DC magnetic field $\underline{H}$.) This phenomenon of dependence of intensity on θ is more pronounced in the materials with larger a (cubic field splitting parameter) because the farther the fine-structure components α and β are from the main line γ (see Fig. 17 in Section IV-D) and the higher the temperature, the more destructively they tend to combine. At $\theta = 30°$ the separation of the fine-structure components reduces nearly to zero; therefore the five transitions corresponding to $M_S = -3/2$, $-1/2$, $1/2$, $3/2$, and $5/2$ occur at about the same magnetic field. Figures 3a and 3b clearly manifest the correctness of orientation assignment given to

the crystal.

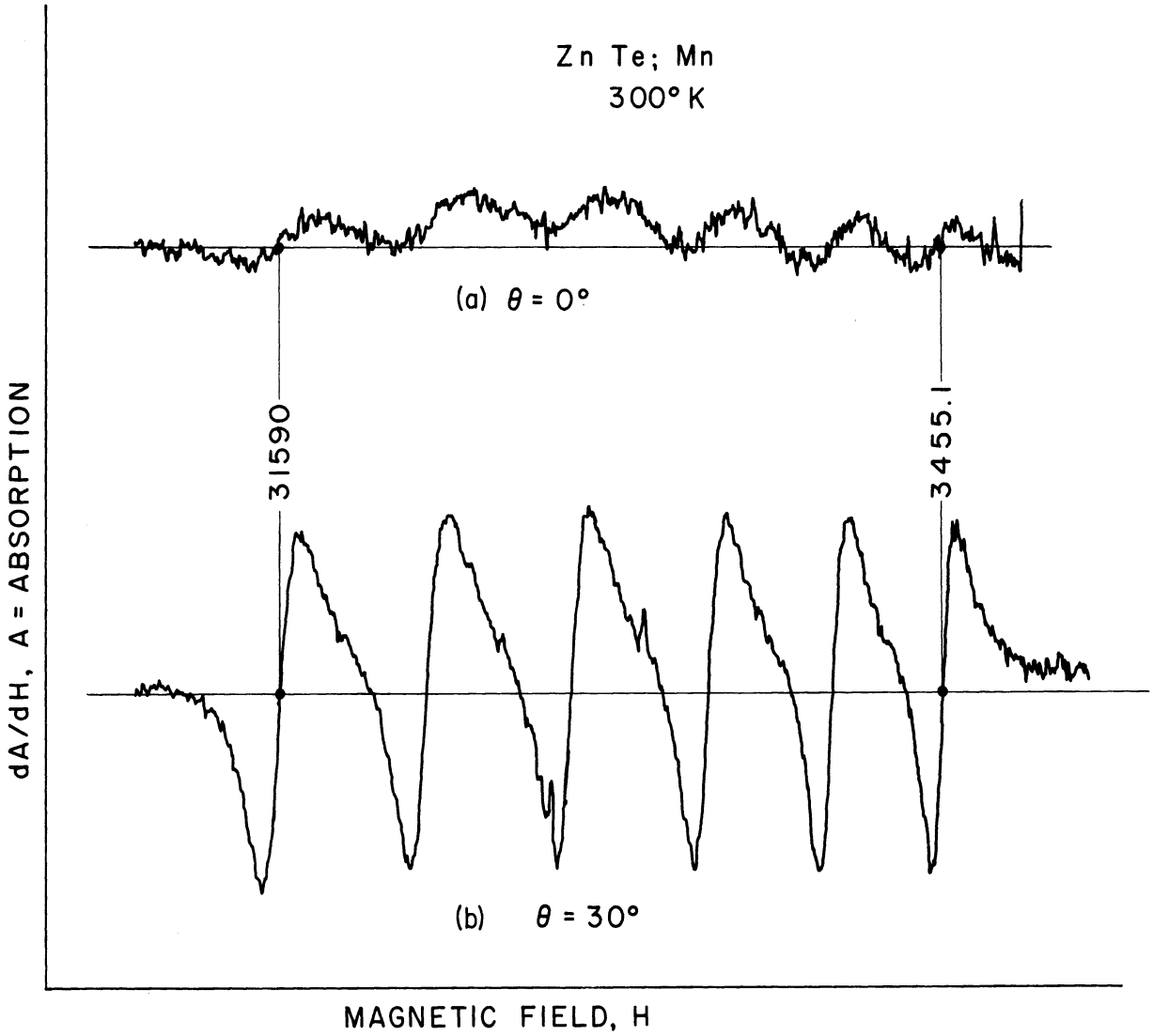

Fig. 3. Mn^{++} ESR spectrum at 300°K: (a) $\theta = 0°$; (b) $\theta = 30°$.

The spectra for T = 78° and 4.2°K at $\theta = 0°$ are given in Figs. 4 and 5 respectively.

2. CdTe:Mn

Measurements were made at 300, 78, and 4.2°K; the corresponding ESR absorption spectrum for 78°K is shown in Fig. 6, and the spectra for 4.2°K ($\theta = 30°$ and $\theta = 0°$) are shown in Figs. 7 and 8 respectively.

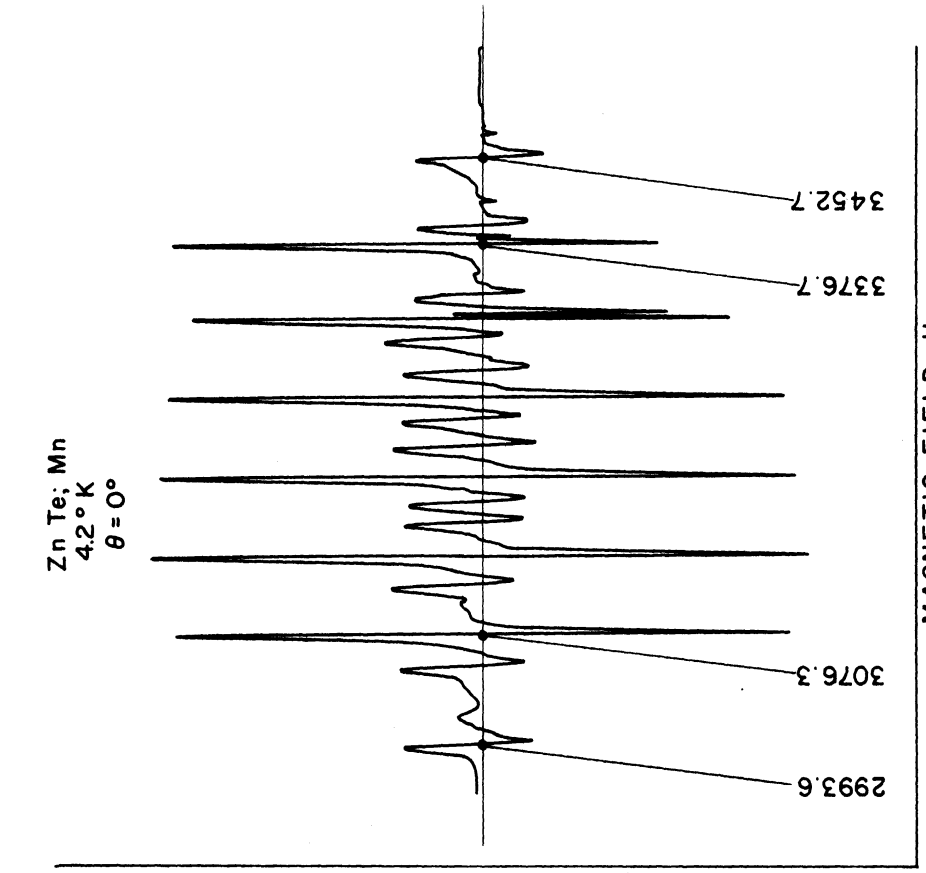

Fig. 5. Differentiation of ESR absorption in CdTe:Mn at 4.2°K.

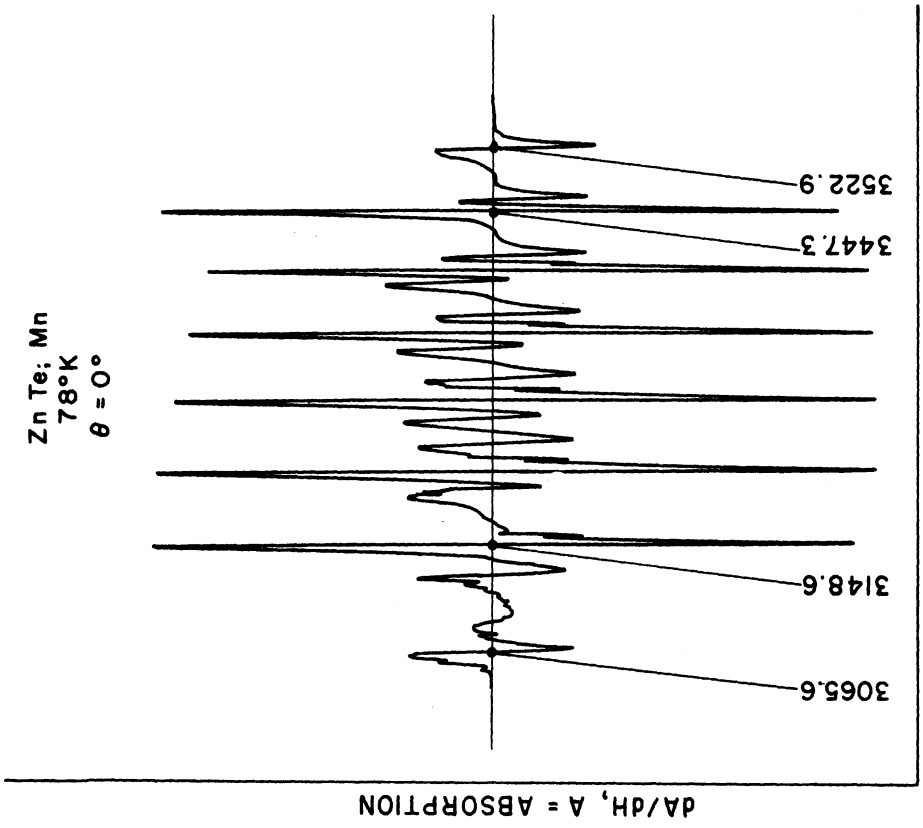

Fig. 4. Differentiation of ESR absorption in ZnTe:Mn at 78°K.

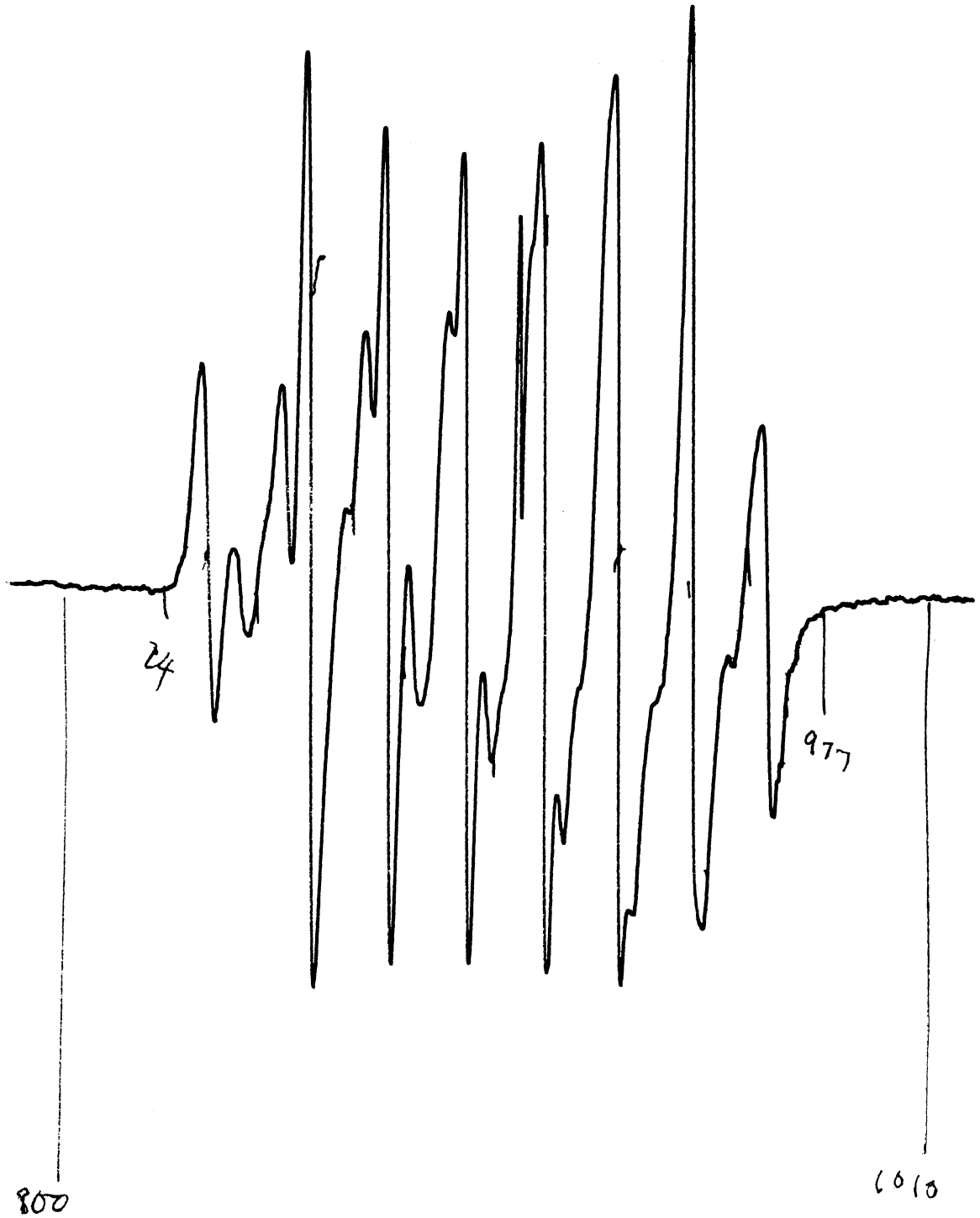

Fig. 6. Mn^{++} ESR spectrum in CdTe single crystals at 78°K, $\theta = 0°$.

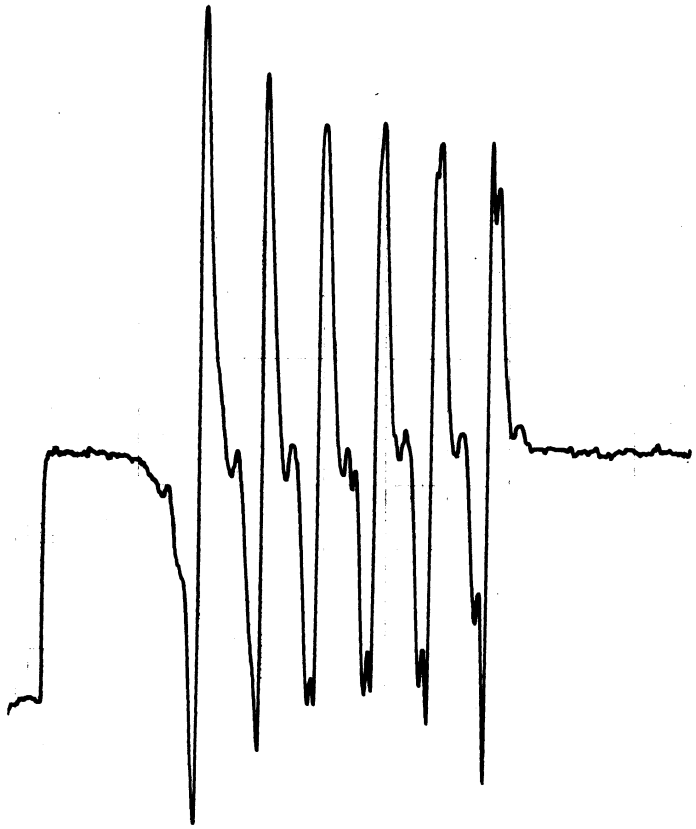

Fig. 7. Mn^{++} ESR spectrum in CdTe single crystals at 4.2°K, $\theta = 30°$.

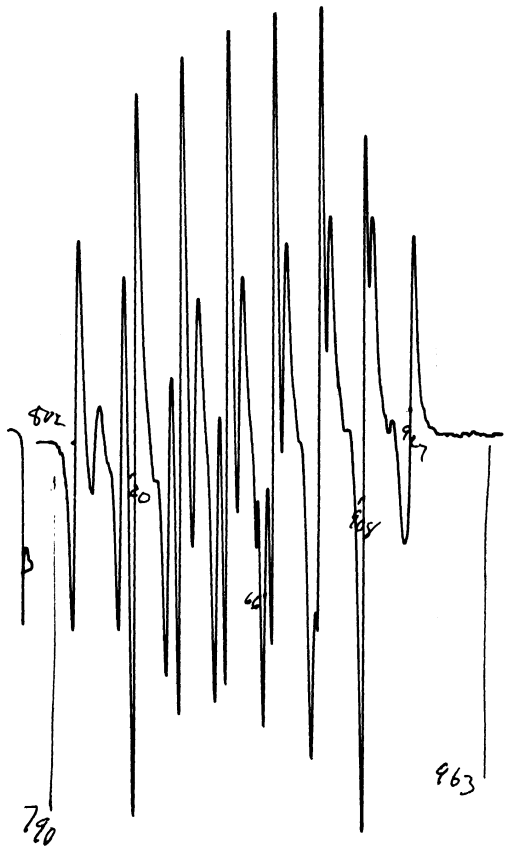

Fig. 8. Mn^{++} ESR spectrum in CdTe single crystals at 4.2°K, $\theta = 0°$.

The superhyperfine structure corresponding to Cd ions was observed both in CdS and CdTe by other investigators.[1]

IV. THEORY

A. GENERAL HAMILTONIAN OF Mn^{++}

To explain the spectra of Mn^{++} shown in Figs. 3-8 we should obtain a relation between (1) the DC magnetic field which is measured experimentally, and (2) the electron spin magnetic quantum number M, the nuclear magnetic quantum number m, the polar angle θ, and the azimuthal angle ϕ. Such a relation is self-evident only if one derives it directly from the following total Hamiltonian of Mn^{++}:

$$\mathcal{H}_t(Mn^{++}) = \sum_{\sigma=1}^{8} \mathcal{H}_\sigma \tag{7}$$

where

$$\mathcal{H}_1 = \sum_{i=1}^{n} (P_i^2/2m_i - Ze^2/r_i) + \sum_{i>j=1}^{n} e^2/r_{ij} \tag{8}$$

$$\mathcal{H}_2 = \sum_{i,j}^{n} (a_{ij}\underline{\ell}^i\cdot\underline{\ell}^j + b_{ij}\underline{\ell}^i\cdot\underline{s}^j + c_{ij}\underline{s}^i\cdot\underline{s}^j) \tag{9}$$

$$\mathcal{H}_3 = \sum_{i>j}^{n} 4\beta^2 r_{ij}^{-5}(r_{ij}^2\underline{s}^i\cdot\underline{s}^j - 3\underline{r}^{ij}\cdot\underline{s}^i\underline{r}^{ij}\cdot\underline{s}^j) \tag{10}$$

$$\mathcal{H}_4 = \sum_{i}^{n} (e\hbar/2mc)(\underline{\ell}^i+2\underline{s}^i)\cdot\underline{H} = \beta(\underline{L}+2\underline{S})\cdot H \tag{11}$$

$$\mathcal{H}_5 = g_N\beta_N 2\beta \sum_{i=1}^{n} \left\{ r_i^{-5}[r_i^2(\underline{\ell}^i-\underline{s}^i)\cdot\underline{I} + 3\underline{r}^i\cdot\underline{s}^i\underline{r}^i\cdot\underline{I}] + \frac{8\pi}{3}\delta(\underline{r}^i)\underline{s}^i\cdot\underline{I} \right\} \tag{12}$$

$$\mathcal{H}_6 = \frac{e^2Q}{2I(2I-1)} \sum_i^{\mathcal{N}} r_i^{-5}[I^{*2}r_i^2 - 3(\underline{r}^i\cdot\underline{I})^2] \text{ with } I^* = \sqrt{I(I+1)} \quad (13)$$

$$\mathcal{H}_7 = \sum_{j=1}^{p}\sum_{i=1}^{\mathcal{N}} V(r_j, r_i, \theta_i, \phi_i) \quad (14)$$

$$\mathcal{H}_8 = -g_N\beta_N\underline{H}\cdot\underline{I} \quad (15)$$

$\mathcal{H}_1$ [Eq. (8)] is the sum of the kinetic energies of electrons; the coulomb interaction of the electrons with the nucleus of the ion and each other, the $\mathcal{N}$ is the number of electrons around the Mn^{++} nucleus; $\mathcal{N} = Z-2 = 23$.

$\mathcal{H}_2$ [Eq. (9)] is the spin orbit interaction. The proportionality constants a_{ij}, b_{ij}, and c_{ij} are in general functions of quantum numbers (n^i, ℓ^i, m^i). The expression $a_{ij}\underline{\ell}^i\cdot\underline{s}^j$, for instance, refers to the energy associated with the force which the orbital angular momentum of the ith electron exerts on the spin of the jth electron. In general

$$|a_{ii}| > a_{ij}$$

It can be shown that[8]

$$a_{ii} = \frac{\hbar^2}{2m^2c^2}\frac{Z_{eff}e^2}{\langle r_i^3\rangle} \quad (16)$$

where r is the position of the electron with respect to the nucleus. c_{ij}'s are primarily due to Heisenberg's exchange effect, which appear in the interaction terms between the two electrons i and j:

$$V_{ij} = K_{ij} - (1/2 - 2\underline{s}^i \cdot \underline{s}^j) J_{ij} \tag{17}$$

where

$$K_{ij} = \langle i|\mathcal{V}_{ij}|i\rangle = \langle j|\mathcal{V}|j\rangle \tag{18}$$

and

$$J_{ij} = \langle i|\mathcal{V}_{ij}|j\rangle \tag{19}$$

Though the dependence of $J_{ij}\underline{s}^i \cdot \underline{s}^j$ on the angle between the spins is similar to that of the mutual potential energy of two magnetic dipoles

$$r^{-5}(r^2 \underline{\mu}^i \cdot \underline{\mu}^j - 3\underline{\mu}^i \cdot \underline{r}\underline{\mu}^j \cdot \underline{r}),$$

they are two entirely different things.

$\mathcal{H}_3$ [Eq. (10)] is the magnetic dipole-dipole interaction and it can be simply derived by finding the magnetic field $\underline{H}^{ij}$ produced by ith dipole at the position of jth dipole:

$$\underline{H}^{ij} = \underline{\nabla}^i x \underline{A}(r_{ij}) = -\underline{\nabla}^i x [\underline{\mu}^i x \underline{\nabla}^i (1/r_{ij})]$$

$$= \underline{\nabla}^i x \left(- \frac{\underline{\mu}^i x \underline{r}^{ij}}{r_{ij}^3} \right)$$

$$= \frac{1}{r_{ij}^3} \underline{\nabla}^i x (\underline{\mu}^i x \underline{r}^{ij}) - \frac{3\underline{r}^{ij}}{r_{ij}^5} x (\underline{\mu}^i x \underline{r}^{ij})$$

$$= r_{ij}^{-3} \left[\underline{\nabla}^i \cdot \underline{r}^{ij} \underline{\mu}^i - \underline{\nabla}^i \cdot \underline{\mu}^i \underline{r}^{ij} + \underline{r}^{ij} \cdot \underline{\nabla}^i \underline{\mu}^i - \underline{\mu}^i \cdot \underline{\nabla}^i \underline{r}^{ij} - 3\underline{\mu}^i + \frac{3\underline{r}^{ij} \cdot \underline{\mu}^i \underline{r}^{ij}}{r_{ij}^2} \right]$$

$$\simeq r_{ij}^{-5} (-r_{ij}^2 \underline{\mu}^i + 3\underline{r}^{ij} \cdot \underline{\mu}^i \underline{r}^{ij})$$

and

$$\mathcal{H}_3^{ij} = -\underline{\mu}^j \cdot \underline{H}^{ij} = r_{ij}^{-5} (r_{ij}^2 \underline{\mu}^i \cdot \underline{\mu}^j - 3\underline{\mu}^i \cdot \underline{r}^{ij} \underline{\mu}^j \cdot \underline{r}^{ij})$$

Let

$$\underline{\mu}^i = 2\beta\underline{s}^i \quad \text{and} \quad \underline{\mu}^j = 2\beta\underline{s}^j$$

Then

$$\mathcal{H}_3^{ij} = 4\beta^2 r_{ij}^{-5}(r_{ij}^2 \underline{s}^i \cdot \underline{s}^j - 3\underline{r}^{ij} \cdot \underline{s}^i \underline{r}^{ij} \cdot \underline{s}^j)$$

and

$$\mathcal{H}_3 = \sum_{i>j=1}^{n} \mathcal{H}_3^{ij} = \sum_{i>j=1}^{n} 4\beta^2 r_{ij}^{-5}(r_{ij}^2 \underline{s}^i \cdot \underline{s}^j - 3\underline{r}^{ij} \cdot \underline{s}^i \underline{r}^{ij} \cdot \underline{s}^j) \quad . \quad (20)$$

$\mathcal{H}_4$ [Eq. (11)] is again the interaction of the magnetic moments of all ion electrons with the external DC magnetic field, and it is evident that if the DC magnetic field is not strong enough to decouple the angular momenta of the electrons then the result of interaction on the closed shells is zero. For the last shell this result is as shown in Eq. (11).

$\mathcal{H}_5$ [Eq. (12)] is exactly like $\mathcal{H}_3$, the only difference being that the total number of Z protons and A-Z neutrons is assumed to be a particle with angular momentum I at the origin; therefore the contribution of the orbital angular momentum $\underline{\ell}^i$ of the electron is just

$$\lambda^i = 2\beta g_N \beta_N \underline{\ell}^i \cdot \underline{I}/r_i^3 \quad (21)$$

where the contribution of the ith electron spin σ^i is

$$\sigma^i = -2g_N\beta_N\beta \left\{ r_i^{-5}[r_i^2 \underline{s}^i \cdot \underline{I} - 3\underline{r}^i \cdot \underline{s}^i \underline{r}^i \cdot I - 8\pi\delta(\underline{r}^i)\kappa \underline{s}^i \cdot I/3] \right\} \quad (22)$$

The first part of Eq. (22) is due to dipole-dipole interaction and the second to the electrons present at origin. Therefore Eq. (23) results (see Fig. 9):

$$\mathcal{H}_s = \sum_{i=1}^{n} (\lambda+\sigma)_i = 2g_N\beta_N\beta \sum_{i=1}^{n} \left\{ r_i^{-5}[r_i^2(\underline{\ell}^i - \underline{s}^i)\cdot I + 3\underline{r}^i\cdot\underline{s}^i\underline{r}^i\cdot I] + 8\pi\kappa\delta(\underline{r}^i)\underline{s}^i\cdot I \right\} \tag{23}$$

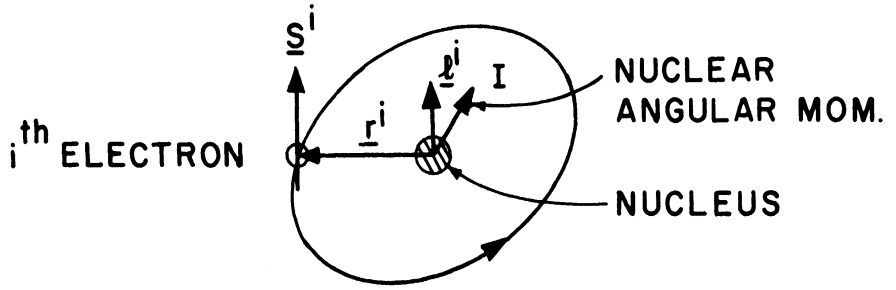

Fig. 9. Schematic representation of electron-nucleus magnetic interaction.

$\mathcal{H}_e$ [Eq. (13)] is the electric quadrupole moment. Consider that the nth nucleon potential on the ith electron is (see Fig. 10):

$$V^{ni} = \sum_{\ell=0}^{\infty} \frac{e_i e_n}{r_i} \rho_{ni}^{\ell} P_\ell(\xi_{ni})$$

and

$$V_{NE} = \sum_{i=1}^{n}\sum_{n=1}^{A} V^{ni} = \sum_{i=1}^{n}\sum_{n=1}^{A}\sum_{\ell=0}^{\infty} \frac{e_i e_n}{r^i} \rho_{ni}^{\ell} P_\ell(\xi_{ni})$$

$$\cong \sum_{i,n} \frac{e_i e_n}{r^i} [\rho_{ni}^{o} P_o(\xi_{ni}) + \rho_{ni}^{1} P_1(\xi_{ni}) + \rho_{ni}^{2} P_2(\xi_{ni}) + \text{-}]$$

$$= V_o + V_1 + V_2 \tag{24}$$

where

$$\xi_{ni} = \cos\theta_{ni} = (x_i X_n + y_i Y_n + z_i Z_n)/r_i R_n \tag{25}$$

and

$$\rho_{ni}^{\ell} = (R_n/r_i)^{\ell} \tag{26}$$

$$V_o = \sum_{i,n} \frac{e_i e_n}{r^i} = -\sum_{i} Ze^2/r_i \qquad (27)$$

$$V_1 = \sum_{i,n} \frac{e_i e_n}{r_i^3 R_n} (x_i X_n + y_i Y_n + z_i Z_n) \qquad (28)$$

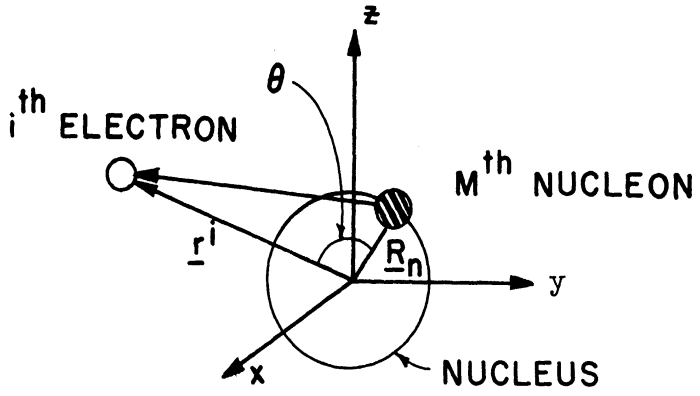

Fig. 10. Schematic representation of electron-nucleon coulomb interaction.

The matrix elements of V_1 correspond to the nuclear electric dipole moment which vanishes, and

$$V_2 = \sum_{i,n} r_i^{-1} e_i e_n \rho_{ni}^2 P_2(\xi_{ni}) = \sum_{i,n} r_i^{-3} e_i e_n R_n^2 (3\xi_{ni}^2 - 1)/2 \qquad (29)$$

Substituting Eqs. (25) and (26) we have:

$$V_2 = \frac{1}{2}\sum_{i,n} r_i^{-3}R_n^2 e_i e_n[3r_i^{-2}R_n^{-2}(x_i^2X_n^2+y_i^2Y_n^2+z_i^2Z_n^2+2x_iy_iX_nY_n+2y_iz_iY_nZ_n+2z_ix_iZ_nX_n)-1]$$

$$= \frac{3}{2}\sum_{i,n} r_i^{-5}e_i e_n[x_i^2X_n^2+y_i^2Y_n^2+z_i^2Z_n^2+2x_iy_iX_nY_n+2y_iz_iY_nZ_n+2z_ix_iZ_nX_n$$

$$- (x_i^2+y_i^2+z_i^2)(X_n^2+Y_n^2+Z_n^2)/3]$$

$$= \frac{1}{6}\sum_{i,n} r_i^{-5}e_i e_n[9(x_i^2X_n^2+y_i^2Y_n^2+z_i^2Z_n^2) + 18(x_iy_iX_nY_n+\cdots) - 3r_i^2R_n^2]$$

$$= \frac{1}{6}\sum_{i,n} r_i^{-5}e_i e_n[(r_i^2-3x_i^2)(R_n^2-3X_n^2) + (r_i^2-3y_i^2)(R_n^2-3Y_n^2) + (r_i^2-3z_i^2)(R_n^2-3Z_n^2)$$

$$+ 18(x_iy_iX_nY_n+\cdots)]$$

$$= \frac{1}{6}\sum_{i} r_i^{-5}e_i \sum_{n} e_n[(r_i^2-3x_i^2)(R_n^2-3X_n^2) + (r_i^2-3y_i^2)(R_n^2-3Y_n^2) + (r_i^2-3z_i^2)(R_n^2-3Z_n^2)$$

$$+ 18(x_iy_iX_nY_n+\cdots)] \qquad (30)$$

Consider now[9]

$$\sum_n e_n(R_n^2-3X_n^2) = -\frac{eQ}{I(2I-1)}(I^{*2}-3I_x^2) \qquad (31)$$

$$\sum_n e_nX_nY_n = -\frac{eQ}{I(2I-1)}\frac{1}{2}(I_xI_y+I_xI_y) \qquad (32)$$

Thus we obtain:

$$V_2 = \frac{1}{6}\sum_i \frac{e_i}{r_i^5} - \frac{eQ}{I(2I-1)}\{I^{*2}(3r_i^2-3r_i^2)-3r_i^2(I_x^2+I_y^2+I_z^2)+9(I_x^2x_i^2\cdots)+18(x_iy_iI_xI_y+\cdots) \qquad (33)$$

For all electrons the e_i's are the same, $e_i = -e$; therefore Eq. (33) reduces to:

$$\mathcal{H}_6 = V_2 = V_Q = + \frac{e^2Q}{2I(2I-1)} \sum_i r_i^{-5}[I(I+1)r_i^2 - 3(\underline{r}^i \cdot \underline{I})^2] \quad (34)$$

$\mathcal{H}_7$ [Eq. (14)] describes the effect of the sum of the coulomb potentials produced by the neighboring ions at the ith electron. In the case of approximation of the closest neighbors in ZnTe and CdTe, this is the sum of the potentials produced by the four closest Te ions. $\mathcal{H}_7$ is discussed in Section IV-C.

$\mathcal{H}_8$ [Eq. (15)] is the direct interaction of the DC magnetic field $\underline{H}$ and nuclear spin $\underline{I}$ with the gyromagnetic ration g_N. $g_N\beta_N\underline{I}\cdot\underline{H}$ is considered as a constant and neglected.

B. SPIN HAMILTONIAN

In case of II-VI compounds and for $3d^n$ ions, $\mathcal{H}_1 > \mathcal{H}_7 > \mathcal{H}_2 + \mathcal{H}_3$; therefore the ground-state electronic configuration of Mn^{++} is still $3d^5$. The terms associated with this configuration are:

$$S,P,D,F,G,H, \text{ and } I. \quad (35)$$

One way of studying the effect of different Hamiltonians on these terms is to transform them into functions of angular momentum operators, L, S, and I, which facilitates the theoretical calculations considerably and does not affect the ESR experimental calculations. This transformation is carried out in Appendix B. The result [Eq. (B-14) of Appendix B] is:

$$\mathcal{H}_C^1(L,S,I) = \mathcal{H}_t - \mathcal{H}_1 + C = K\underline{L}\cdot\underline{S} - M[(L\cdot S)^2 + \tfrac{1}{2}\underline{L}\cdot\underline{S} - L^{*2}S^{*2}/3]$$

$$+ \beta(\underline{L}+2\underline{S})\cdot\underline{H} - g_N\beta_N\underline{H}\cdot\underline{I}$$

$$+ N\{a[L^{*2}\underline{S}\cdot\underline{I} - 3(\underline{L}\cdot\underline{S}\underline{L}\cdot\underline{I}+\underline{L}\cdot\underline{I}\underline{L}\cdot\underline{S})/2] + \underline{L}\cdot\underline{I} - \kappa\underline{S}\cdot\underline{I}\}$$

$$+ p[(\underline{L}\cdot\underline{I})^2 - \underline{L}\cdot\underline{I}/2 - L^{*2}I^{*2}/3] + \mathcal{H}_7 \qquad (36)$$

where

$$L^* = \sqrt{L(L+1)}\ ; \qquad S^* = \sqrt{S(S+1)}\ ; \qquad I^* = \sqrt{I(I+1)}$$

and K, M, N, p, and κ are independent of $\underline{L}$, $\underline{S}$, $\underline{I}$, M_L, M_S or M_I. The energy of each of the terms of Eq. (35) is calculated in Appendix A. Equations (A-28) of this appendix give for Mn^{++} $(3d^5)$

$$\frac{E(3d^5, L^{2S+1}, B/C=.5, C) - 10A}{C} = \begin{cases} +\ 0.5 & \text{for } {}^4F \\ -\ 4.0 & \text{for } {}^4D \\ -\ 7.0 & \text{for } {}^4P \\ -\ 7.50 & \text{for } {}^4G \\ -17.50 & \text{for } {}^6S \end{cases} \qquad (37)$$

where A,B,C are Racah's coefficients.

Thus the ^6S state lies the lowest; considering Eqs. (36) and (37) one finds that in the case of Mn^{++} the eigenvalues for operators including L will be zero. Thus:

$$< LM_L|\mathcal{H}_C^1|LM_L > = \mathcal{H}_C^S = 2\beta\underline{S}\cdot\underline{H} + \underline{S}\cdot\underline{I} + \mathcal{H}_7(S) - g_N\beta_N\underline{H}\cdot\underline{I} \qquad (38)$$

where

$$A = -N\kappa$$

Therefore, for Mn^{++} in the intermediate crystalline field appropriate to II-VI compounds such as MgO, ZnS, ZnTe, and CdTe, the spin Hamiltonian—which is derived from the total Hamiltonian after the latter has been transformed into functions of orbital and spin angular momenta and then integrated over orbital angular momenta L—is:

$$\mathcal{H}_c^S(\underline{S},\underline{I}) + g_N\beta_N\underline{H}\cdot\underline{I} = \mathcal{H}_S = 2\beta\underline{S}\cdot\underline{H} + A\underline{S}\cdot\underline{I} + \mathcal{H}_7(S) \qquad (39)$$

where

$$A = -N\kappa$$

and $g_N\beta_N\underline{H}\cdot\underline{I}$ is assumed to remain constant. On the basis of the assumptions made to derive $\mathcal{H}_t$, in Eqs. (7)-(15), one finds that:

(1) The gyromagnetic ratio of Mn^{++} outer shell electronic cloud should be the same as that of free electrons.

(2) Any difference between electronic spin states $M_I(-5/2,\cdots 5/2)$ should result from $\mathcal{H}_7(S)$ and $A\underline{S}\cdot\underline{I}$ in Eq. (39).

C. CRYSTALLINE FIELD

The crystalline field in II-VI compounds of zincblende structure can be obtained from Fig. 11 and Eq. (40).

$$V(r) = \sum_{n=0}^{\infty}\sum_{m=-n}^{n} A_{nm}r^n Y_{nm}(\theta,\phi) \qquad (40)$$

Symmetry considerations will reduce the number of terms in Eq. (40).

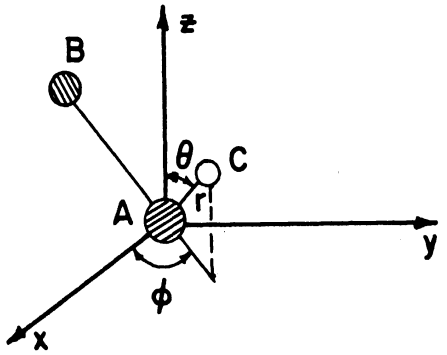

Fig. 11. Schematic representation of crystalline field. (A is the ion, B is its closest neighbor, and C is its electron.)

For d electrons one has to consider only expansions up to n = 4. No terms with odd n in a given configuration will contribute in ground-state splitting, regardless of whether the center of symmetry is present or not. The term A_0^0 is a constant shifting all of the levels of a given configuration by the same amount. Therefore:

$$V_{eff} = A_{20}r^2Y_{20} + A_{22}r^2Y_{22} + A_{40}r^4Y_{40} + A_{44}Y_{44} + A_{4-4}Y_{4-4}$$

The choice of z axis parallel to the fourfold rotary reflection axis S_4 facilitates the determination of the coefficients in the above relations. Furthermore consider that

$$V(r,\theta,\phi) = \sum_{nm} \alpha_{nm}\xi^{n-m}e^{im\phi}$$

where

$$\alpha_{nm} = f(r,n,m) \text{ only}$$

and

$$\xi = \cos\theta$$

Thus

$$S_4 V(r,\theta,\phi) = V(r\theta+\pi,\ \phi + \frac{\pi}{2}) = V(r,\theta,\phi)$$

results in

$$[\cos(\theta+\pi)]^{n-m}\ e^{im(\phi+\pi/2)} = (\cos\theta)^{n-m}\ e^{im\phi}$$

or

$$m = 0, \pm 4 .$$

Now consider that reality condition requires that

$$V^* = V$$

or each term having the same condition, i.e.,

$$(A_{44}Y_{44})^* = A_{44}^* Y_{44}^* = A_{4-4}Y_{4-4}$$

since

$$Y_{44}^* = (-1)^4 Y_{4-4} = Y_{4-4} \Rightarrow A_{44}^* = A_{4-4}$$

The presence of reflection planes σ requires that

$$A_{nm} = A_{n-m} \tag{41b}$$

Conditions (41a) and (41b) result in:

$$(A_{nm})^* = A_{n-m} = A_{nm} , \tag{41c}$$

namely, A_{nm}'s are real. In our experiments no axial dependence of the field on θ was observed; therefore the field set up by four tellurium ions around Mn^{++} electronic cloud is

$$V = A_{40}r^4[Y_{40} + (A_{44}/A_{40})(Y_{44}+Y_{4-4})]$$

$$= A_{40}r^4(35\cos^4\theta - 30\cos^2\theta + 3) + r^4A_{44}\sqrt{70}\sin^4\theta\cos^4\phi \qquad (42)$$

Now consider Fig. 12. We have

$$V_A(r,\theta = 0,\phi = 0) = V_B(r,\theta = \pi/2,\phi = 0)$$

or

$$8r^4A_{40} = 3A_{40}r^4 + r^4\sqrt{70}\,A_{44}$$

or

$$(A_{44}/A_{40}) = \sqrt{5/14}$$

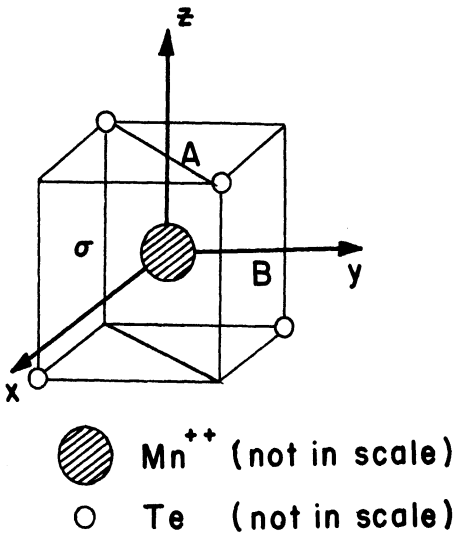

Fig. 12. A unit cell of cubic ZnTe single crystal showing a Mn^{++} ion surrounded by four Te ions and the reflection planes σ.

Therefore

$$_7(r,\theta,\phi) = V = A_{40}r^4[Y_{40}+(5/14)^{1/2}(Y_{44}+Y_{4-4})] \qquad (43)$$

and Eqs. (B-28) of Appendix B give:

$$\mathcal{H}_7[(r,r')_n, L_x, L_y, L_z] = B[L_x^4 + L_y^4 + L_z^4 - \frac{L^{*2}}{5}(3L^{*2}-1)] \qquad (44)$$

In the ^6S state of Mn^{++}, for H parallel to z axis, one finds from Eqs. (39) and (44) that

$$< M,n|\mathcal{H}^S|M,m > - < M-1,m|\mathcal{H}^S|M-1,m > = 2\beta H(M,m) + mA = h\nu_o = 2\beta H_o \qquad (45)$$

and

$$H(M,m) = H_o - mA' \qquad A' = A/2\beta \qquad (46)$$

where

m = nuclear magnetic quantum number.

Equations (45) and (46) indicate that there should be six absorptions only (see Fig. 13).

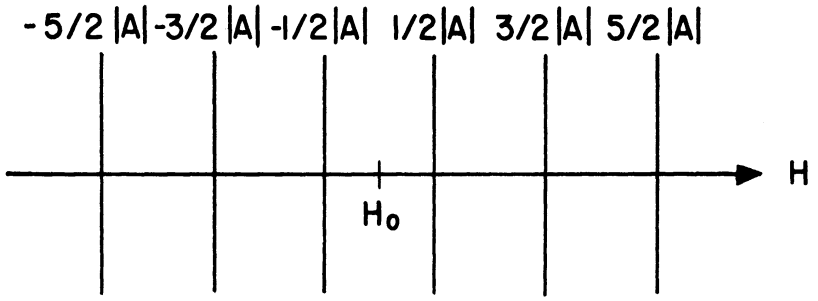

Fig. 13. Theoretical prediction of Mn^{++} ESR spectrum.

These absorptions are observed only in powders and we realize that to describe the spectra shown in Figs. 3-8 a further refinement of theory is necessary. Bleaney and Stevens,[10] after a phenomological argument, conclude that a more realistic representation of the crystal potential for Mn^{++} in II-VI compounds may be written as:

$$\mathcal{H}_7[(r,r')_n,L,S] = B[L_x^4 + L_y^4 + L_z^4 - L^{*2}(3L^{*2}-1)/5] + P[S_x^4 + S_y^4 + S_z^4 - S^{*2}(3S^{*2}-1)/5] \quad (47)$$

Therefore

$$\mathcal{H}^S_{cubic}(Mn^{++}) \cong \langle 0|\mathcal{H}'_t|0\rangle + \sum_n{}' |\langle 0|\mathcal{H}'_i|n\rangle|^2/[E(0)-E(n)]$$

$$= g\beta\underline{H}\cdot\underline{S} + A\underline{S}\cdot\underline{I} + P[S_x^4 + S_y^4 + S_z^4 - S^{*2}(3S^{*2}-1)/5] \quad (48)$$

Owing to the fact that P is a measure of $\mathcal{H}^S_{cubic}$ when $\underline{H} = 0$ it is called the zero field splitting factor. Bethe[11] shows that the state $^6S_{5/2}$ will be split into $^2\Gamma_7$ and $^4\Gamma_8$ under the effect of a tetrahedral field created by the four closest tellurium ions of Zn, Cd, and Te. To correlate P and $\Delta E = {}^4\Gamma_8 - {}^2\Gamma_7$ use is made of T tensors given as:[12,13]

$$T_{\ell q\pm 1} = [\ell(\ell+1) - q(q\pm 1)]^{-1/2}(S_\pm, T_{\ell q}) \quad (49)$$

$$S_\pm = S_x \pm iS_y$$

$$T_{4\pm 4} = \sqrt{70}/(16)\ S_\pm{}^4 \quad (50)$$

$$S_x = (S_+ + S_-)/2 \qquad S_y = (S_+ + S_-)/2i \quad (51)$$

Consider that

$$S_x^4 = (S_+ + S_-)^4/16 = (S_+^4 + S_-^4)/16 + f(S_+^3 + \cdots S_-^3)$$

$$S_y^4 = (S_+ + S_-)^4/16 = (S_+^4 + S_-^4)/16 + h(S_+^3 + \cdots S_-^3)$$

Then

$$P(S_x^4 + S_y^4) = \frac{P}{8}(S_+^4 + S_-^4) + f' + h' = \frac{2P}{\sqrt{70}}(T_{44} + T_{4-4}) + f'' + h'' \tag{52}$$

Evaluating $S_\pm$ from Eq. (49) and substituting in Eq. (52) one gets:

$$\mathcal{H}^S_{\text{cubic}}(Mn^{++}) = g\beta \underline{S}\cdot\underline{H} + A\underline{I}\cdot\underline{S} + \frac{2P}{5}[T_{40} + \sqrt{5/14}(T_{44} + T_{4-4}) \tag{53}$$

where

$$T_{40} = \frac{1}{8}(35S_z^4 - 30S^{*2}S_z^2 + 25S_z^2 - 6S^{*2} + 3S^{*4}) \qquad S^* = \sqrt{S(S+1)} \tag{54}$$

The matrix elements of the $2P[T_{40} + \sqrt{5/14}(T_{44}+T_{4-4})]/5$ can be found very easily, and the result is as shown in Table II.

TABLE II

MATRIX ELEMENTS OF $\frac{2P}{5}[T_{40} + \sqrt{5/14}(T_{44}+T_{4-4})]$

M' =	$\pm\frac{1}{2}$	$\pm\frac{3}{2}$	$\pm\frac{5}{2}$
$M = \pm\frac{1}{2}$	6P	0	0
$\pm\frac{3}{2}$	0	-9P	$3\sqrt{5}P$
$\pm\frac{5}{2}$	0	$3\sqrt{5}P$	3P

In the secular equation

$$\|\mathcal{H}_{ij} - \delta_{ij}\epsilon\| = (6P-\epsilon)[(-9P-\epsilon)(3P-\epsilon) - 45P^2] = 0$$

giving

$$\epsilon_1(\pm \tfrac{1}{2}) = 6P, \qquad \epsilon_2 = 6P, \qquad \epsilon_3 = -12P \tag{55}$$

ϵ_1 and ϵ_2 correspond to four eigen functions with energy 6P above the ground state of the free ion. Thus the situation shown in Fig. 14 results:

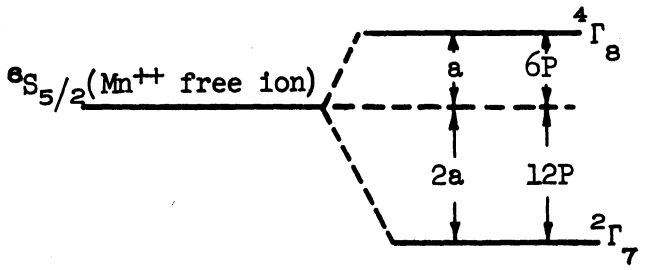

Fig. 14. Effects of cubic field on $^6S_{5/2}$ levels.

The splitting of $^6S_{5/2}$ state in a tetrahedral field is given by

$$^4\Gamma_8 - {}^2\Gamma_7 = 18P = 3a \tag{56}$$

where

$$a = 6P$$

Substituting for Pin Eqs. (52) and (53), one finds expressions similar to those given by Bleaney and Stevens[10] and by Lambe et al.[1]:

$$\mathcal{H}^{S'}_{cubic} = -g_N\beta_N\underline{H}\cdot\underline{I} + \mathcal{H}^{S}_{cubic} = g\beta\underline{S}\cdot\underline{H} + a[S_x^4+S_y^4+S_z^4-S^{*2}(3S^{*2}-1)/5]/6$$

$$+ A\underline{I}\cdot\underline{S} - g_N\beta_N\underline{H}\cdot\underline{I} \tag{57}$$

or

$$\mathcal{H}^{S}_{\text{cubic}} = g\beta \underline{S}\cdot\underline{H} + A\underline{I}\cdot\underline{S} + a[T_{40} + \sqrt{5/14}\,(T_{44}+T_{4-4})]/15 \qquad (58)$$

To find the energy corresponding to electronic and nuclear spin levels we set up the secular equation for fine-structure Hamiltonian $\mathcal{H}^{S}_{\text{f.s.}}$:

$$\mathcal{H}^{S}_{\text{f.s.}} = \mathcal{H}^{S} - A\underline{I}\cdot\underline{S} = g\beta\underline{S}\cdot\underline{H} + a(35S_z^4 - 30S^{*2}S_z^2 + 25S_z^2 - 6S^{*2} + 3S^{*4})/120 + a(S_+^4 + S_-^4)/48 \qquad (59)$$

For the DC magnetic field $\underline{H}$ parallel to one of the principal axes of the cube, namely the z axis, we will find the matrix elements of

$$\mathcal{H}^{S}_{\text{f.s.}}(H\|Z\|S_4) = g\beta HS_z + a(35S_z^4+25S_z^2-30S^{*2}S_z^2-6S^{*2}+3S^{*4})/120 + a(S_+^4+S_-^4)/48 \qquad (60)$$

The first and second term are diagonal while the third term is off-diagonal; therefore

$$< M|g\beta HS_z + a(35S_z^4-30S^{*2}S_z^2+25S_z^2-6S^{*2}+3S^{*4})/120 + a(S_+ + S_-)/48|M' >$$

$$= < M|g\beta HS_z + a(35S_z^4-30S^{*2}S_z^2+25S_z^2-6S^{*2}+3S^{*4})/120|M' >$$

$$+ < M|a(S_+^4+S_-^4)/48|M' > = A\delta_{MM'} + B\delta_{M,M'\pm4} \qquad (61)$$

with

$$A = [2M\epsilon + a(14M^4-95M^2+189)/48]$$

$$B = \sqrt{5}\,a/2 \qquad \epsilon = g\beta H/2$$

The secular equations (determinant) can be constructed from

$$\| (\mathcal{H}^{S}_{f.s.})_{MM'} - E\delta_{MM'} \| = 0 \qquad (62)$$

Thus

M \ M'	5/2	3/2	1/2	-1/2	-3/2	-5/2
5/2	$5\epsilon+a/2-E$	0	0	0	$\sqrt{5}\ a/2$	0
3/2	0	$3\epsilon-3a/2-E$	0	0	0	$\sqrt{5}\ a/2$
1/2	0	0	$\epsilon+a-E$	0	0	0
-1/2	0	0	0	$-\epsilon+a-E$	0	0
-3/2	$\sqrt{5}\ a/2$	0	0	0	$-3\epsilon-3a/2-E$	0
-5/2	0	$\sqrt{5}\ a/2$	0	0	0	$-5\epsilon+a/2-E$

$\Delta =$ $= 0$

(63)

The determinant is an equation of 6th power in E. To solve consider

$$\Delta = \begin{vmatrix} \alpha & 0 & 0 & 0 & \gamma & 0 \\ 0 & \beta & 0 & 0 & 0 & \gamma \\ 0 & 0 & \delta & 0 & 0 & 0 \\ 0 & 0 & 0 & \lambda & 0 & 0 \\ \gamma & 0 & 0 & 0 & \zeta & 0 \\ 0 & \gamma & 0 & 0 & 0 & \eta \end{vmatrix} = \delta\lambda(\alpha\zeta-\gamma^2)(\beta\eta-\gamma^2) = 0 \qquad (64)$$

giving

$$E_1 = a+\epsilon \qquad E_2 = a-\epsilon$$

or, provided $\epsilon \gg a$,

$$
\begin{aligned}
E_3 &= \epsilon - \frac{a}{2} + \sqrt{(4\epsilon+a)^2+5a^2/4} \cong \epsilon - \frac{a}{2} + 4\epsilon + a + \frac{5a^2}{4}/8\epsilon \\
E_4 &= \epsilon - \frac{a}{2} - \sqrt{(4\epsilon+a)^2+5a^2/4} \cong \epsilon - \frac{a}{2} - 4\epsilon - a - \frac{5a^2}{4}/8\epsilon \\
E_5 &= -\frac{2\epsilon+a}{2} + \sqrt{(4\epsilon-a)^2+5a^2/4} \cong -\epsilon - \frac{a}{2} + 4\epsilon - a + \frac{5a^2}{4}/8\epsilon \\
E_6 &= -\frac{2\epsilon+a}{2} - \sqrt{(4\epsilon-a)^2+5a^2/4} \cong -\epsilon - \frac{a}{2} - 4\epsilon + a - \frac{5a^2}{4}/8\epsilon
\end{aligned}
\tag{65}
$$

It is obvious that the states $M = \pm 1/2$ do not mix and that E_1 and E_2 therefore belong to $M = 1/2$ and $M = -1/2$. For other M's one has, provided $a/\epsilon \ll 1$.

$$
\begin{aligned}
E^{f.s.}_{\pm\frac{1}{2}} &= a \pm \epsilon \\
E^{f.s.}(M = \pm\tfrac{3}{2}) &= -\frac{3a}{2} \pm 3\epsilon \pm \frac{5a^2}{4}/8\epsilon = -\frac{3a}{2} \pm 3\epsilon \pm 5a^2/32\epsilon \\
E^{f.s.}(M = \pm\tfrac{5}{2}) &= \frac{a}{2} \pm 5\epsilon \pm \frac{5a^2}{4}/8\epsilon = \frac{a}{2} \pm 5\epsilon \pm 5a^2/32\epsilon
\end{aligned}
\tag{66}
$$

Thus, the energy diagram of spin levels for $H \| Z$ and in the absence of nuclear spin effect is as shown in Fig. 15 and Table III.

TABLE III

VARIATION OF SEPARATION OF Mn^{++} ESR FINE-STRUCTURE COMPONETS AT $\theta = 0$ AS A FUNCTION OF $\rho = g\beta H/2a = \epsilon/a$

ρ	$E_{-5/2}-E_F$	$E_{-3/2}-E_F$	$E_{-1/2}-E_F$	$E_{1/2}-E_F$	$E_{3/2}-E_F$	$E_{5/2}-E_F$
0	- 2.00	- 2.00	1.00	1.00	1.00	1.00
1	- 4.71	- 4.62	0.00	2.00	1.71	5.62
2	- 9.59	- 7.57	- 1	3	4.59	10.57
3	- 14.56	- 10.55	- 2	4	7.05	15.55
4	- 19.54	- 13.54	- 3	5	10.54	20.54
5	- 24.53	- 16.53	- 4	6	13.53	25.54
6	- 29.52	- 19.53	- 5	7	16.53	30.52
7	- 34.52	- 22.52	- 6	8	19.52	35.52
10	- 49.52	- 31.51	- 9	11	28.51	50.5
100	-499.5	-301.50	-99	101	298.5	500.5

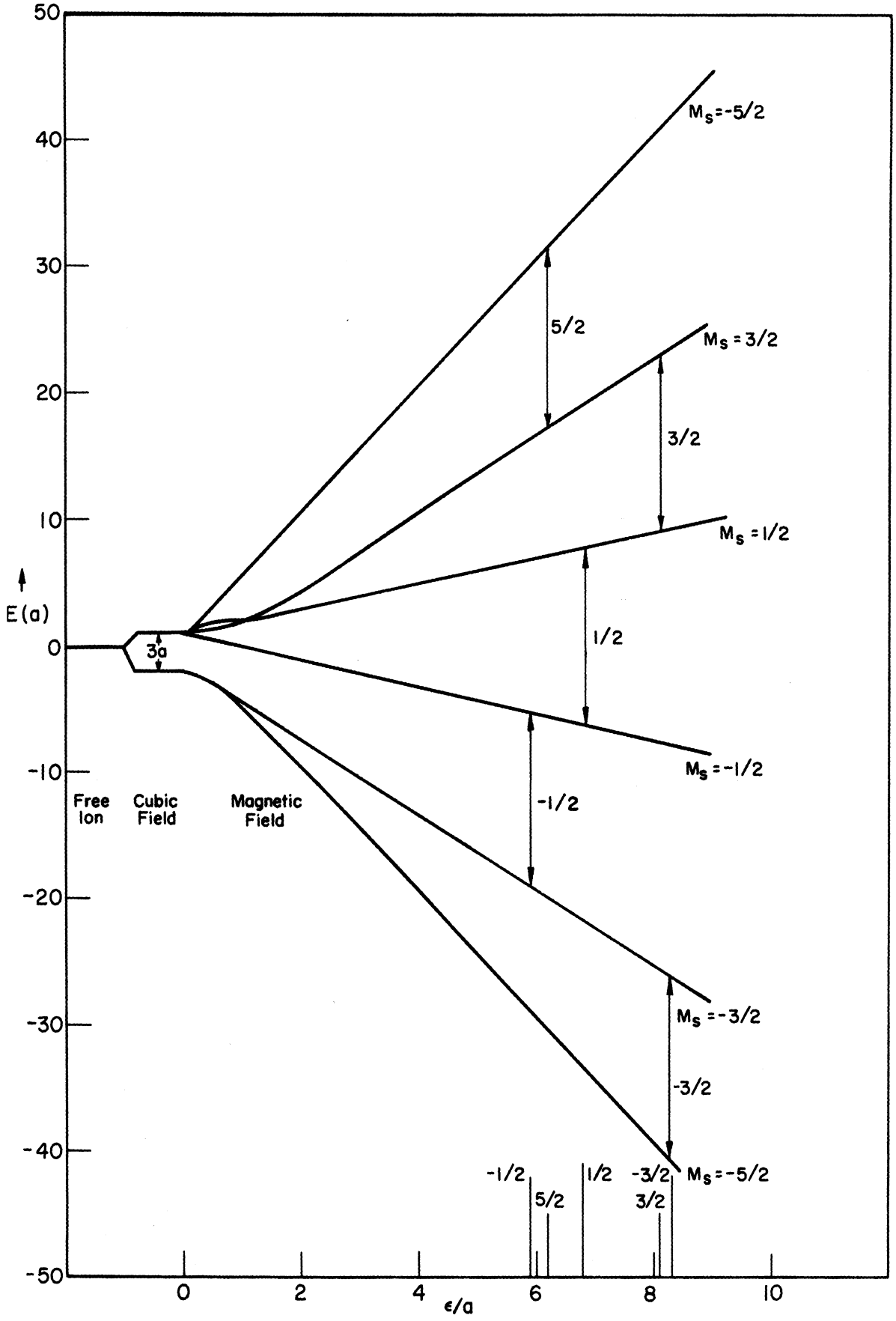

Fig. 15. Energy level scheme of $3d^5\ {}^6S_{5/2}$ (Mn^{++}) in a tetrahedral field at $\theta = 0°$.

For the case where H has direction cosines α, β, and γ with coordinate axes,

$$g\beta\underline{H}\cdot\underline{S} = g\beta[H_zS_z + \frac{1}{2}(H_+S_- + H_-S_+)] = 2\epsilon(\gamma S_z + \lambda_+S_- + \lambda_-S_+) \tag{67}$$

where

$$2\epsilon = g\beta H \quad \text{and} \quad \lambda_\pm = (\alpha \pm i\beta)/2 \tag{68}$$

and the energy levels are[14]

$$\begin{aligned} E_{\pm 1/2} &= pa \pm \epsilon + r_1a^3/\epsilon^2 \pm q_1a^2/\epsilon \\ E_{\pm 3/2} &= -3pa/2 \pm 3\epsilon + r_2a^3/\epsilon^2 \pm q_2a^2/\epsilon \\ E_{\pm 5/2} &= 5pa/2 \pm 5\epsilon + r_3a^3/\epsilon^2 \pm q_3a^2/\epsilon \end{aligned} \tag{69}$$

where

$$\begin{aligned} p &= [1 - (\alpha^2\beta^2 + \beta^2\gamma^2 + \gamma^2\alpha^2)] = 1 - \delta \\ q_1 &= -5\delta(7 - 25\delta)/6 \\ q_2 &= 5[1 + \delta(22 - 75\delta)]/32 \\ q_3 &= 5[1 + \delta(50 - 113\delta)/3]/32 \end{aligned} \tag{70}$$

and

$$\begin{aligned} r_1 &= -5\delta(196 - 1635\delta + 3125\delta^2)/144 \\ r_2 &= 5[1 + 3\delta(79 - 615\delta + 1125\delta^2)]/128 \\ r_3 &= -5[1 - 5\delta(113 - 705\delta + 1075\delta^2)/9]/128 \end{aligned} \tag{71}$$

D. HYPERFINE SPLITTING

The hyperfine splitting Hamiltonian for a cubic field is:

$$\mathcal{H}_{hf.s.} = \underline{S}\cdot A\cdot\underline{I} = A\underline{S}\cdot\underline{I} = AS_zI_z + A(S_+I_- + S_-I_+)/2 \tag{72}$$

The exact energy to be assigned to each state M,m requires solution of a 36 x 36 secular equation. An approximate method is to use time-independent perturbation theory up to a sufficiently high order with respect to the diagonalized Hamiltonian for $H\|Z\|S_4$.

Let

$$\mathcal{H} = \mathcal{H}_o + \mathcal{H}_1 \tag{73}$$

$$\mathcal{H}_o = g\beta HS_Z \tag{74}$$

$$\mathcal{H}_1 = AS_ZI_Z + A(S_+I_- + S_-I_+)/2 + \mathcal{H}_{crystalline} \tag{75}$$

Then, taking free ion energy as zero, one has:

$$E_{M,m} = E^{(0)}_{M,m} + E^{(1)}_{M,m} + E^{(2)}_{M,m} \tag{76}$$

where

$$E^{(0)}_{M,m} = \langle M,m|\mathcal{H}_o|M,m\rangle \tag{77}$$

$$E^{(1)}_{M,m} = \langle M,m|\mathcal{H}_1|M,m\rangle \tag{78}$$

$$E^{(2)}_{M,m} = \sum_{M',m'}{}' \; |\langle M,m|\mathcal{H}_1|M',m'\rangle|^2/[E^{(0)}_{M,m} - E^{(0)}_{M',m'}] \tag{79}$$

Then the energy associated with each level M,m is given by

$$E_{M,m}(\Theta = 0) = E^{f.s.}_M + E^{hf.s.}_{M,m}$$

where

$$E^{hf.s.}_{M,m} \cong E^{(1)}_{M,m} + E^{(2)}_{M,m} \tag{80}$$

The values of $E^{f.s.}_{M,m}$ are given by Eq. (66) and $E^{(1)}_{M,m}$ and $E^{(2)}_{M,m}$ are:

$$E^{(1)}_{M,m} = AM,m \tag{81}$$

$$E^{(2)}_{M,m} = \sum_{M',m'}{}' \; | < M,m|A(S_+I_-+S_-I_+)/2|M',m'>|^2/[E^{(0)}_{M,m} - E^{(0)}_{M',m'}]$$

$$= \frac{A^2}{4} \sum (< M,m|S_+I_-|M',m'>< M,m|S_-I_+|M',m'>)$$

$$(x) < M',m'|S_+I_- + S_-I_+|M,m >/[E^{(0)}_{M,m} - E^{(0)}_{M',m'}] \tag{82}$$

$$= \frac{A^2}{4} < M,m|S_+I_-|M-1,m+1 > < M-1,m+1|S_-I_+|M,m >/[E^{(0)}_{M,m} - E^{(0)}_{M-1,m+1}]$$

$$+ \frac{A^2}{4} < M,m|S_-I_+|M+1,m-1 > < M+1,m-1|S_+I_-|M,m >/[E^{(0)}_{M,m} - E^{(0)}_{M+1,m-1}]$$

Consider

$$\begin{aligned} S_+I_-|M-1,m+1> &= [S^{*2} - (M-1)M]^{1/2}[I^{*2} - (m+1)m]^{1/2}|M,m > \\ S_-I_+|M,m > &= [S^{*2} - M(M-1)]^{1/2}[I^{*2} - m(m+1)]^{1/2}|M-1,m+1 > \\ \text{and} \qquad S_-I_+|M+1,m-1 > &= [S^{*2} - (M+1)M]^{1/2}[I^{*2} - (m-1)m]^{1/2}|M,m > \\ S_+I_-|M,m > &= [S^{*2} - M(M+1)]^{1/2}[I^{*2} - m(m-1)]^{1/2}|M+1,m-1 > \end{aligned} \tag{83}$$

Consider also

$$E^{(0)}_{M,m} \cong g\beta HM, \qquad E^{(0)}_{M\pm1,m\mp1} \cong g\beta H(M\pm1), \qquad E^{(0)}_{M,m} - E^{(0)}_{M\mp1,m\pm1} = \pm g\beta H \tag{84}$$

Substituting Eqs. (82) and (83) in Eq. (84), one finds:

$$E^{(2)}_{M,m} = \frac{A^2}{4}\left[\frac{(S^{*2}-M^2+M)(I^{*2}-m^2-m)}{g\beta H} - \frac{(S^{*2}-M^2-M)(I^{*2}-m^2+m)}{g\beta H}\right]$$

$$= \frac{A^2}{4g\beta H}\left[M(I^{*2}-m^2) - m(S^{*2}-M^2) + M(I^{*2}-m^2) - m(S^{*2}-M^2)\right] \qquad (85)$$

$$= \frac{A^2}{2g\beta H}\left\{M[I(I+1) - m^2] - m[S(S+1) - M^2]\right\}$$

Considering Eqs. (67), (75), (80), (81), and (85) one finds for $(H\|Z\|S_4)$:

$$E_{5/2,m} \cong \epsilon - \frac{a}{2} + \sqrt{(4\epsilon+a)^2+5a^2/4} + 5Am/2 + A^2[5(35/4-m^2)/2-5m/2]/2g\beta H$$

$$E_{3/2,m} \cong -\epsilon - \frac{a}{2} + \sqrt{(4\epsilon-a)^2+5a^2/4} + 3Am/2 + A^2[3(35/4-m^2)/2-13m/2]/2g\beta H$$

$$E_{1/2,m} \cong \epsilon + a + Am/2 + A^2[(35/4-m^2)/2-17m/2]/2g\beta H \qquad (86)$$

$$E_{-1/2,m} \cong -\epsilon + a - Am/2 + A^2[-(35/4-m^2)/2-17m/2]/2g\beta H$$

$$E_{-3/2,m} \cong \epsilon - \frac{a}{2} - \sqrt{(4\epsilon+a)^2+5a^2/4} - 3Am/2 + A^2[-3(35/4-m^2)/2-13m/2]/2g\beta H$$

$$E_{-5/2,m} \cong -\epsilon - \frac{a}{2} - \sqrt{(4\epsilon-a)^2+5a^2/4} - 5Am/2 + A^2[-5(35/4-m^2)/2-5m/2]/2g\beta H$$

For a given m there are six energy levels; therefore five absorption transitions will occur, giving rise to five resonance lines corresponding to a given m and to different M values. The ESR spectrum of Mn^{++} clearly shows this feature (see Fig. 16).

Considering Fig. 16 one notes that associated with each m the spectrum at $\Theta = 0$ has the form shown in Fig. 17. To identify the M values to which the lines α, β, γ, δ, and λ are associated we must find the intensity I_M of each line. This is proportional to magnetic dipole absorption probability;

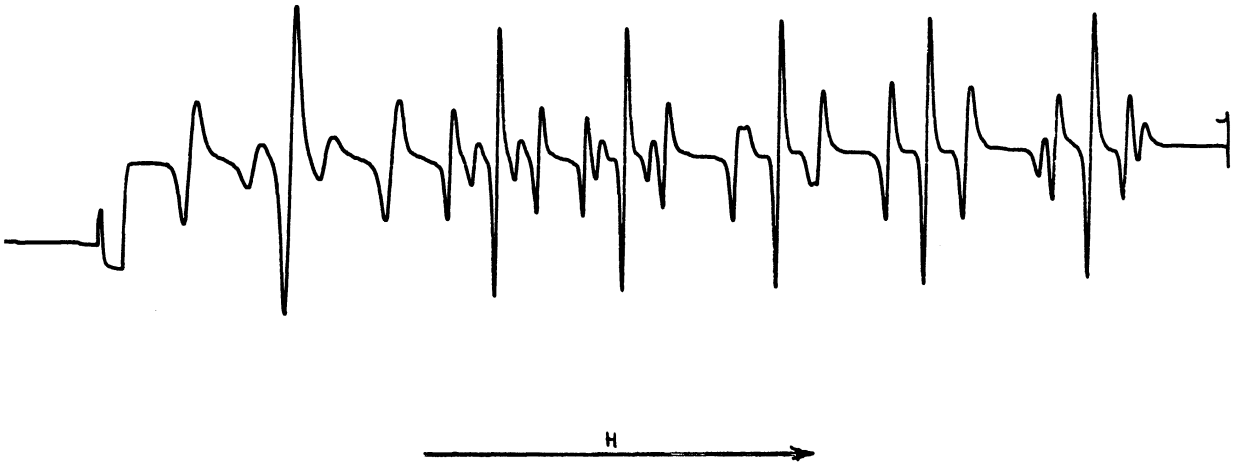

Fig. 16. Mn^{++} ESR spectrum in ZnS (cubic) at 300°K, $\theta = 0°$.

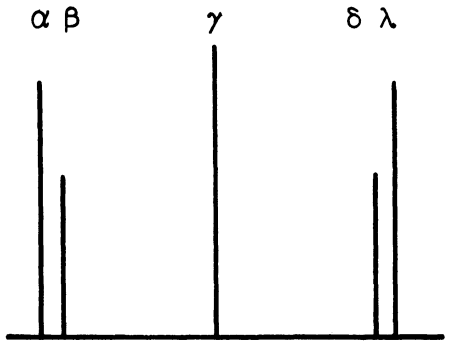

Fig. 17. Mn^{++} ESR due to a given m.

and the ratio of intensities of two lines is as follows:[15]

$$\frac{I_M}{I_{M'}} = \frac{|< M\text{-}1|\underline{r}K\cdot\underline{r}|M >|^2}{|<M'\text{-}1|\underline{r}K\cdot\underline{r}|M'>|^2} \tag{87}$$

But, from replacement theory, vectors of position and linear momentum can be substituted by angular momentum operators $\underline{L}$ or $\underline{S}$, namely

$$\underline{\hat{r}}\underline{\hat{K}}\cdot\underline{\hat{r}} = \underline{\hat{r}}\,\frac{1}{\hbar}\,\underline{P}\cdot\underline{\hat{r}} \propto \underline{\hat{L}}\underline{\hat{L}}\cdot\underline{\hat{L}} = \hat{L}L^{*2} \text{ or } \hat{S}S^{*2} \tag{88}$$

where

$$\underline{\hat{S}} = \hat{S}_z + \xi_- S_+ + \xi_+ S_- \qquad \xi_\pm = (1\pm i)/2 \qquad i = \sqrt{-1}$$

and

$$\frac{I_M}{I_{M'}} = \frac{\langle M-1|\xi_+ S_-|M\rangle\langle M|\xi_- S_+|M-1\rangle}{\langle M'-1|\xi_+ S_-|M'\rangle\langle M'|\xi_- S_+|M'-1\rangle} = \frac{S(S+1) - M(M-1)}{S(S+1) - M'(M'-1)}$$

Thus

$$I_{5/2}:I_{3/2}:I_{1/2}:I_{-1/2}:I_{-3/2} = 5:8:9:8:5 \tag{89}$$

Note also that the separation of the measured magnetic field corresponding to each line with intensity I_M, $\sigma_{MM'}$, ρ for $\theta = 0$ can be obtained as follows:

$$E_{M,m} - E_{M-1,m} = g\beta H_{M,m} + f'_{M,m} = g\beta H_o = h\nu_o \text{ for all } M,m \tag{90}$$

Thus

$$\frac{E_{M,m}-E_{M-1,m}}{g\beta} = \frac{E_{M',m}-E_{M'-1,m}}{g\beta} \Longrightarrow H_{M,m} + f_{M,m} = H_{M',m} + f_{M',m} \tag{91}$$

or

$$\sigma_{MM'} = H_{M',m} - H_{M,m} = f_{M,m} - f_{M',m} \qquad f = f'/g\beta \tag{92}$$

where $f'_{M,m}(A,a)$'s are given in Eq. (86) and one considers the fact that in $A_{II}B_{VI}$ compounds $|a_{Mn^{++}}| < |A_{Mn^{++}}|$, $f_{M,m}$ must be found up to a^2, i.e.,

$$\sqrt{(4\epsilon \pm a)^2 + 5a^2/4} \;\cong\; 4\epsilon \pm a + 5a^2/16g\beta H \qquad g\beta H = 2\epsilon \tag{93}$$

Substituting Eq. (93) into Eq. (86) one finds $\sigma_{MM'}$'s, e.g.,

$$\sigma_{1/2,5/2} = \sigma_{5/2} = H_{5/2} - H_{1/2} = f_{1/2} - f_{5/2} \tag{94}$$

where

$$f_{1/2} = \frac{E_{1/2} - E_{-1/2}}{g\beta} - H_{1/2}$$

Equations (86) give

$$\frac{E_{1/2} - E_{-1/2}}{g\beta} = \frac{2\epsilon + mA + A^2(35/4 - m^2)/2g\beta H}{g\beta}; \quad 2\epsilon/g\beta = H_{1/2} \tag{95}$$

Thus

$$f_{1/2} = mA' + A'^2[(35/4 - m^2)]/2H \qquad A' = A/g\beta, \quad a' = a/g\beta$$

and

$$f_{5/2} = mA' + 2a' + A'^2(35/4 - m^2 + 8m)$$

Therefore

$$\sigma_{5/2} = -2a' - 2mA'^2/H$$

Similarly

$$\begin{aligned} \sigma_{3/2} &= 5a'/2 - 5a'^2/16H - mA'^2/H \\ \sigma_{1/2} &= 0 \\ \sigma_{-1/2} &= -5a'/2 - 5a'^2/16H + mA'^2/H \\ \sigma_{-3/2} &= 2a' + 2mA'^2/H \end{aligned} \tag{96}$$

Considering Eqs. (89) and (96), and also the fact that the two fine-structure components tend to merge (see Figs. 17 and 18) at higher field one can deter-

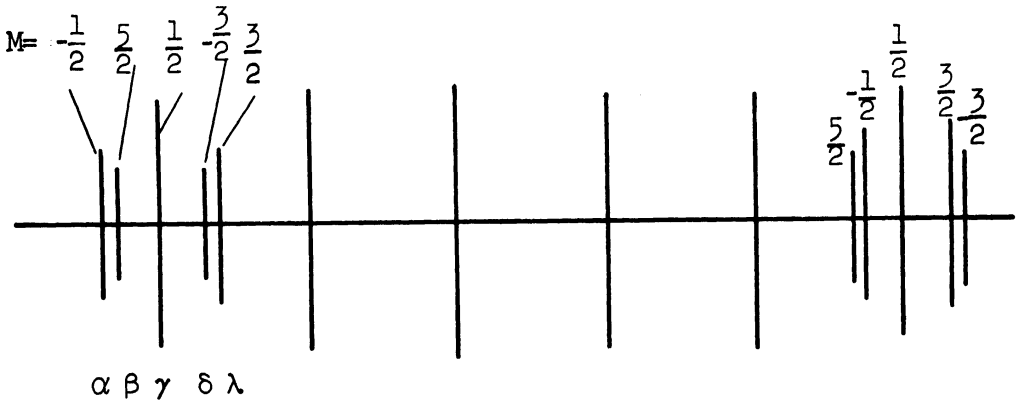

Fig. 18. Schematic plot of fine structure of ESR spectrum of Mn^{++} in cubic ZnS for m = -5/2 and 5/2.

mine that A and a have opposite signs. According to Watanabe[5] a $\propto (Dq)^2$ and thus $A < 0$. Since $(|5a'/2|)/(|5A'^2/H|)$ is 8, 28, and 29 for ZnS, CdTe, and ZnTe respectively, the measured DC magnetic field determines the M to be assigned to the lines α, β, γ, δ, λ; e.g., α corresponds to the M giving maximum separation, etc. The result (see Fig. 18) is

$$\alpha \rightarrow M = -1/2; \quad \beta \rightarrow 5/2; \quad \gamma \rightarrow 1/2; \quad \delta \rightarrow -3/2; \quad \lambda \rightarrow 3/2 \qquad (97)$$

Consider Eqs. (91) and (95), as well as the fact that $A' \leq 0$ and

$$H_{M,m'} - H_{M,m} = f_{M,m} - f_{M,m'}$$

Then

$$H_{1/2,m'} - H_{1/2,m} = A'(m-m') + A'^2(m'^2-m^2)/2H_0 \begin{cases} > 0 & m' > m \\ < 0 & m' < m \end{cases} \qquad (98)$$

Therefore, the lowest group of five fine-structure components α, β, γ, δ, and λ (see Fig. 18) belongs to m = -5/2, where the group at the high-side

field belongs to m = +5/2.

E. DETERMINATION OF $3a = {}^4\Gamma_8 - {}^2\Gamma_7$ PARAMETERS

The ${}^6S_{5/2}$ electronic level of the Mn^{++} ion is split into two levels, ${}^4\Gamma_8$ and ${}^2\Gamma_7$, due to the presence of a cubic field. This energy difference is easily obtained from Eq. (96):

$$\frac{3}{5}\left[|\sigma(M = -1/2, m = -5/2)| + |\sigma(M = 3/2, m = 5/2)|\right]$$

$$= \frac{3}{5}\left[|-5a'/2 - 5a'^2/16H - 5A'^2/2H| + |5a'/2 - 5a'^2/16H - 5A'^2/2H|\right]$$

$$= 3[|5a'/2 + 5a'^2/16H + 5A'^2/2H| + |5a'/2 - 5a'^2/16H - 5A'^2/2H|]/5 = 3a'$$

and

$$3a = g\beta\ 3a'(\text{erg}), \quad 3a'(\text{gauss}), \quad \text{or} \quad \frac{3a'g\beta}{hc}\ (\text{cm}^{-1}) \tag{99}$$

F. DETERMINATION OF HYPERFINE SPLITTING CONSTANT A'

Equation (98) gives

$$H_{1/2,5/2} - H_{1/2-5/2} = -5A' \qquad A' = -1/5\ (H_{1/2,5/2} - H_{1/2-5/2}) < 0 \tag{100}$$

$$A = g\beta A'(\text{erg}) \quad \text{or} \quad A'(\text{gauss}) \quad \text{or} \quad g\beta A'/hc \quad \text{in } (\text{cm}^{-1})$$

APPENDIX A

DETERMINATION OF Mn^{++} GROUND STATE

The electronic configuration of Mn^{++} is

$$1s^2\ 2s^2\ 2p^6\ 3s^2\ 3p^6\ 3d^5 \tag{A-1}$$

According to Griffith[16] the relative energy levels of the ion can be obtained by considering only the last five electrons in the partially filled shell of 3d. The energy terms corresponding to these electrons can be found simply by the "counting method." This method consists of setting up a table with possible positive M_S and M_L values in rows and columns, respectively, with determining the number of times that each M_S occurs for a given M_L by constructing all possible wavefunctions corresponding to M_L. In Eq. (A-2) a set of wave functions of $M_L = 2$ is given.

$$\begin{aligned}
&|2^+\ 2^-\ 1^+\ -1^+\ -2^+\rangle \quad \text{with} \quad M_L = 2 \quad \text{and} \quad M_S = 3/2 \\
&|2^+\ 2^-\ 1^+\ -1^+\ -2^-\rangle \quad \text{with} \quad M_L = 2 \quad \text{and} \quad M_S = 1/2 \\
&|2^+\ 2^-\ 1^+\ -1^-\ -2^+\rangle \quad \text{with} \quad M_L = 2 \quad \text{and} \quad M_S = 1/2 \\
&|2^+\ 2^-\ 1^-\ -1^+\ -2^+\rangle \quad \text{with} \quad M_L = 2 \quad \text{and} \quad M_S = 1/2
\end{aligned} \tag{A-2}$$

One can, with the same procedure, find that there are nine other wave functions with $M_S = 1/2$ and two more with $M_S = 3/2$. The result for other M_L values can be obtained much easier; they are given in Table A-I. Among the sixteen terms in Table A-I the sextet ^6S and quartets ^4G, ^4F, ^4D and ^4P are the most responsible terms which account for the observed optical and EPR

TABLE A-I

$M_S M_L$ TABLE FOR $3d^5$ CONFIGURATION

M_L \ M_S	Total Number			Difference			Energy Terms
	1/2	3/2	5/2	1/2	3/2	5/2	
6	1	0	0	1	0	0	^2I
5	2	0	0	1	0	0	^2H
4	5	1	0	3	1	0	^2G, ^2G and ^4G
3	8	2	0	3	1	0	^2F, ^2F and ^4F
2	12	3	0	4	1	0	^2D, ^2D, ^2D and ^4D
1	14	4	0	2	1	0	^2P and ^4P
0	16	5	1	2	1	1	^2S and ^6S

experimental results. According to Racah[12] these terms can be calculated from the terms of $3d^2$ because $3d^5$ is an $n\ell^{2\ell+1}$ configuration and because the sextet and quartet terms have the spin $S = \ell+1/2$ and $S = \ell-1/2$. The $3d^2$ $M_S M_L$ table (Table A-II) reveals that for $3d^2$ there are five energy terms,

$$^1G,\ ^3F,\ ^1D,\ ^3P \text{ and } ^1S\ , \tag{A-3}$$

whose energies can be obtained by using the diagonal-sum rule. In this way one finds the sum of the energies of several terms from the relation:

$$|\mathcal{H}_{ij} - E\delta_{ij}| \equiv 0 \equiv \prod_{\sigma=1}^{p} P_\sigma \tag{A-4}$$

where P_σ is a polynomial of m_σth power provided

$$\sum_{\sigma=1}^{p} m_\sigma = n'$$

TABLE A-II

$M_S M_L$ TABLE FOR $3d^2$ CONFIGURATION

M_L \ M_S	Total Number		Difference		Energy Terms
	1	0	1	0	
4	0	1	0	1	^1G
3	1	2	1	1	^3F
2	1	3	0	1	^1D
1	2	4	1	1	^3P
0	2	5	0	1	^1S

with n' the number of electrons in the partially filled shell ($n' \leq 2\ell+1$).

Each P_σ satisfies the relation

$$P_\sigma = E^{m_\sigma} - E^{m_\sigma - 1} \sum_{i=1}^{m_\sigma} \mathcal{H}_{ii} + \cdots = 0 \qquad \text{(A-5)}$$

The coefficient of $-E^{m_\sigma - 1}$ in Eq. (A-5) is the desired diagonal-sum which we must find. It can be obtained from the relation

$$\sum_{i=1}^{m_\sigma} \mathcal{H}_{ii} = \sum_{\kappa,\lambda} J(\kappa,\lambda) \qquad \text{(A-6)}$$

where $J(\kappa,\lambda)$ is the coulomb integral defined as

$$J(i,j) = \sum_{k=0}^{\infty} a^k(i,j) F^k(i,j) \qquad \text{(A-7)}$$

F^k is the so-called Slater-Condon parameter which for a pair of electrons i and j with the same n and ℓ takes the form

$$F^k_{n\ell}(i,j) = e^2 \int_0^\infty \int_0^\infty (r_<^k / r_>^{k+1}) [R_{n\ell}(i)]^2 [R_{n\ell}(j)]^2 r_i^2 r_j^2 \, dr_i dr_j \qquad \text{(A-8)}$$

and $a^k(i,j)$ in this case (same n and ℓ) can be given as:

$$a^k(i,j) = c^k_\ell(m^i,m^i) c^k_\ell(m^j,m^j) \qquad \text{(A-9)}$$

with

$$c^k_\ell(m,m') = \left[\frac{4\pi}{(2k+1)}\right]^{1/2} \int_0^{2\pi} \int_0^{\pi} Y^*_{\ell m}(\theta,\phi) \; Y_{km-m'}(\theta,\phi) \; Y_{\ell m'}(\theta,\phi) \sin\theta \, d\theta d\phi \qquad \text{(A-10)}$$

From the diagonal-sum rule which is described in Eqs. (A-4), (A-5), and (A-6) we can write the energies of the terms of $3d^2$ as follows:

$$E(^1G) = J(2,2) \qquad \text{(A-11a)}$$

$$E(^3F) + E(^1G) = J(2,1) + J(1,2) \qquad \text{(A-11b)}$$

$$E(^1D) + E(^3F) + E(^1G) = J(2,0) + J(1,1) + J(0,2) \qquad \text{(A-11c)}$$

$$E(^3P) + E(^1D) + E(^3F) + E(^1G) = J(2,-1) + J(1,0) + J(0,1) + J(-1,2) \qquad \text{(A-11d)}$$

and

$$E(^1S) + E(^3P) + E(^1D) + E(^3F) + E(^1G) = J(2,-2) + J(1,-1) + J(0,0) + J(-1,1) + J(-2,2) \qquad \text{(A-11e)}$$

Equations (A-6)-(A-10) reveal that J(i,j)'s of Eqs. (A-11) can be obtained from the much simpler relation

$$J(i,j) = \sum_{k=0}^{\ell} a^{2k} F^{2k} = \sum_{k=0}^{\ell} a_{2k} F_{2k} = a_0 F_0 + a_2 F_2 + a_4 F_4 \qquad \text{(A-12)}$$

In Table A-III the integrals J(i,j) of Eqs. (A-11) are given in terms of the coefficients A, B, and C defined as

$$A = F_o - 49F_2 \tag{A-13a}$$

$$B = F_2 - 5F_4 \tag{A-13b}$$

$$C = 35F_4 \tag{A-13c}$$

TABLE A-III

J(m,m') INTEGRALS IN TERMS OF A, B, AND C

m	m'	J(m,m')
2	±2	A + 4B + 2C
2	±1	A - 2B + C
2	0	A - 4B + C
1	±1	A + B + 2C
1	0	A + 2B + C
0	0	A + 4B + 3C

Substituting for J(i,j) in Eqs. (A-11) one finds the relative energy levels as follows:

$$E(^1G) = A + 4B + 2C \tag{A-14a}$$

$$E(^3F) = A - 8B \tag{A-14b}$$

$$E(^1D) = A - 3B + 2C \tag{A-14c}$$

$$E(^3P) = A + 7B \qquad \text{(A-14d)}$$

$$E(^1S) = A + 14B + 7C \qquad \text{(A-14e)}$$

Equations (A-14) reveal that the relative energy levels for the terms with $S = n'/2$ (n' being the number of electrons) can be express as[16]

$$E[d^{n'}, {}^{n'+1}T(L)] = n'(n'-1)(A-8B)/2 + 3[6n' - L(L+1)]B/2 \qquad \text{(A-15)}$$

and therefore the energy of the triplets of $3d^2$, quartets of $3d^3$, quintets of $3d^4$ and sextets of $3d^5$ can be found easily, e.g.,

$$E(d^5, {}^6S) = 10A - 35B \qquad \text{(A-16)}$$

The energies of the quartets of $3d^5$ cannot be obtained as easily, it can, however, be shown that they may be derived from Eqs. (A-14). Consider that each quartet of d^5 has four electrons with α spin and one with β spin. We construct the wave functions $\phi_1(m,m')$ of the quartet ^4F of d^5 so that, compared with the wave functions $\psi_1(m^1 \cdots m^6)$ of the quintet ^5D of d^6

$$\psi_1(m^1 \cdots m^6, d^6, {}^5D) = |2^+\ 2^-\ 1^+\ 0^+\ -1^+\ -2^+\rangle\ , \qquad \text{(A-17)}$$

it will have the form

$$\phi_1(m^1 \cdots m^5, d^5, {}^4F) = \phi_1(2,1) = |2^+\ 2^-\ 1^+\ 0^+\ -2^+\rangle\ . \qquad \text{(A-18)}$$

In Eq. (A-18), $m(2)$ stands for the m_ℓ of one-electron wave function with β spin and $m'(1)$ stands for the $-m_\ell$ of the extra electron in the quintet ^5D of d^6 configuration. The diagonal elements of $\phi(m,m')$ can be obtained by relating

them to the corresponding elements of the ^5D terms of d^4 and d^6 configurations. These terms can be found from the relation[16]

$$E(d^6,{}^5D) = \sum_{\kappa<\lambda=2}^{6} [J(m^\kappa,m^\lambda) - K(m^\kappa,m^\lambda)]$$

$$= \sum_{\kappa<\lambda=2}^{5} [J(m^\kappa,m^\lambda) - K(m^\kappa,m^\lambda)] + \sum_{\kappa=0}^{5} [J(m^\kappa,m^6) - K(m^\kappa,m^6)] \qquad \text{(A-19)}$$

$$= E[\phi(m,m')] + J(m,m') - K(m,m') + \sum_{\kappa=1}^{5} f(m^\kappa,m^\lambda)$$

where

$$K(m,m') = \delta(\underline{s},\underline{s}') \sum_{k=0}^{2} b^{2k} F_{n\ell}^{2k} = 0 \qquad \underline{s} \neq \underline{s}' \qquad \text{(A-20a)}$$

and

$$f(m^\kappa,m^\lambda) = J(m^\kappa,m^\lambda) - K(m^\kappa,m^\lambda). \qquad \text{(A-20b)}$$

Thus Eq. (A-19) can be rewritten as

$$E(d^6,{}^5D) = E[\phi(m,m')] + J(m,m') + \sum_{\kappa=1}^{5} f(m^\kappa,-m'). \qquad \text{(A-21)}$$

We have also

$$E(d^5,{}^6S) = \sum_{\kappa<\lambda=2}^{5} [J(m^\kappa,m^\lambda) - K(m^\kappa,m^\lambda)]$$

$$= \sum_{\kappa=1}^{5} f(m^\kappa,m2) + \sum_{\kappa<\lambda=3}^{5} f(m^\kappa,m^\lambda) \qquad (A\text{-}22)$$

$$= \sum_{\kappa=1}^{5} f(m^\kappa,-m') \sum_{\kappa<\lambda=2}^{4} f(m^\kappa,m^\lambda)$$

$$= \sum_{\kappa=1}^{5} f(m^\kappa,-m') + E(d^4,{}^5D)$$

A comparison of Eqs. (A-21) and (A-22) gives:

$$E[\phi(m,m')] = E(d^6,{}^5D) + E(d^4,{}^5D) - E(d^6,{}^6S) - J(m,m') \qquad (A\text{-}23)$$

Equation (A-23) gives the energy levels associated with the sextet and the quartets of Mn^{++} and Fe^{+++} within a constant which can be found by considering Eqs. (A-14), (A-16), and (A-23) for the case where $M_L = m+m' = 0$:

$$E[\phi(m,m'), M_L = 0] = E(d^5,{}^6S) = C' - E(d^2,{}^1S) \qquad (A\text{-}24)$$

where

$$C' = E(d^5,{}^6S) + E(d^2,{}^1S) = 10A - 35B + A + 14B + 7C$$

$$= 11A - 21B + 7C \; . \qquad (A\text{-}25)$$

Equations (A-24) and (A-25) reveal that

$$E[d^5,{}^4T(L)] = 11A - 21B + 7C - E[d^2,{}^{2S+1}T(L)] \qquad (A\text{-}26)$$

Substituting from Eqs. (A-14) for $E[d^2, {}^{2S+1}T(L)]$ we find the relative energies of the quartets ^4G, ^4F, ^4D and ^4P of $3d^5$ configuration

$$E(^4G) = 10A - 25B + 5C \qquad \text{(A-27a)}$$

$$E(^4F) = 10A - 13B + 7C \qquad \text{(A-27b)}$$

$$E(^4D) = 10A - 18B + 5C \qquad \text{(A-27c)}$$

$$E(^4P) = 10A - 28B + 7C \qquad \text{(A-27d)}$$

The relative energies of these levels for the case B/C = .5 and in units of C can be computed with the result as

$$\frac{E[d^5, {}^{2S+1}T(L);\ B/C = .5] - 10A}{C} = \begin{cases} 0.5 & \text{for } {}^4F & \text{(A-28a)} \\ -4.0 & \text{for } {}^4D & \text{(A-28b)} \\ -7.0 & \text{for } {}^4P & \text{(A-28c)} \\ -7.5 & \text{for } {}^4G & \text{(A-28d)} \\ -17.5 & \text{for } {}^6S & \text{(A-28e)} \end{cases}$$

A careful study of Fig. 4.4, Ref. 16, indicates that only at $B/C \leq .08$ do the quartets lie lower compared with the doublets; but even at this region Hund's Rule does not hold completely, and the ^4D is lower than ^4F.

APPENDIX B

REDUCTION OF THE $\mathcal{H}_t$-$\mathcal{H}_1$ TO A FUNCTION OF $\underline{L}$, $\underline{S}$ AND $\underline{I}$

To derive the spin Hamiltonian Eq. (35), use is made of the replacement theory:[17]

$$(\alpha' Km' |\underline{I}|\alpha Km) = \frac{(\alpha' K\|\underline{L}\cdot\underline{I}\|\alpha K)}{L(L+1)} (Km' |\underline{L}|Km)$$
$$= B(\alpha',\alpha)(Km' |\underline{L}|Km) \ . \tag{B-1}$$

where $\underline{I}$ can represent such vectors as $\underline{r}$ or $\underline{p}$. Thus we can replace the position coordinates with angular momentum components as follows:

$$x \to L_x, \quad xy = (L_xL_y+L_yL_x)/2, \quad x^n \to L_x^n \ , \tag{B-2}$$

$\mathcal{H}_2$ [Eq. (9)] is already independent of position vector and assuming that Russel-Saunders coupling holds and that $b_{ii} \gg b_{ij}$, it will take the form:

$$\mathcal{H}_2 = K\, \underline{L}\cdot\underline{S} \tag{B-3}$$

where K is a constant, $\underline{L}$ is total angular momentum and $\underline{S}$ is the total spin.

$\mathcal{H}_3$ [Eq. (10)] is one of the Hamiltonians containing position vectors $\underline{r}^{ij}$ in conjunction with $\underline{s}^i$ and $\underline{s}^j$. To replace position coordinates with the components of angular momentum we expand $\mathcal{H}_3$ as follows:

$$\mathcal{H}_3 = \sum_{i>j}^{n} 4\beta^2 r_{ij}^{-5}[r_{ij}^2(s_x^is_x^j+s_y^is_y^j+s_z^is_z^j) - 3(\xi s_x^i+\eta s_y^i+\zeta s_z^i)(\xi s_x^j+\eta s_y^j+\zeta s_z^j)] \tag{B-4}$$
$$= R_x + R_y + R_z$$

where ξ, η and ζ are the Cartesian coordinates of $\underline{r}^{ij}$ and

$$R_X = \sum_{i>j}^{n} 4\beta^2 r_{ij}^{-5} \left\{ r_{ij}^2 s_X s_X - 3[\xi^2 s_X^i s_X^j + \eta\zeta(s_y^i s_z^j + s_z^i s_y^j)] \right\} \tag{B-5}$$

$$= \sum_{i>j}^{n} C_1(i,j) \left\{ L(L+1) s_X^i s_X^j - 3[L_X^2 s_X^i s_X^j + \tfrac{1}{2}(L_y L_z + L_z L_y)(s_y^i s_z^j + s_z^i s_y^j)] \right\}$$

Recalling that

$$\overline{s_X^i s_X^j} = \alpha_i S_X \alpha_j S_X = \beta_{ij} S_X^2 , \tag{B-6}$$

by substituting for $s_X^i s_X^j$ in Eq. (B-5) one finds:

$$R_X = \sum_{i>j}^{n} C_1(i,j)\beta_{ij} \left\{ L(L+1) S_X^2 - 3[L_X^2 S_X^2 + \tfrac{1}{2}(L_y L_z + L_z L_y)(S_y S_z + S_z S_y)] \right\}$$

$$= -\overline{r^{-3}}\, p[3 L_X^2 S_X^2 + \tfrac{3}{2}(L_y L_z + L_z L_y)(S_y S_z + S_z S_y) - L^{*2} S_X^2] \tag{B-8}$$

$$= -\overline{r^{-5}}\, p[(3L_X^2 - L^{*2}) S_X^2 + \tfrac{3}{2}(iL_X + 2L_z L_y)(-iS_X + 2S_y S_z)]$$

$$= -\overline{r^{-5}}\, p[(3L_X^2 - L^{*2}) S_X^2 + \tfrac{3}{2}(L_X S_X + 6 L_z L_y S_y S_z)] + \cdots$$

The result for R_y and R_z can be obtained from R_X [Eq. (B-8)] and $\mathcal{H}_3$ can be expressed as

$$\mathcal{H}_3(L,S) = -M[(\underline{L}\cdot\underline{S})^2 + \tfrac{1}{2}(\underline{L}\cdot\underline{S}) - L(L+1)S(S+1)/3] \tag{B-9}$$

Since $\mathcal{H}_4$ [Eq. (11)] is already given in terms of L and S, $\mathcal{H}_5$ [Eq. (12)] will be considered now. Each of the three parts $r_{ij}^2(\underline{\ell}^i - \underline{s}^i)\cdot\underline{I}$, $3\underline{r}^i\cdot\underline{s}^i\underline{r}^i\cdot\underline{I}$ and $8\pi\delta(r^i)s^i\cdot I/3$ will be treated separately as follows:

$$\mathcal{H}_5' = N' \sum_i \frac{(\underline{\ell}^i - \underline{s}^i)\cdot \underline{I}}{r_i^3} \longrightarrow N'(\underline{L}\cdot\underline{I} - \kappa \underline{S}\cdot\underline{I}) \qquad \text{(B-10)}$$

$$\mathcal{H}_5'' = N_1 \sum_i 3\underline{r}^i\cdot\underline{s}^i\ \underline{r}^i\cdot\underline{I}/r_i^5$$

$$= N_2[\tfrac{3}{2}(L_xS_xL_xI_x+L_xI_xL_xS_x+L_xS_xL_zI_z+L_zI_zL_xS_x+L_xS_xL_yI_y+L_yI_yL_zS_z)$$

$$+ \tfrac{3}{2}(x\to y, y\to x, z\to z) + \tfrac{3}{2}(x\to z, z\to x, y\to y)]$$

$$= \tfrac{3}{2} N''[(L_xS_x+L_yS_y+I_zS_z)(L_xI_x+L_yI_y+L_zI_z)$$

$$+ (L_xI_x+L_yI_y+L_zI_z)(L_xX_x+L_yS_y+L_zS_z)]$$

$$= \tfrac{3}{2} N''[\underline{L}\cdot\underline{S}\ \ \underline{L}\cdot\underline{I} + \underline{L}\cdot\underline{I}\ \underline{L}\cdot\underline{S}] \qquad \text{(B-11)}$$

$$\mathcal{H}_5''' = N_3 \sum_i \frac{8\pi}{3}\delta(\underline{r}^i)\underline{s}^i\cdot\underline{I} = N'''\, L^{*2}\ \underline{S}\cdot\underline{I} \qquad \text{(B-12)}$$

and finally we have

$$\mathcal{H}_5 = N\left\{a[L^{*2}\underline{S}\cdot\underline{I} - \tfrac{3}{2}(\underline{L}\cdot\underline{S}\ \underline{L}\cdot\underline{I} + \underline{L}\cdot\underline{I}\ \underline{L}\cdot\underline{S})] + \underline{L}\cdot\underline{I} - \kappa\ \underline{S}\cdot\underline{I}\right\} \qquad \text{(B-13)}$$

where N and a are constants. In the same way, $\mathcal{H}_6$ [Eq. (13)] can be changed into a function of $\underline{L}$, $\underline{S}$ and $\underline{I}$. The final result is

$$\mathcal{H}'(L,S,I) = \mathcal{H}_t - \mathcal{H}_1$$

$$= K\,\underline{L}\cdot\underline{S} - M[(\underline{L}\cdot\underline{S})^2 + \underline{L}\cdot\underline{S}/2 - L^{*2}S^{*2}/3]$$

$$+ \beta(\underline{L}+2\underline{S})\cdot\underline{H} - \gamma\beta_N\underline{I}\cdot\underline{H}$$

$$+ N\{a[L^{*2}\underline{S}\,\underline{I} - 3(\underline{L}\cdot\underline{S}\,\underline{L}\cdot\underline{I}+\underline{L}\cdot\underline{I}\,\underline{L}\cdot\underline{S})/2] + \underline{L}\cdot\underline{I} - \kappa\,\underline{S}\cdot\underline{I}\} \qquad \text{(B-14)}$$

$$+ p[(\underline{L}\cdot\underline{I})^2 + \underline{L}\cdot\underline{I}/2 - L^{*2}I^{*2}/3]$$

$$+ \mathcal{H}_7$$

where K, M, N, p, a, β and γ are independent of operators $\underline{L}$, $\underline{S}$, and $\underline{I}$, and $\mathcal{H}_7$ [Eq. (14)] is to be obtained for each particular crystalline field. ZnTe and CdTe single crystals have cubic structure with each Zn or Cd surrounded by four tetrahedrally positioned Te ions. The crystalline field appropriate to this structure is [see Eq. (43)]:

$$\mathcal{H}_7(r,\theta,\phi) = A_{4o}r^4\{Y_{4o}(\theta,\phi) + (5/14)^{1/2}[Y_{44}(\theta,\phi) + Y_{4-4}(\theta,\phi)]\}$$

$$= A_{4o}[\alpha_{4o}/8(35z^4-30r^2z^2+3r^4) + \sqrt{5/14}\,\frac{105}{8}\,\alpha_{44}(3r^4$$

$$-4r^4\cos 2\theta+r^4\cos 4\theta)\cos 4\phi] \qquad \text{(B-15)}$$

$$= A_{4o}[\alpha_{4o}/8\,(35z^4-30r^2z^2+3r^4) + \sqrt{5/14}\,105r^4\sin^4\theta\cos 4\phi].$$

Recalling that

$$\cos 4\phi = 8\cos^4\phi - 8\cos^2\phi + 1$$

$$r^4\sin^4\theta = (x^2+y^2)^2 = r^4 - 2r^2z^2 + z^4$$

one finds that

$$r^4\sin^4\theta \cos 4\phi = x^4 + y^4 - 6x^2y^2 \tag{B-16}$$

Equations (B-15) and (B-16) reveal that

$$\mathcal{H}_7 = (A_{40}/8)[\alpha_{40}(35z^4-30r^2z^2+3r^4) + 1680\sqrt{5/14}\ \alpha_{44}(x^4+y^4-6x^2y^2)] \tag{B-17}$$

where

$$\alpha_{n,m} = (-1)^n\left[\frac{(2n+1)(n-|m|)!}{2(n+m)!}\right]^{1/2}\left(1/\sqrt{2\pi}\right)$$

Thus

$$\alpha_{44} = (9/2(8)!2\pi)^{1/2} \tag{B-18}$$

and

$$\alpha_{40} = (9/2\pi)^{1/2} \tag{B-19}$$

Substituting for $\alpha_{n,m}$ in Eq. (B-17) one finds:

$$\begin{aligned}\mathcal{H}_7 &= (3A_{40}/8\sqrt{2\pi})[(35z^4-30r^2z^2+3r^4) + 5(x^4+y^4-6x^2y^2)] \\ &= (15A_{40}/\sqrt{2\pi})(x^4+y^4+z^4 - 3r^4/5).\end{aligned} \tag{B-20}$$

The next step is to transform r^4 into a function of angular momentum components. Consider that

$$r^4 = x^4 + y^4 + z^4 + 2(x^2y^2+y^2z^2+z^2x^2) \tag{B-21}$$

and

$$x^2y^2 \Longrightarrow \frac{1}{6}(L_x^2L_y^2+L_y^2L_x^2+L_xL_yL_yL_x+L_yL_xL_xL_y+L_xL_yL_xL_y+L_yL_xL_yL_x) \tag{B-22}$$

where

$$L_x L_y L_y L_x + L_y L_x L_x L_y = 2L_z^2 + 2L_x^2 L_y^2 - L_x^2 - L_y^2 \qquad \text{(B-23)}$$

and

$$L_x L_y L_x L_y + L_y L_x L_y L_x = L_z^2 + 2L_x^2 L_y^2 - L_x^2 - L_y^2 \qquad \text{(B-24)}$$

Equations (B-22), (B-23), and (B-24) reveal that

$$x^2y^2 \Longrightarrow \frac{1}{6}\left(2L_x^2L_y^2+4L_x^2L_y^2+3L_z^2-2L_x^2-2L_y^2\right) = \frac{1}{6}\left(6L_x^2L_y^2+3L_z^2-2L_x^2-2L_y^2\right) \qquad \text{(B-25)}$$

The expressions corresponding to y^2z^2 and z^2x^2 can be obtained from Eq. (B-25) by proper substitution of x, y, and z. The sum of these expressions which is needed for evaluating Eq. (B-21) is:

$$\begin{aligned} 6(x^2y^2+y^2z^2+z^2x^2) \Longrightarrow\ & 6(L_x^2L_y^2+L_y^2L_z^2+L_z^2L_x^2) \\ & + 3(L_z^2+L_x^2+L_y^2) - 2(L_x^2+L_y^2+L_z^2) \\ & - 2(L_y^2+L_z^2+L_x^2) \\ \Longrightarrow\ & 6(L_x^2L_y^2+L_y^2L_z^2+L_z^2L_x^2) - (L_x^2+L_y^2+L_z^2) \end{aligned} \qquad \text{(B-26)}$$

Now note that

$$L_x^2L_y^2 + L_y^2L_z^2 + L_z^2L_x^2 = L^{*4} - (L_x^4+L_y^4+L_z^4) - (L_x^2L_y^2+L_y^2L_z^2+L_z^2L_x^2)$$

or

$$6(L_x^2L_y^2 + L_y^2L_z^2 + L_z^2L_x^2) = 3[L^{*4} - (L_x^4+L_y^4+L_z^4)] \qquad \text{(B-27)}$$

Equations (B-20) through (B-27) reveal that

$$\mathcal{H}_7(L) = B[L_x^4 + L_y^4 + L_z^4 - \frac{3}{5}(L^{*4} - \frac{1}{3}L^{*2})]$$

$$= B[L_x^4 + L_y^4 + L_z^4 - \frac{1}{5}L^{*2}(3L^{*2}-1)] \qquad \text{(B-28)}$$

$$= B[L_x^4 + L_y^4 + L_z^4 - \frac{1}{5}L(L+1)(3L^{*2}+3L-1)]$$

Equation (B-28) is similar to the Bleaney's[10] results for this case and B here is a constant obtained as a result of transforming $\mathcal{H}_7(r,\theta,\phi)$ into $\mathcal{H}_7(L)$.

REFERENCES

1. Lambe et al., Phys. Rev. 119, 1256 (1960).

2. Azarbayejani et al., Bull. of Am. Phys. Soc. 6, 117 (1961).

3. Kikuchi et al., Suppl. Phys. Soc. Japan 17, 435 (B-1, 1962).

4. Semiconductor Laboratory Procedural Manual (DRM60-00169).

5. Van Wieringen, Physica 19, 397 (1953).

6. Watanabe, Prog. of Theoret. Phys. 18, 405 (1957).

7. Matarrese et al., J. Chem. Phys. of Solids 1, 117 (1956).

8. Thomas, Nature 117, 514 (1926).

9. Mack, Rev. of Mod. Phys. 22, 64 (1950).

10. Bleaney and Stevens, Repts. Prog. Phys. 16, 108 (1953).

11. Bethe, Ann. Physik 3, 133 (1929).

12. Racah, Phys. Rev. 62, 438 (1942).

13. AFOSR TN59-220 (1959).

14. deKronig et al., Physica 6, 290 (1939).

15. Hitler, Quantum Theory of Radiation, Oxford, Clarendon Press, p. 180 (1954).

16. Griffith, The Theory of Transition Metal Ions, Cambridge (1961).

17. Feenberg, notes on Quantum Theory of Angular Momentum, p. 34, Stanford University Press (1959).

PART IV

SOLID STATE INSTRUMENTATION

by

Glenn G. Sherwood*

*Captain, USAF, in Civilian Institutions Program, AFIT, at The University of Michigan.

This research project is concerned with the design and development of a solid state charged particle dE/dx detector to replace the traditional gaseous ion chamber. The advantages of the solid state counter over the gas counter are:

(a) Resolving times of less than 0.1 microsecond due to short collection times in the semiconductor.

(b) Less scattering of particles out of the beam by multiple coulomb interactions, and hence greater counting efficiency.

(c) Ionization efficiency which is 10 times greater than that of the gas counter, and hence some probable improvement in resolution.

(d) Fast rise time, which permits high counting rates and the possibility of using pulse shaping techniques to discriminate against background gamma radiation.

Some work on semiconductor dE/dx detectors was done by H. E. Wegner of Los Alamos Laboratory in 1960. He developed a diffused junction dE/dx detector with a thickness of 50 microns and a diameter of 3/16-in. As Wegner reported out of six original detectors this was the only one which survived the difficult grinding and etching process to give a workable thin detector. However, this one was enough to demonstrate the feasibility and advantages of semiconductor dE/dx detectors.

Our research project, wherein we are attempting to measure the spatially dependent fast neutron fission spectra through several types of semi-infinite media, requires a proton recoil telescope spectrometer which has a resolving

time of less than 1 microsecond and is relatively insensitive to background neutrons and gammas. Previous telescopes with gaseous counters had extreme limitations imposed by the large resolving times, and this restricted their performance so greatly that experiments with fission sources were virtually impossible, as explained by Johnson.[1]

Our prescription for a possible method of measuring the spectra is shown in Fig. 1. Here is depicted a proton recoil telescope with a semiconductor detector preceded by a semiconductor dE/dx detector. The proton recoils in energy range 1 to 12 Mev must pass the dE/dx detector and stop in the thick E detector. Only those pulses which pass through both detectors and are hence in time coincidence are allowed to enter the pulse height analyzer. This reduces the large neutron background produced by the Si^{28} (n,p) and Si^{28} (n,α) reactions as well as betas from the walls of the instrument.

The portion of this telescope spectrometer project covered herein involves the development of the dE/dx detector. Three factors dictate the size of the thin detector: noise, counting statistics and thickness. The energy of the protons require a detector of about 25 microns so that 1.5 Mev protons will pass into the second detector. So that the efficiency can be kept in the order of magnitude of 10^{-6} or greater (corresponding to an energy resolution of 15-20%) for reasonable counting statistics, the diameter of the finished detector should be as close to 2 cm as possible. Noise will limit the achievement of the ultimate resolution and efficiency. Theoretically, the noise of this detector should be about 85 Kev if predicted by the noise analysis of Goulding.[2] This would be acceptable because the 12-Mev

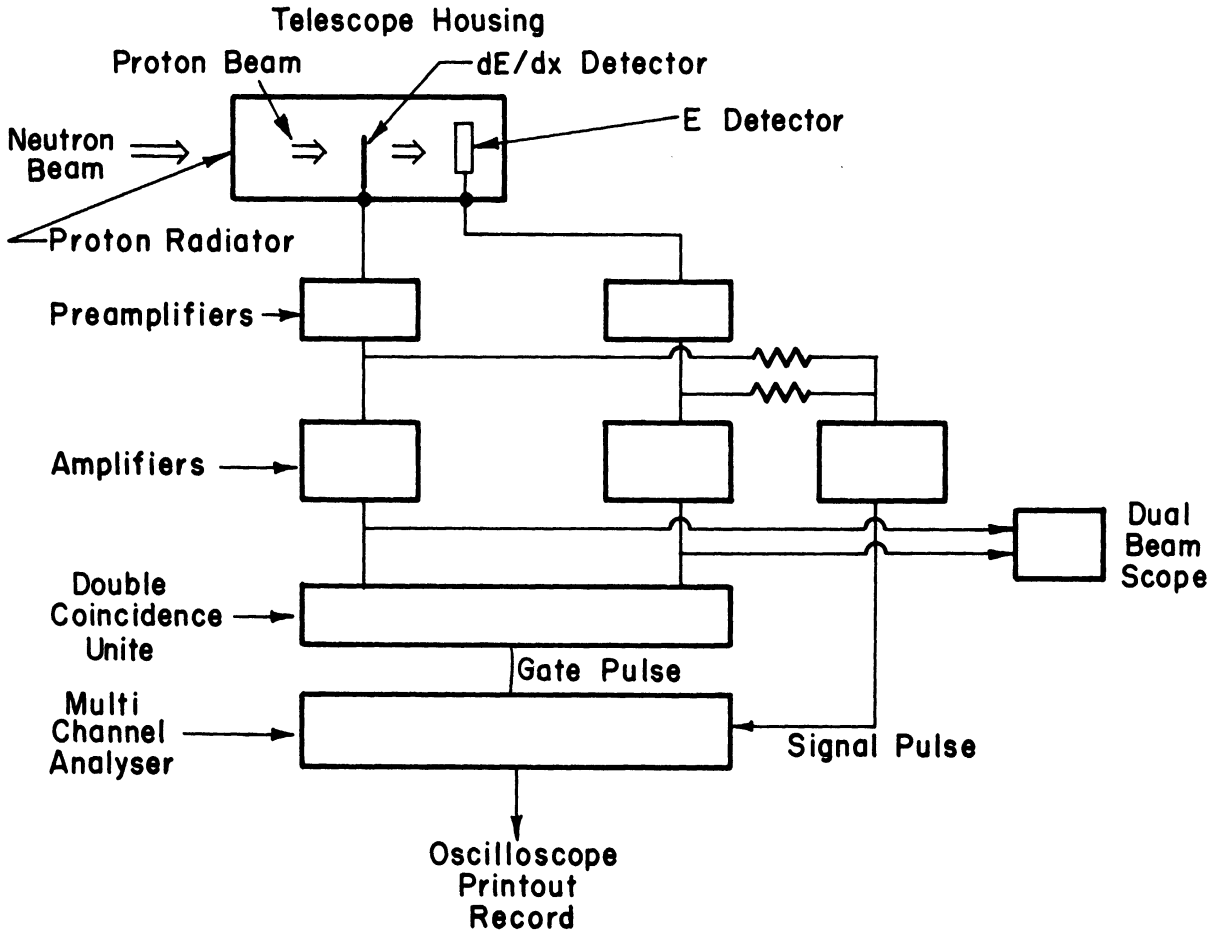

Fig. 1. Block diagram of telescope spectrometer and necessary circuitry for coincidence counting.

proton deposits about 150 Kev in 25 microns of silicon.

In attempting to develop high quality semiconductor detectors the surface barrier technique appears superior to the diffused junction method as used by Wegner because:

(a) The surface barrier method does not require excessive heat which degrades the performance of the completed diode.

(b) The p-n junction diode has a "window" of several microns which degrades the energy of slower protons without collecting charge.

With these advantages in mind work was started in February 1962 to develop these solid state devices.

A 2000 ohm-cm, 500-microsecond, vacuum zone floated N-type silicon, 24 mm in diameter, is waxed into a circular pyrex boat which is in turn waxed to a flat aluminum plate. The silicon is then cut into discs .035-in. thick with a high speed diamond impregnated blade on a Di Met No. 120BQ cutoff machine. The silicon disc is then waxed to a pyrex optical disc 3 in. in diameter (see Fig. 2). Three small blocks of silicon are waxed 120 degrees apart, as shown in the figure, and it is the purpose of these blocks to maintain the parallelism between the face of the silicon crystal and the pyrex blocks.

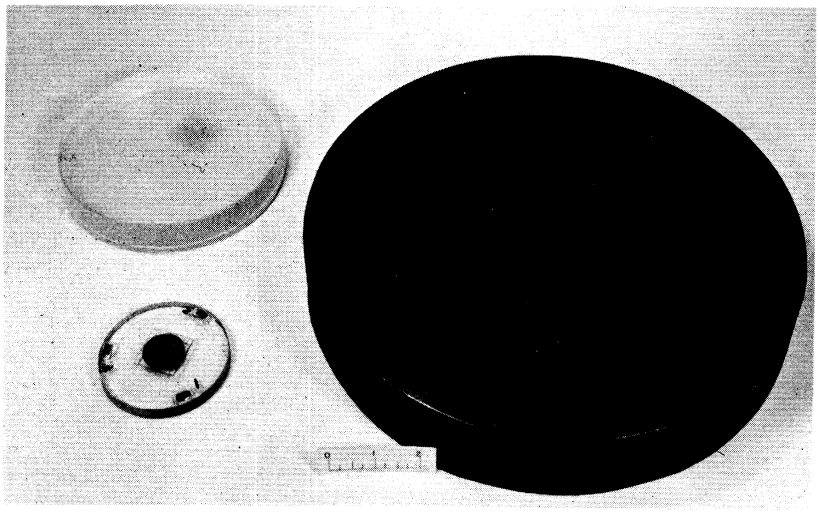

Fig. 2. The silicon wafer is shown mounted on a pyrex polishing disc. The optical glass flat and the iron flat are used in the lapping process.

Two types of optical lapping flats are used in this process, a 12-in. iron flat and a 6-in. glass flat. The iron flats are used with silicon carbide abrasive and the pyrex flats with aluminum oxide abrasive. The final

polishing is done with Linde A alumina on Buehler AB Metcloth with the Buehler polishing wheel. Both iron and pyrex flats are checked periodically to ensure that they do not loose their flatness.

The silicon crystal is first lapped with No. 400 silicon carbide in water on the metal flat to remove the silicon damaged by the saw. The crystal is then lapped with No. 600 silicon carbide and then with No. 1200 aluminum oxide in water. The polishing blocks are measured regularly during this process with a micrometer to maintain them at an even height with respect to the back of the polishing block. In this way the removal of silicon by lapping can be controlled so that the crystal is ground with parallel surfaces. When the pits have all been removed by the No. 1200 abrasive, as observed with a metallurgical microscope of power 110, the crystal is transferred to the glass optical flat and lapped with No. 3200 aluminum oxide. The crystal is then polished to a mirror finish with the Linde A until all pits and scratches are removed. At this point the surface should have minimum damage (about 1 micron) but should still exhibit a relatively high surface recombination velocity.

The crystal is then turned over on the 3-in. pyrex flat, polished side down, and the reverse side of the crystal is lapped and polished in the manner explained above. The crystal is polished down to 45-micron thickness, with particular care being taken to insure that the crystal is planar. This can be controlled by measuring the edges with a microscope.

The crystal is removed from polishing by gentle heating. It is washed in successive baths of trichloroethylene, alcohol, and distilled water, dried in a clean glove box, and finally cemented to a lavite type A ring with

Araldite No. 951 amine-type epoxy (see Fig. 2).

The back of the crystal is protected by sax while the entire crystal and holder is immersed in an etch bath (nitric acid, hydrofluoric acid, and acetic acid in volume proportions 2:1:1) for two minutes. After washing in distilled water, the wax is removed from the back. After 24 hours, 75 micrograms/cm^2 of gold is evaporated on the front and the same quantity of aluminum is evaporated on the back. The semiconductor dE/dx detector is allowed to age for several days and is then completed.

Experimentation with several etches showed that the most controlled etch producing a chemical polish on the 1/2-micron polished surface of the silicon was of the above noted composition, maintained at 0°C for about 2 minutes. This procedure removes evenly about 10 microns, leaving a polished surface which appears to produce the surface barrier required.

The important aspect of this technique is that we have apparently been able to control the etch rate without any preferential action on the part of the etch solution. Using this procedure on the face of the silicon crystal apparently provides the density of fast states necessary for the inversion layer. With evaporation of a gold layer, the rectifying junction appears to be complete.

We are still experimenting with back contacts to achieve a stable or ohmic contact which is free from injection. We have only partially achieved this because the back contacts still provide some rectifying action. The tests to show the amount of minority carrier injection are still inconclusive.

The latest dE/dx detectors have progressed to the point where we are now producing detectors 3-cm^2 in finished area, and 30 microns thick, with stable characteristics over periods of weeks. Resolution for Po^{210} is 5.8% (see Fig. 3) and the peak noise extends to channels corresponding to about 280 Kev. Improvement in the back contact should help to decrease the noise to the acceptable level of 150 Kev. Figure 4 shows the pulse shape versus bias for Po^{210} alphas.

The dE/dx detector in conjunction with a thick detector is now operating in a proton recoil test spectrometer with coincidence equipment. This telescope spectrometer, shown in Fig. 5, is being used to help find those sources of noise which can be removed. (Since tests have just started there are no conclusive results as yet.) The mechanism shown in Fig. 5 is the telescope, which operates in a vacuum housing. The front wheel holds the polyethylene radiators, which are of different thickness. Behind the front wheel is the dE/dx detector, and behind this detector is the E detector. The rear of the device holds the motor for positioning the different radiators corresponding to various parts of the neutron energy spectrum being sampled.

The instrument has been initially tested with a weak Pu-Be source. Figure 6 shows the response of the dE/dx detector and E detector to recoil protons. The picture is poor because the count rate is low and a 30-45 second exposure was necessary. The coincidence counting rate is about 1 per minute. In January the instrument will be tested with the Michigan Van de Graaff.

Initial results indicate at least partial success with the new semiconductor dE/dx detectors and some success with the telescope. As far as we can determine no other group has achieved success as yet in producing these solid state counters.

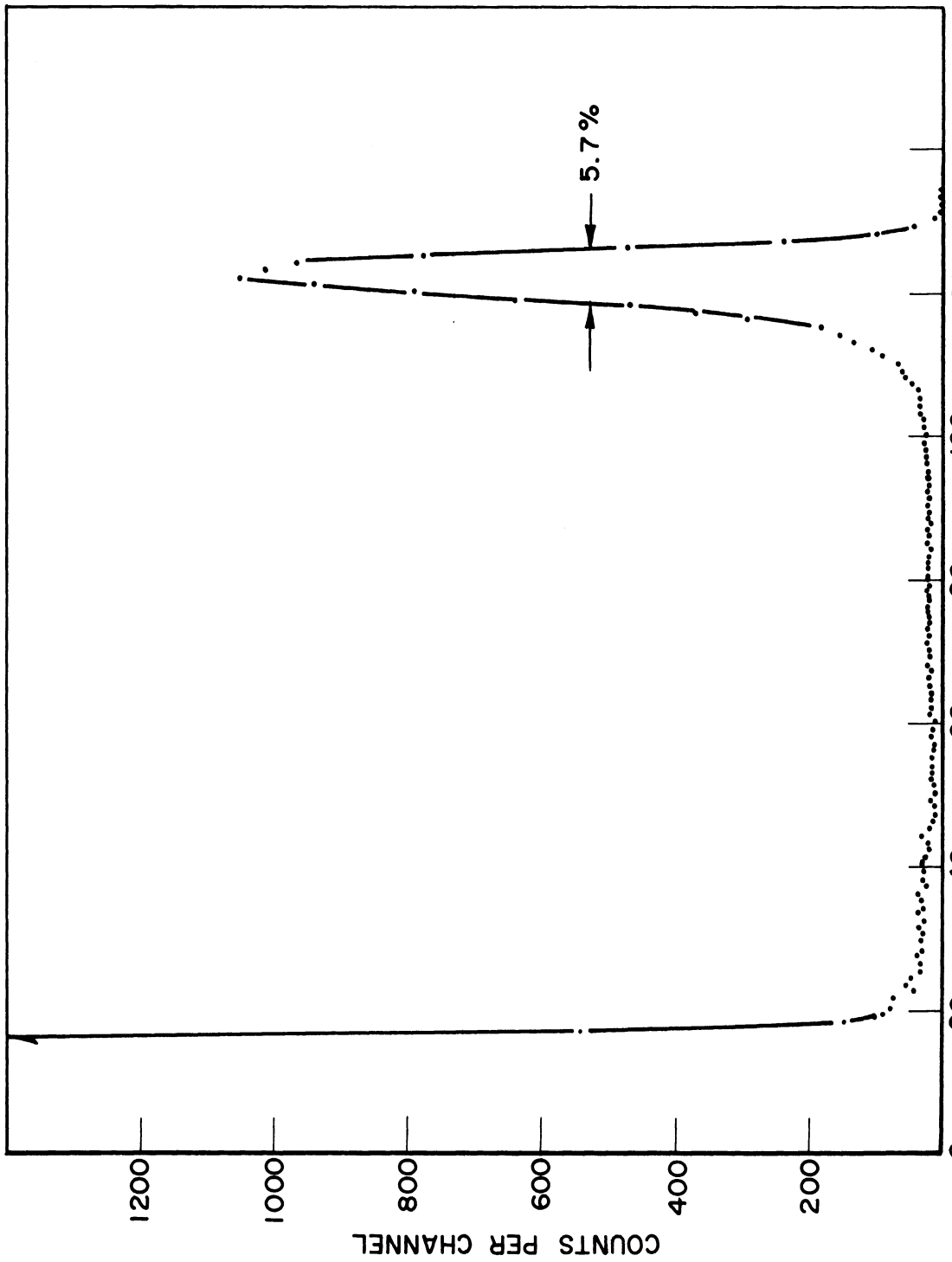

Fig. 3. Response of the silicon dE/dx detector to Po^{210} alphas.

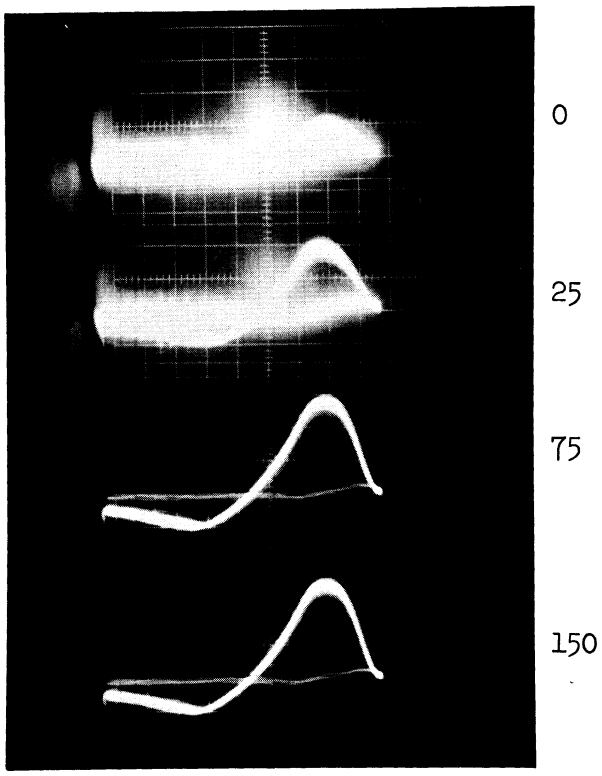

Fig. 4. Pulse shape of large area dE/dx detector to Po^{210} alphas vs. bias across the detector and 22-meg load resistor. Voltage is 0, 25, 75, and 150 volts; the leakage current is over 1 microampere.

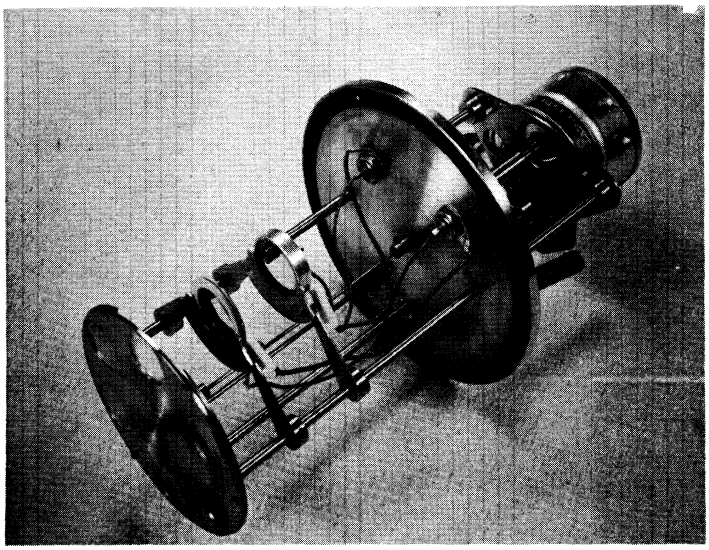

Fig. 5. The telescope spectrometer. The detector nearest to the proton radiator wheel is the dE/dx detector. The second detector is a semi-conductor E detector.

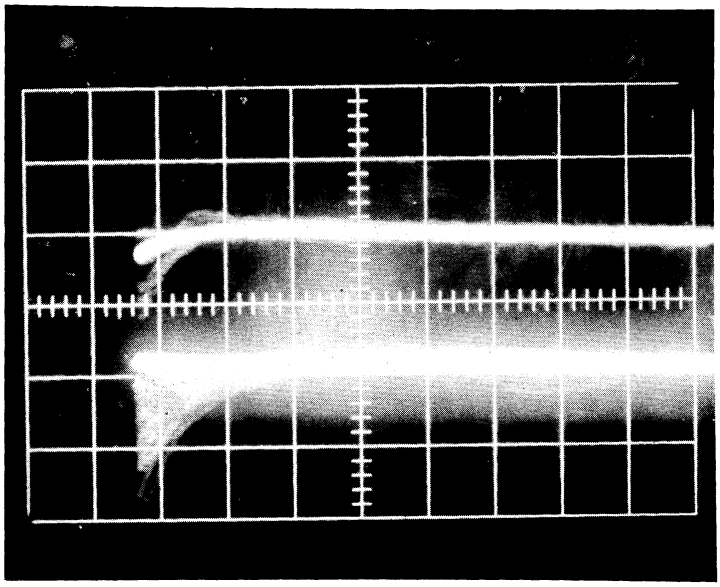

Fig. 6. The top line shows the response of the dE/dx detector and the bottom the E detector to proton recoils using a Pn-Be source.

REFERENCES

1. In Marion, J. B. and J. L. Fowler, Fast Neutron Physics, Vol. IV, Interscience Publishers, N. Y. (1960).

2. Goulding, F. S. and W. L. Hansen, Leakage Current in Semiconductor Junction Radiation Detectors and Its Influence on Energy Resolution Characteristics, UCRL 9436, November 1960.

PART V

PUBLICATIONS AND PRESENTATIONS COMPLETED UNDER CONTRACTS NO. AF-49(638)-68 AND AF-49(638)-987

I. UNIVERSITY OF MICHIGAN TECHNICAL REPORTS AND INTERNAL MEMORANDUMS

Baker, J., and Lambe, J., Luminescence of Color Centers in KCl, Technical Report 2616-5-T, January, 1959.

Chen, S. H., Evaluation of Matrix Elements in Crystalline Field Theory, Technical Report 04275-1-T, October, 1962.

Kikuchi, C., Makhov, G., Lambe, J., and Terhune, R., Ruby as a Maser Material, Technical Report 2616-6-R, May, 1959.

Kikuchi, C., Sum Rules and Relative Intensities for Paramagnetic Ions of Spin 3/2, Technical Report 2616-8-R, June, 1959.

Kikuchi, C., Resonance Absorption of Paramagnetic Ions with Spin 5/2: $CaCO_3$: Mn, Technical Report 2616-10-R, August, 1959.

Kikuchi, C., and King, J. E., Azimuthal Dependence of Spin Resonance Spectrum for S = 5/2, Internal Memorandum Z-1214, April 14, 1959.

Kikuchi, C., and Lambe, J., Spin Resonance of V^{2+}, V^{3+}, V^{4+} in α-Al_2O_3, Technical Report 2616-12-R, November, 1959.

Kikuchi, C., and Sims, C., Resonance Absorption of Ruby at Low Magnetic Fields, Internal Memorandum, Z-1101, August 25, 1958.

Kikuchi, C., and Sims, C., Relative Intensities of Ruby Resonance Lines, Internal Memorandum, Z-1102, August 27, 1958.

Makhov, G., Kikuchi, C., Lambe, J., and Terhune, R. W., Maser Action in Ruby, Technical Report 2616-1-T, June, 1958.

II. JOURNAL ARTICLES, PAPERS, AND PRESENTATIONS

Azarbayejani, G. H., Kikuchi, C., and Mason, D.,"Paramagnetic Resonance of ZnTe:Mn," Bull. Am. Phys. Soc. 6, 117 (1961).

Baker, J., Lambe, J., and Kikuchi, C., "Photosensitive Spin Resonance in CdS," Phys. Rev. Ltrs. 3, 270 (1959).

Borcherts, R., Wepfer, G., and Kikuchi, C., "Paramagnetic Resonance Spectrum of Vanadyl Ammonium Sulfate," Bull. Am. Phys. Soc. 7, 118 (1962).

Kikuchi, C., "Certain Sum Rules Applicable to Paramagnetic Ions of Spin 3/2," Bull. Am. Phys. Soc. 4, 261 (1959).

Kikuchi, C., "MASER," presentation at Sylvania Products, Bayside, New York (April, 1957).

Kikuchi, C., "Ruby Maser," Proceedings of NSIA-ARDC Conference on Molecular Electronics (1958).

Kikuchi, C., "Experimental Work on Ruby Masers," invited paper at American Physical Society Meeting (November, 1958), Chicago, Illinois.

Kikuchi, C., and Ager, R., "Doublets in the Electron Spin Resonance Spectrum of Mn^{++} in Calcite," Bull. Am. Phys. Soc. 3 (march, 1958).

Kikuchi, C., Ager, R., and Matarrese, L., "Doublets in the Electron Spin Resonance Spectrum of Mn^{++} in Calcite," presentation at American Physical Society Meeting, Chicago, Illinois (March, 1958).*

Kikuchi, C., and Azarbayejani, G. H., "Spin Resonance Properties of ZnTe:Mn and of Other $A_{II}B_{VI}$ Compounds," J. Phys. Soc. Japan 17, Suppl. B-I, 453 (1962).

Kikuchi, C., and Lambe, J., "Spin Resonance Investigation of Certain Sapphires," invited paper at American Physical Society Meeting, Honolulu, Hawaii (August, 1959).

Kikuchi, C., and Lambe, J., "Spin Resonance of V^{2+}, V^{3+}, V^{4+}, in α-Al_2O_3,+ Phys. Rev. 118, 71 (1960).

*This is essentially the same paper as Technical Report 2616-12-R, November, 1959.

Kikuchi, C., Lambe, J., Makhov, G., and Terhune, R. W., "Development of a Ruby Maser at Willow Run Laboratories," presentation at Fort Monmouth, New Jersey (1958).

Kikuchi, C., Lambe, J., Makhov, G., and Terhune, R. W., "Ruby Maser," presentation at Electron Rube Research Conference, Laval Univ., Quebec, Canada (June, 1958).

Kikuchi, C., Lambe, J., Makhov, G., and Terhune, R. W., "Induced Microwave Emission in Ruby," Solid State Physics in Electronics and Tele-Communications, Vol. IV: Magnetic and Optical Properties, Part 2, Academic Press, London (1960).

Kikuchi, C., Lambe, J., and Terhune, R., "Maser Action in Ruby," Phys. Rev. 109, 1399 (February, 1958).

Kikuchi, C., Makhov, G., Lambe, J., and Terhune, R., "Ruby as a Maser Material," J. Appl. Phys. 20, 1061 (July, 1959).

Kikuchi, C., and Matarrese, L. M., "Paramagnetic Resonance Absorption of Ions with Spin 5/2: Mn^{++} in Calcite," J. Chem. Phys. 33, 601 (1960).

Lambe, J., and Ager, R., "Microwave Cavities for Magnetic Resonance Spectrometers," Rev. Sci. Inst. 30, 599 (July, 1959).

Lambe, J., Ager, R., and Kikuchi, C., "Electron Spin Resonance of V^{2+} and V^{3+} in Corundum," Bull. Am. Phys. Soc. 4, 261 (1959).

Lambe, J., and Baker, J., "Effect of Bleaching on F-Center Paramagnetic Resonance," Bull. Am. Phys. Soc. 3 (March, 1958).

Lambe, J., and Baker, J., "Optical Effects on F-Center Spin Resonance at Low Temperatures," presentation at Quantum Mechanics Conference, High View, New York (Sept., 1959).

Lambe, J., Baker, J., and Scarisbrick, I., "Spin Resonance of Atomic Tritium at 4.2°K," Bull. Am. Phys. Soc. 4, 418 (1959).

Lambe, J., and Kikuchi, C., "Spin Resonance of Donors in CdS," J. Phys. Chem. Solids 8, 492 (January, 1958).

Lambe, J., and Kikuchi, C., "Spin Resonance Mn^{++} in CdTe," Bull. Am. Phys. Soc. 5, 158 (1960).

Lambe, J., and Kikuchi, C., "Paramagnetic Resonance of CdTe; Mn and CdS:Mn," Phys. Rev. 119, 1256 (1960).

Mathews, J. H., and Lambe, J., "X-Ray Coloration of Ruby," Bull. Am. Phys. Soc. 4, 284 (1959).

Scarisbrick, I., "Spin Resonance of Gamma Irradiated Alkali Hydrides," Bull. Am. Phys. Soc. 4 (June, 1959).

Terhune, R. W., Kikuchi, C., Lambe, J., and Baker, J., "Hyperfine Structure of the $(Cr53)^{+++}$ Ion in Ruby by Double Resonance," Bull. Am. Phys. Soc. 5, 157 (1960).

Terhune, R. W., Lambe, J., Kikuchi, C., and Baker, J., "Hyperfine Spectrum of Chronium 53 in Al_2O_3," Phys. Rev. 123, 1265 (1961).

DISTRIBUTION LIST

(One copy unless otherwise indicated)

Air Force Office of Scientific Research
Washington 25, D. C.
Attn.: Solid State Sciences Div. 3
Attn.: Technical Library (SRGL) 2

Armed Services Technical Information Agency 10
Arlington Hall Station
Arlington 12, Virginia
Attn.: TIPCR

Air Research and Development Command
Andrews Air Force Base
Washington 25, D. C.
Attn.: RDRS

European Office
Air Research and Development Command
47 Cantersteen
Brussels, Belgium

Hq., United States Air Force
Washington 25, D. C.
Attn.: AFDRT

Aeronautical Research Laboratory
Building 450
Wright-Patterson AFB, Ohio
Attn.: Technical Library

Wright Air Development Division
Wright-Patterson AFB, Ohio
Attn.: WWAD

Wright Air Development Division
Materials Central
Wright-Patterson AFB, Ohio
Attn.: Metals and Ceramics Lab.
Attn.: Physics Lab.
Attn.: Materials Informantion Branch

Institute of Technology
MCLI-LIB, Bldg. 125, Area B
Wright-Patterson AFB, Ohio
Attn.: (AU) Library

Aeronautical Research Laboratory
AFRD
Wright-Patterson AFB, Ohio
Attn.: Metallurgy
Attn.: Physics, Solid State

Air Force Office of Science Research
Holloman AFB, New Mexico
Attn.: SRLTL

Air Force Cambridge Research Lab.
Laurence G. Hanscom Field
Bedford, Massachusetts
Attn.: CRRELA

Air Force Flight Test Center
Edwards AFB, California
Attn.: FTCTL

Arnold Engineering Development Center
Arnold Air Force Station
Tennessee
Attn.: AEOIM

Air Force Special Weapons Center
Kirtland AFB, New Mexico
Attn.: SWOI

Commander 2
Army Rocket and Guided Missile Agency
Redstone Arsenal, Alabama
Attn.: ORDXR-OTL

DISTRIBUTION LIST (Continued)

Office of the Chief of Research
and Development
Department of the Army
Washington 25, D. C.
Attn.: Scientific Information

Army Research Office (Durham)
Box CM, Duke Station
Durham, North Carolina
Attn.: CRD-AA-IP

Commanding Officer
Ordnance Materials Research Office
Watertown Arsenal
Watertown 72, Massachusetts
Attn.: PS and C Div.

Commanding Officer
Watertown Arsenal
Watertown 72, Massachusetts
Attn.: Watertown Arsenal Lab.
Tech. Reports Section

Commander
Signal Corps Engineering Lab.
Fort Monmouth, New Jersey
Attn.: SIGFM/EL-RPO

Director
U.S. Naval Research Laboratory
Washington 25, D. C.
Attn.: Library

Department of the Navy
Office of Naval Research
Washington 25, D. C.
Attn.: Code 423
Attn.: Code 421

Officer in Charge
Office of Naval Research
Navy No. 100
Fleet Post Office
New York, New York

Commanding Officer
Naval Radiological Defense Lab.
San Francisco Naval Shipyard
San Francisco 24, California

Dr. D. F. Bleil
Associate Technical Director
for Research
U.S. Naval Ordnance Lab.
White Oak
Silver Spring, Maryland

National Aeronautics and Space
Agency
1520 H St., N.W.
Washington 25, D. C.
Attn.: Library

Ames Research Center (NASA)
Moffett Field, California
Attn.: Tech. Library

High Speed Flight Station (NASA)
Edwards AFB, California
Attn.: Tech. Library

Langley Research Center (NASA)
Langley AFB, Virginia
Attn.: Tech. Library

Lewis Research Center (NASA)
21000 Brookpark Road
Cleveland 35, Ohio
Attn.: Tech. Library

Wallops Station (NASA)
Wallops Island, Virginia
Attn.: Tech. Library

U.S. Atomic Energy Commission
Library Branch
Tech. Information Div., ORE
P. O. Box E
Oak Ridge, Tennessee

DISTRIBUTION LIST (Concluded)

Division of Research
U.S. Atomic Energy Commission
Division Office
Washington 25, D. C.

Major John Radcliffe
ANP Office
U.S. Atomic Energy Commission
Washington 25, D. C.

Oak Ridge National Laboratory
Post Office Box P
Oak Ridge, Tennessee
Attn.: Central Files

Brookhaven National Laboratory
Upton, Long Island, New York
Attn.: Research Laboratory

Argonne National Laboratory
9700 South Cass Avenue
Argonne, Illinois
Attn.: Librarian

Knolls Atomic Power Laboratory
P. O. Box 1072
Schenectady, New York
Attn.: Document Librarian

National Science Foundation
1901 Constitution Avenue, N.W.
Washington 25, D. C.

National Bureau of Standards Library
Room 203, Northwest Building
Washington 25, D. C.

Document Custodian
Los Almos Scientific Laboratory
P. O. Box 1663
Los Alamos, New Mexico

Ames Laboratory
Iowa State College
P. O. Box 14A, Station A
Ames, Iowa

Director
Office of Technical Services
Department of Commerce
Technical Reports Branch
Washington 25, D. C.

Chairman
Canadian Joint Staff (DRB/DSIS)
2450 Massachusetts Ave., N. W.

Defense Research Member
Canadian Joint Staff
Director of Engineering Research
Ottawa, Canada
Attn.: Mr. H. C. Oatway

Institute of the Aeronautical Sciences
2 East 64th Street
New York 21, New York
Attn.: Librarian

RAND Corporation
1700 Main Street
Santa Monica, California